IMPACT OF SOLAR PHOTOVOLTAICS ON THE SYSTEM STABILITY OF THE ZAMBIA NATIONAL GRID

By

Phiri David Chifundo

A dissertation submitted to the University of Zambia in partial fulfilment of the requirements for a Master's Degree in Electrical Power Engineering

The University of Zambia

Lusaka

2021

Copyright Declaration

Declaration

I, Phiri David Chifundo, do declare that this work is my own and that the work of other persons utilized in this dissertation has been duly acknowledged. This work presented here has not been previously presented at this or any other university for similar purposes.

Signature: …….…… Date…….…….
Phiri David Chifundo
(Candidate)

We the undersigned have read this dissertation and have approved it for examination;

Dr. Ackim. Zulu (PhD)
Lecturer
Department of Electrical and Electronics Engineering
The University of Zambia

Signature: …….…….

Date…….……

Certificate of Approval

This dissertation by Phiri David Chifundo is in partial fulfillment of the requirements for the award of the Master of Electrical Power Engineering by The University of Zambia.

Examiner 1

Name: ……

Signature: ……...

Date: …….

Examiner 2

Name: ……

Signature: ……...

Date: …….

Examiner 2

Name: …….

Signature: ……...

Date: ……...

Chairperson of the Board of Examiners

Name: …….

Signature: ……...

Date: ……...

Abstract

The use of renewable energy sources is one of the crucial components of the contemporary issues of sustainable development. Sustainable energy development gives a rationale to have resources that are economical, environmentally friendly and whose social effects are acceptable. However, the potential for a large-scale shift from the use of conventional fuels to renewable energy for electricity generation remains a highly debated issue especially in developing countries. The major argument is that large-scale implementation of renewable energy poses significant challenges to legacy power systems due to temporal fluctuations, geographical dispersion of renewable energy resources and the presumed inadequacy of the existing power grids which are still dependent on traditional power generation technologies. In this study, the impacts of integrating Solar PV power generation on an existing grid were investigated. The investigations were performed by modelling and simulations in power system software (DIgSILENT PowerFactory). The highlights of the investigation results are that there was alteration of voltage levels, changes of line losses, reversal of power flows and improvement in steady state voltage stability depending on level of penetration of Solar PV and the operating condition of the given injection point. The study concluded that a loss of Solar PV power generation had more adverse effects than a startup of such a power plant. Further, the study concluded that changes in solar irradiance may not result in adverse impacts on the stability of the grid provided that the generation is within the limits for which the grid is capable of handling a total loss of generation. For the Zambian grid, the study concluded that with a non-cumulative scenario, up to 123 MW at Leopards Hill and 121 MW at Lusaka West Substations of Solar PV could be injected into the 132 kV busbars resulting in additional loading of about 25.5 % and 31.5 % on the respective busbars, without adverse effects. However, an uncontrolled loss of generation for the 123 MW and 121 MW Solar PV power at Leopards Hill and Lusaka West would result in a total system failure for each non-cumulative scenario. System stability could be achieved for a total loss of generation of 43.6 MW of Solar PV generation at the Leopards Hill and Lusaka West resulting in additional loading of about 9.2 % and 11.5 % as a maximum on the respective busbars, thereafter reinforcements on the national grid may be necessary. Arising from the study the Kabwe Pensulo line was identified as a weak link therefore lending itself to further investigation for a Solar PV power plant at the Pensulo Substation. It was found that a maximum of 130 MW could be injected on to the 66 kV Pensulo Busbar but only 49.5 MW Solar PV generation on the 66 kV busbar at Pensulo could retained system stability after total loss of generation, resulting in 240 % maximum additional loading but only 51.3 % additional loading on the 66 kV bus bar could yield system stability after total loss of generation. In view of the need to diversify from hydroelectricity power generation which is highly susceptible to hydrological fluctuations, the study recommended the scaling up of Solar PV power generation through the modification of legislation and associated regulations and codes that were developed for conventional power generation so as to enable flexibility in the design, construction and operations of future power (generation and Transmission) infrastructure.

Keywords: Power System Stability, Renewable Energy, Solar Photovoltaic, Utility Scale, Integration, National Grid, PowerFactory DIgSILENT

Dedications

This research work is dedicated to members of my family who have continuously encouraged and supported me through my academic and professional life. Special dedications are extended to my wife Dabwitso Chapema Phiri and to my late mother Esther Kabamba-Phiri, who identified the engineer in me. Further, worthy of mention are my sons David Chifundo Phiri III and Declan Chisomo Phiri for their companionship during the study period.

Acknowledgements

To God Almighty, be the Glory;

Sincere gratitude to Dr. Ackim Zulu and Dr. Luka Ngoyi for the guidance before, during and after the course of this study;

Appreciation to my employers, the Ministry of Energy and particularly the Office for Promoting Private Power Investment for the support; and

Appreciation to everyone that contributed to the development of this report.

Table of Contents

Copyright Declaration ii
Declaration iii
Certificate of Approval v
Abstract vi
Dedications vii
Acknowledgements viii
Table of Contents ix
List of Figures xii
List of Tables xiv
List of Symbols xv
Acronyms and Abbreviations xvi
1. INTRODUCTION 1
1.1. Background 1
1.2. Problem Statement 3
1.3. Scope of the Study 5
1.3.1. Scope 5
1.3.2. Delimitation 5
1.3.2.1. Focus of the Study 5
1.3.2.2. State of Simulation Model 5
1.3.3. Limitation 6
1.4. Objectives 6
1.5. Research Questions 6
1.6. Rationale for the Study 6
1.7. Presentation of the Report 7
2. LITERATURE REVIEW 8
2.1. Solar Resource 8
2.1.1. Solar Photovoltaic Energy 8
2.1.2. Solar Resource in Zambia 9
2.2. The Traditional Power System 10
2.3. Power System Stability 11
2.3.1. Rotor Angle Stability 13
2.3.2. Frequency Stability 13
2.3.3. Voltage Stability and Voltage Collapse 14
2.3.4. Mutually Exclusivity of Stability Events 15

2.4. Variability and Uncertainty of Solar PV Generation 16
2.5. Managing Variability and Uncertainty 18
2.5.1. Predictability and Modelling of Fluctuations 18
2.5.2. Smart Grid Mitigation Measures 20
2.6. Support for Variable Solar PV Power 22
2.7. Solar PV Power Developments 23
2.7.1. Global Solar Power Generation 23
2.7.2. Solar PV Power Developments in Zambia 24
3. METHODOLOGY 26
3.1. Study Design 26
3.2. Data collection 26
3.2.1. Site visits 26
3.2.2. Participation in Solar PV development Work Groups 26
3.2.3. Review of Secondary Sources 26
3.3. Modelling of the Zambia National Grid 27
3.3.1. PowerFactory DIgSILENT 27
3.3.2. Modelling of the Zambian Power System 28
3.3.3. Modelling of a PV System in PowerFactory DIgSILENT 33
3.4. Simulations in Power factory DIgSILENT 34
3.4.1. Simulation Packages in PowerFactory DIgSILENT 34
3.4.2. Study Criteria 35
3.4.3. The choice of study areas – Leopards Hill and Lusaka West Substations 36
3.4.4. Simulation Flow Process 38
3.5. Data Analysis 39
3.6. Comparison of Results with Other Studies Conducted by Other Researchers 40
4. RESULTS AND DISCUSSIONS 41
4.1. Overview 41
4.2. Base Case 41
4.3. Impact of Solar PV on the stability of the Zambia National Grid 43
4.3.1. Injection of Solar PV at the 132 kV Leopards Hill Substation 43
4.3.2. Injection of Solar PV at the 132 kV Lusaka West Hill Substation 49
4.3.3. Injection of Solar PV at the 66 kV Pensulo Substation 53
4.4. Comparison of Solar PV Plant with Equivalent Rotational Plant 57
4.4.1. Hydro Equivalent Plant at the 132 kV Leopards Hill Busbar 57
4.4.2. Hydro equivalent plant at the 132 kV Lusaka West Busbar 61
4.4.3. Hydro equivalent plant at the 66 kV Pensulo Busbar 64

4.5. Summary of Results 66
5. CONCLUSIONS AND RECOMMENDATIONS 68
5.1. Conclusions 68
5.1.1. Impact on the Stability of the Zambia National Grid 68
5.1.2. Solar PV Power Injected at Specific Points on The Zambian Grid 68
5.1.3. Comparison of Solar PV Plant with Equivalent Rotational Plant 69
5.2. Recommendations 71
5.2.1. Recommendations 71
5.2.2. Further Studies 71
6. REFERENCES 72
7. APPENDICES 74
7.1. Appendix 1: Utility Scale Solar PV Technology i
7.2. Appendix 2: Classical Methods for Analysis of Power System Stability i
7.3. Appendix 3: System Setup for the Model Zambia National Grid i
7.4. Appendix 4: Modelling and Simulation in PowerFactory DIgSILENT iv
7.5. Appendix 5: Causes of System Collapse in PowerFactory DIgSILENT xix

List of Figures

Fig 1: World Gross Electricity Consumption 1974 – 2018 (IEA, 2020) 2
Fig 2: GTI – Global irradiation on tilted surface [kWh/m^2/day] (World Bank, 2014) 10
Fig 3: Subdivisions of power system stability (Kundur et al, 2004) 12
Fig 4: Atmospheric Radiation Measurement (Perez et al., 2009) 19
Fig 5: SLD of the ZESCO Power System 30
Fig 6:SLD of the CEC Power System 31
Fig 7:Depiction of the model of the Zambia National Grid 32
Fig 8:Functional Diagram of the PV plant (DIgSILENT, 2018) 33
Fig 9: Study Flow Chart 39
Fig 10: Voltage level (pu) with no solar injection on the power grid (base case) 42
Fig 11: % Line Loading with no solar injection on the power grid (base case) 42
Fig 12: DIgSILENT model of the Leopards Hill Substation 43
Fig 13: System collapse with 200 MW of Solar PV at 132 kV Leopards Hill Substation 44
Fig 14: Voltage Level (pu) for self-stabilizing capability at 132 kV L/Hill 45
Fig 15: Voltage Level (pu) for loss of 123 MW Solar PV generation at 132 kV L/Hill 45
Fig 16: Voltage Level (pu) for loss of 43.6MW of Solar PV generation at 132 kV L/Hill 46
Fig 17: % Line Loading for 43.6 MW Switch Off at 132 kV Leopards Hill 47
Fig 18: Per Unit Voltage Level for Selected Bus bars Solar injection at Leopards Hill 48
Fig 19: % Line Loading for Solar injection at Leopards Hill 49
Fig 20: Line Losses for Solar injection at Leopards Hill 49
Fig 21: DIgSILENT model of the Lusaka West Substation 50
Fig 22: Voltage Level (pu) for loss of 43.6 MW Solar Plant Switch Off at L/West 132 kV 51
Fig 23: Per Unit Voltage Level for Selected Bus bars Solar injection at Lusaka West 52
Fig 24: % Line Loading for solar injection at Lusaka West 53
Fig 25: % Line Losses for Solar Injection at Lusaka West Substation 53
Fig 26: Voltage Oscillations on the 330 kV Kabwe – Pensulo Transmission line 54
Fig 27: DIgSILENT model of the Pensulo Substation 54
Fig 28: Reversed power flows on the 330 kV Kabwe Pensulo Line 55
Fig 29: Per Unit Voltage Level for Selected Bus bars Solar injection at Pensulo 56
Fig 30: % Line Loading for solar injection at Pensulo Substation 57
Fig 31: Line Losses for Solar injection at Pensulo Substation 57
Fig 32: Voltage Levels (pu) for 120 MW Hydro Equivalent at L/Hill 132 kV 58
Fig 33: Voltage Level (pu) for 43.6MW Hydro Equivalent Switch off at L/Hill 132 kV 58
Fig 34: Voltage Level (pu) for 36MW Hydro Equivalent Switch off at L/Hill 132 kV 59
Fig 35: Per Unit Voltage Level for Selected Bus bars with hydro-equivalent model 60

Fig 36: % Line Loading for Selected Lines with hydro-equivalent model 60
Fig 37: MW Line Losses for Selected Lines with hydro-equivalent model..... 60
Fig 38: Voltage levels (pu) for 123MW Hydro Equivalent at Lusaka West 132 kV 61
Fig 39: Voltage Level (pu) for 36 MW Hydro Equivalent Switch off at LW 132 kV 62
Fig 40: Per Unit Voltage Level for Selected Bus bars with hydro-equivalent model 63
Fig 41: % Line Loading for Selected Lines with hydro-equivalent model 63
Fig 42: MW Line Losses for Selected Lines with hydro-equivalent model..... 63
Fig 43: Voltage Level (pu) for 130 MW Hydro Equivalent at Pensulo 66 kV 64
Fig 44: Voltage Level (pu) for 130MW Solar PV Plant Switch off at Pensulo 66kV 65
Fig 45: Voltage Level (pu) for 50MW Hydro Equivalent Plant Switch off at Pensulo 65
Fig 46: summary of % injection levels on identified busbars 70

List of Tables

Table 1: Advantages and Disadvantages of Solar PV Technologies (Wikipedia, 2019) 9
Table 2: Forms of Energy Storage Systems 21
Table 3: Timeline of the largest PV power stations in the world (Wikipedia, 2019) 23
Table 4: List of generation plants in the Model 28
Table 5: Frequency load shedding settings 36
Table 6: Transmission Line Parameters 43
Table 7: Per Unit Voltage for Selected Busbars for Solar PV Injection at Leopards Hill 47
Table 8: Transmission Line parameters at steady state at Leopards Hill 48
Table 9: Per Unit Voltage for Selected Busbars for Solar PV Injection at Lusaka West 51
Table 10: Transmission Line parameters at steady state for Lusaka West 52
Table 11: Per Unit Voltage for Selected Busbars for Solar PV Injection at Pensulo 55
Table 12: Steady state transmission line parameters for solar injection at Pensulo 56
Table 13: Per Unit Voltage Results at Selected Busbars 66
Table 14: Penetration Level at the Busbars 66
Table 15: Per Unit Voltage Results at Selected Busbars 67

List of Symbols

Δ	Rate of Change
f	Frequency
H	inertia constant
K	Damping factor
P	Real Power
Q	Reactive Power
t	time
V	Voltage

Acronyms and Abbreviations

ac	Alternating Current
CBD	Central Business District
CEC	Copperbelt Energy Corporation
dc	Direct Current
EAPP	East Africa Power Pool
ENTSO-E	European Network of Transmission System Operators
EPFI	Equator Principles Financial Institution
ERB	Energy Regulation Board
GET FiT	Global Energy Transfer Feed in Tariff
GIS	Gas Insulated Substation
HVDC	High Voltage Direct Current
IDC	Industrial Development Corporation
IDC	Industrial Development Corporation
IEEE	Institute of Electrical and Electronics Engineers
IEEE	Institute of Electrical and Electronics Engineers
IFC	International Finance Corporation
IRENA	International Renewable Energy Agency
IRENA	International Renewable Energy Agency
JICA	Japanese International Corporation Agency
kV	kilovolt
kWh	Kilowatt-hour
LS MFEZ	Lusaka South Multi Facility Economic Zone
MFEZ	Multi-Facility Economic Zone
MVA	Megavolt Ampere
MVAr	Megavolt Ampere Reactive
MW	Megawatt
MW	Megawatt
NERC	North American Electric Reliability Corporation
OECD	Organisation for Economic Co-operation and Development
PV	Photovoltaic
RE-FiT	Renewable Energy Feed-in-Tariff
RES	Renewable Energy Resources
RES	Renewable Energy Source
SAPP	Southern Africa Power Pool
SI	Statutory Instrument
SLD	Single Line Diagram
UN	United Nations
VG	Variable Generation

1. INTRODUCTION

This chapter provides a background on the impacts of integrating Solar PV power into an existing transmission grid. The chapter outlines the problem and further points to the specific study interest by defining the scope and objectives of the study.

1.1. Background

The concepts of sustainable energy development and energy sufficiency have become a matter of priority in many countries spanning from productivity and economic factors, to issues of national security. The major factors considered under sustainable development are environmental health in the wake of increased productivity for socio-economic development, occurring in a global village where peace and security are a necessity for the well-being of mankind.

The philosophy of sustainable energy development has established itself firmly among government systems, financial markets and environmental lobby groups, thereby presenting itself as a major consideration for development thereby leading to a rise in the exploitation of the so-called Renewable Energy Resources (RES) (Ayhan, 2006) and other alternative energy sources. Renewable energy resources include non-diminishing natural resources such as solar irradiance, wind power systems, geothermal manifestations, biomass decomposition etc. that are considered virtually inexhaustible in duration. The most advanced societies such as the USA, UK, Japan, Sweden and Germany, have aligned themselves towards self-sufficiency in the quest for energy development and therefore carried out extensive research on renewable energy development.

Despite being virtually inexhaustible in duration, renewable resources are limited in the amount of energy that is available per unit of time. The energy available varies from time to time depending on many factors such as prevailing weather and climatic conditions. Such variable renewable energy generators are, however, expected to be integrated seamlessly with the constant generation of traditional power systems in order for the renewables to retain a certain level of economic justification.

Because traditional power systems are designed to operate within defined operating parameters, integration of Solar PV power is likely to impact on the active and reactive power reliability of the system as a whole. The impact on the reliability of the power will in turn affect the general stability of the interconnected power grid.

The International Energy Agency (IEA) reports that in OECD countries, the gross electricity production from renewable products (excluding generation from pumped storage plants) reached 2,731.8 TWh in 2017 (IEA, 2018), representing about 5.1% gross electricity production. The IEA further projects that the global Solar PV annual additions are expected to reach 140 GW by 2023 (IEA, 2018).

As of 2020, the IEA makes a pre-COVID 19 prediction of 12% growth in the global energy demand between 2019 and 2030 (2020). This growth has been adjusted to 9% on assumption that the COVID 19 pandemic is controlled by the year 2021 and 4% where prolonged COVID 19 pandemic causes lasting damage to economic prospects (IEA, 2020).

The world gross electricity consumption for the years 1974 – 2018 are shown in Fig 1 below in which the electricity deficit with respect to the population growth can be seen from the year 1990 onwards.

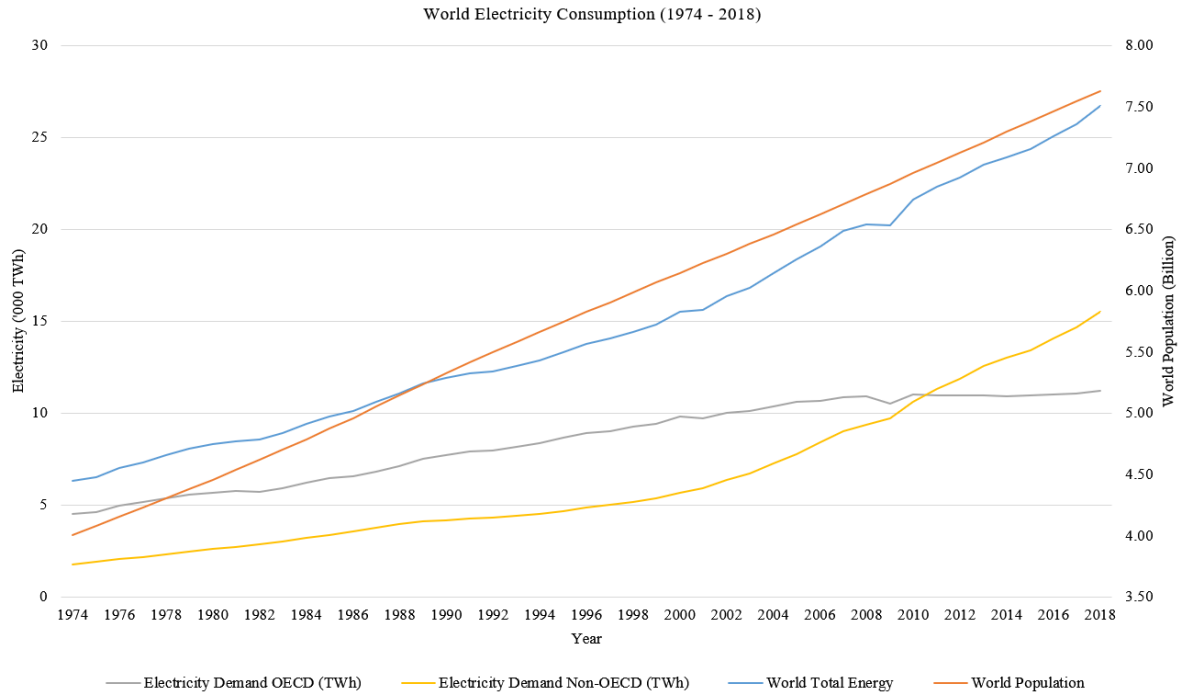

Fig 1: World Gross Electricity Consumption 1974 – 2018 (IEA, 2020)

For the Zambian case, the electricity deficit was recorded at over 800MW in 2020 (xinhuanet, 2020). The deficit was attributed to a looming scarcity of water in a power system that is heavily reliant on hydroelectric power generation. It is for this reason that the country is aggressively taking up the development of Solar PV resources as a measure to diversify the country's generation mix. Various studies are being undertaken by the government to ascertain the behaviour of Solar PV and other renewable resources on the existing national grid. In 2019-2020 the Ministry of Energy conducted a study in partnership with RES4Africa under a program to enhance the renewable energy transition in Zambia that was aimed at highlighting the challenges of renewable technologies on the grid and the mitigation measures thereof. A similar study was undertaken by the IDC as part of the scaling solar Zambia program in 2017.

Due to commercial arrangements and obligations, details contained in the IDC study have not been made available to the public. However, high-level pronouncements of 600 MW Solar PV have been floated by IDC, ZESCO and Government authorities. Further, the RES4Africa project is still underway and the results are yet to be published.

This study investigated the impacts of integrating Solar PV power on the stability of the Zambia national grid from an academic view point. The findings are expected to inform future researchers on what factors are likely to govern the integration of variable energy resources and what measures are required to enable the acceptance of such novice technologies.

1.2. Problem Statement

The use of renewable energy sources is one of the crucial components of sustainable development. Sustainable energy development gives a rationale for the desire to have resources that are economical, environmentally friendly and whose social effects are acceptable. This is the basis for the United Nations Sustainable Development Goal (SDG) No. 7: to ensure access to affordable, reliable, sustainable and modern energy for all (UNDP, 2019).

However, the potential for a large-scale shift from the use of fossil fuels to renewable energy for electricity generation remains a highly debated issue in many countries. Fossil fuels have a considerably high energy density thereby enhancing the cost-effectiveness, dependability and reliability of the fuels. Further, fossil fuels for many years now have influenced economic, military and geopolitical issues the world over and therefore a shift from fossil fuels is likely to overturn the dominances thereof.

From a technical perspective, utility-scale implementation of renewable energy poses significant challenges to traditional power systems due to the geographical dispersion of renewable energy sources, temporal fluctuations associated with weather conditions, and the inadequacies that are inherent in the existing power grids to accommodate variable power generation. Specifically, traditional power systems are still dependent on legacy power generation and control technologies which generally have a slow response time.

Solar energy at a specific location on the earth depends on the movement of the earth around the sun and indeed on its own axis and will thus exhibit annual and diurnal variations. Climate, weather conditions and shading are some of the other factors that affect the availability of solar irradiation at a given place in a given instance. The variability in solar irradiation results in a variable output of power from the generating photovoltaic system and consequently, an erratic response from the interconnected power system. The erratic response is mainly due to the fact that conventional power systems comprise power generation plants that are rotational and are fully dispatchable (controllable), properties that are missing in renewable energy generators.

The rotating elements in conventional power generators form an electromechanical coupling that provides rotational inertia, an important property of frequency dynamics and overall system stability. The generator's rotating mass provides kinetic energy to the grid (or absorbs it from the grid) in case of a frequency deviation and the energy exchanged is proportional to the rate of change of frequency (Kundur, 1994). In that way, the grid frequency is directly coupled to the rotational speed of the generator (active power balance).

The rotational inertia thus minimizes the marginal change in frequency in case of frequency deviations (Kundur, 1994) rendering frequency dynamics in traditional power systems much slower, and thus increases the available response time to react to fault events such as line losses, power plant outages or large-scale set-point changes of either generation or load units. In against this concept that power system protection is developed.

Now, the traditional assumption that grid inertia is sufficiently high with only small variations over time is invalidated for power systems with high penetration of solar photovoltaics (Andreas et. al, 2014). This has implications for frequency dynamics and power system stability and operation in that frequency dynamics now become faster in power systems with low rotational inertia, making frequency control and power system operation challenging (Andreas et. al, 2014). The integration of a high penetration level of solar photovoltaics will thus significantly influence the overall dynamics of the power system.

Notwithstanding the above setbacks of integrating Solar PV on to the grid, Solar PV technology is in no doubt a growing component of electricity grids around the world and this is due to its contributions to (1) energy system de-carbonization; (2) long-term energy security; (3) availability of climate funds that provide incentives and funding for renewable energy projects; and (4) expansion of energy access to new energy consumers in the developing world with the advantage that it can be set up within the shortest possible time.

The power system in Zambia is dominated by rotational hydroelectric power generation which makes the Zambian power system fairly stable. With a Solar PV penetration of just below 3% (ERB, 2019), Zambia can be considered to have a low penetration of renewable energy generators thereby enhancing the stability and control of the system. Nonetheless, despite having a fairly stable operating status, the Zambian power system is susceptible to adverse hydrological conditions that are a result of many factors such as the depleting water resources due to climatic variations and abstraction of water by increasingly competing users situated upstream of the power stations all of which results in reduced power production from the power plants.

The renewable energy subsector in Zambia is relatively in its infancy and not many conclusive studies have been undertaken to understand the behaviour of the system as utility-scale Solar PV injected into the grid. A number of studies have been undertaken on a project-by-project basis however the overall impact on the grid is yet to be fully understood.

The purpose of this study was to evaluate the impacts of solar photovoltaic systems on the Zambia National Grid. The study sought to investigate the steady-state and transient impacts of integrating Solar PV power to an existing grid and propose some of the available mitigation options.

1.3. Scope of the Study

1.3.1. Scope

This study was conducted to determine the impacts of integrating Solar PV power into an existing transmission grid. In the integration process, different penetration levels of the Solar PV power were integrated and analysed. The study involved a review of the literature surrounding Solar PV development, construction and operation. It also included the design and operation of generation and transmission systems with a focus on the Zambia National Grid as of 2019. A representative modelled was developed in PowerFactory DIgSILENT a power system simulation software. Thereafter, the steady-state impacts on the line loading, losses, voltage level, and voltage stability of the grid were investigated.

Both steady-state and transient stability was investigated during the simulations. Transient stability was investigated with the scenario of a loss of power generation for the plant at a given instance.

1.3.2. Delimitation

1.3.2.1. Focus of the Study

The focus of this study was on the stability of the grid with respect to safety performance and reliability of the interconnected grid. Details regarding the design of Solar PV power plants or the mechanisms that are a consequence of the variability in weather conditions were not covered. The impacts of these conditions are mostly attenuated by readily available smart inverters and transformer stations that form the coupling between the solar PV power plant and the interconnected grid. Furthermore, provided that the protection system is sound, limitations in solar plant design coupled with variability in weather conditions will most likely manifest as increased, reduced or total loss of power generation at the point of common coupling whereas the voltage output will be maintained constant by the solar inverters.

The significant loss of output power from the solar plant was thus of more relevancy to the study with respect to the operation of the interconnected grid since the marginal changes in voltage and power output will most likely be present even in conventional power systems.

The design considerations for a Solar PV power plant are however provided discussed in Appendix 1

1.3.2.2. State of Simulation Model

The simulation model used in this study assumed the operating state and condition of the grid as of 2019. Compensation and system improvements were not provided for, thereby avoiding capital investments into the grid for a given quantity of Solar PV injected.

1.3.3. Limitation

The limitations of this study included the unavailability of data for some network equipment and restrictions in access to network infrastructure.

1.4. Objectives

The purpose of this study was to investigate the steady-state impacts of integrating Solar PV power to an existing grid and propose some of the available mitigation options. The objectives of the study were as outlined below:

1. To determine the impact of low rotational inertia solar PV on the stability of the Zambia National Grid;

2. To determine the quantity of solar PV power that can be injected at specific points on the Zambian grid; and

3. To compare the impact on system performance of the maximum determined PV plant with that of the equivalent rotational plant

1.5. Research Questions

In order to meet the objectives, the following were some of the concerns raised:

1. How will the system respond to fluctuations in power due to changes in irradiance when specific amounts of Solar PV are injected into the grid?

2. What is the maximum PV plant that can be injected into the grid without giving rise to system disturbances?

3. What is the impact on the system performance of the maximum determined PV plant compared with that of an equivalent rotational plant?

4. What measures and procedures can be employed to ensure the system regains stability after disturbances from Solar PV installed at given locations?

1.6. Rationale for the Study

This study provides an investigation of the impacts of integrating variable power generation on the existing Zambian national grid. Despite the huge potential for Solar PV generation that has been established through resource assessments by the World Bank, IRENA and the Government of Zambia, the penetration of Solar PV power on to the grid still remains low. It is imperative then that the factors contributing to the low penetration of Solar PV in Zambia are investigated.

Stability issues as related to power system operations in the light of variable power generation in an interconnected grid need to be addressed as these may influence the technical designs and considerations for further grid developments and expansion. The technical considerations will in turn impact the financial and economic viability of the proposed technologies and consequently their acceptance by both the grid operator and the power consumers.

This study was commissioned as the first step in the acceptance of low inertia, variable energy generation on the grid as part of the technical considerations.

1.7. Presentation of the Report

This report was developed and organized five (05) chapters with seven (07) appendices. The report presents the concept of integrating variable Solar PV power generation on to an existing grid and the impacts thereof in comparison with the traditional rotational hydro power unit. The report further discusses some of the mitigation measures that can be exploited in a high Solar PV penetration scenario.

Chapter One of the report defines the study by presenting the problem, the objectives and the scope of works while Chapter Two outlines the principles of Solar PV generation, power system stability and system operations with a focus on how variable Solar PV generation can be seamlessly integrated with the existing traditional power grid. The chapter also provides insight into similar studies carried out in Zambia and around the world.

Chapter three (03) describes the methodology adopted in executing the study. Data acquisition and data analysis tools, methods and procedures regarding the study are presented. The choice of the injection points on the grid is given in Chapter three (03).

Chapter four (04) presents the summary of the results obtained by the study. The impacts of integrating Solar PV on the Zambian Grid are presented in terms of results of loading and voltage changes at the major substations and the loading and associated line losses on the major transmission lines. A comparison of the above parameters is made with a hydro equivalent model replacing the Solar PV plant.

Chapter five (05) draws conclusions of the study based on the findings in Chapter four (04) and makes recommendations for system improvements and policy alterations necessary for the intensification of Solar PV generation. The Chapter also makes recommendations for further studies.

The final section of the report is the appendices that provide supplementary information necessary to complete the study.

2. LITERATURE REVIEW

This chapter outlines the concepts and principles behind solar PV and the integration of Solar PV into an existing power grid. Detailed discussions are presented on Solar PV with respect to power variations, steady-state system stability and related studies that have attempted to study some impacts of renewable energy generation in some parts of the world.

2.1. Solar Resource

Solar energy is the ultimate source of energy form available on earth. The technologies that are currently available to convert solar energy directly to electricity are called photovoltaics due to the photovoltaic effect on which they are based.

2.1.1. Solar Photovoltaic Energy

The photovoltaic (PV) effect is the phenomenon in which an electrical potential is developed between two dissimilar materials when their common junction is illuminated with radiation of photons (Mukund, 2006). The French physicist Alexandre-Edmond Becquerel discovered the PV effect in 1839 and in 1954 Bell Laboratories produced the first silicon cell while the first commercial solar PV panel was developed by Charles Fritts in 1881. The solar cell developed by Fritts is what is called a low impact solar cell and was only able to achieve an energy conversion rate of 1 to 2%. The modern-day solar cell rides on the concept developed by Russel Ohl and has a conversion rate of 15 to 20%

Today, solar photovoltaic technology lends itself to many engineering applications including but not limited to agricultural irrigation, refrigeration in health care services, urban illumination, power supply as part of building services, power supply for terrestrial and extra-terrestrial vehicles.

A description of Solar PV technology as applied to utility-scale Solar PV systems is presented in Appendix 1 while some advantages and disadvantages of solar PV technologies are shown in Table 1 below:

Table 1: Advantages and Disadvantages of Solar PV Technologies (Wikipedia, 2019)

	Advantages	**Disadvantages**
1.	Renewable Energy Source: harnessed in all areas of the world and is available every day. Cannot run out	Cost: High capital investment. However, recent developments in technology are promising a reduction in costs
2.	Reduced Electricity Bills: Generation can be distributed resulting in reduced tariffs	Weather Dependent: Challenges with Availability and Controllability
3.	Diverse Applications: Can be scaled down and applied in diverse engineering applications	Resources cannot be stored: Solar Energy Storage is Expensive
4.	Low Maintenance Costs: Has no moving parts reducing maintenance requirements	Uses a Lot of Space: claims huge potions of land
5.	Technology Developments: Constantly developing increasing its effectiveness	Pollution and Energy in production: Process of producing solar PV cells is energy intensive and involves highly poisonous and environmentally toxic chemical substances.

2.1.2. Solar Resource in Zambia

In Zambia, IRENA approximated average solar insolation of 5.5 kWh/m^2/day at 3,000 sunshine hours annually (IRENA, 2013). Theoretically, from an area of 752,618 km^2, Zambia can potentially harness $1.51x10^{10}$ GWh of solar energy annually. However, the actual amount that can be realized is dependent on several factors such as availability of land, time of the year, the level of sunlight, prevailing weather conditions, type of solar panels used etc. Fig 2 below shows the solar irradiance level for Zambia as surveyed by the World Bank.

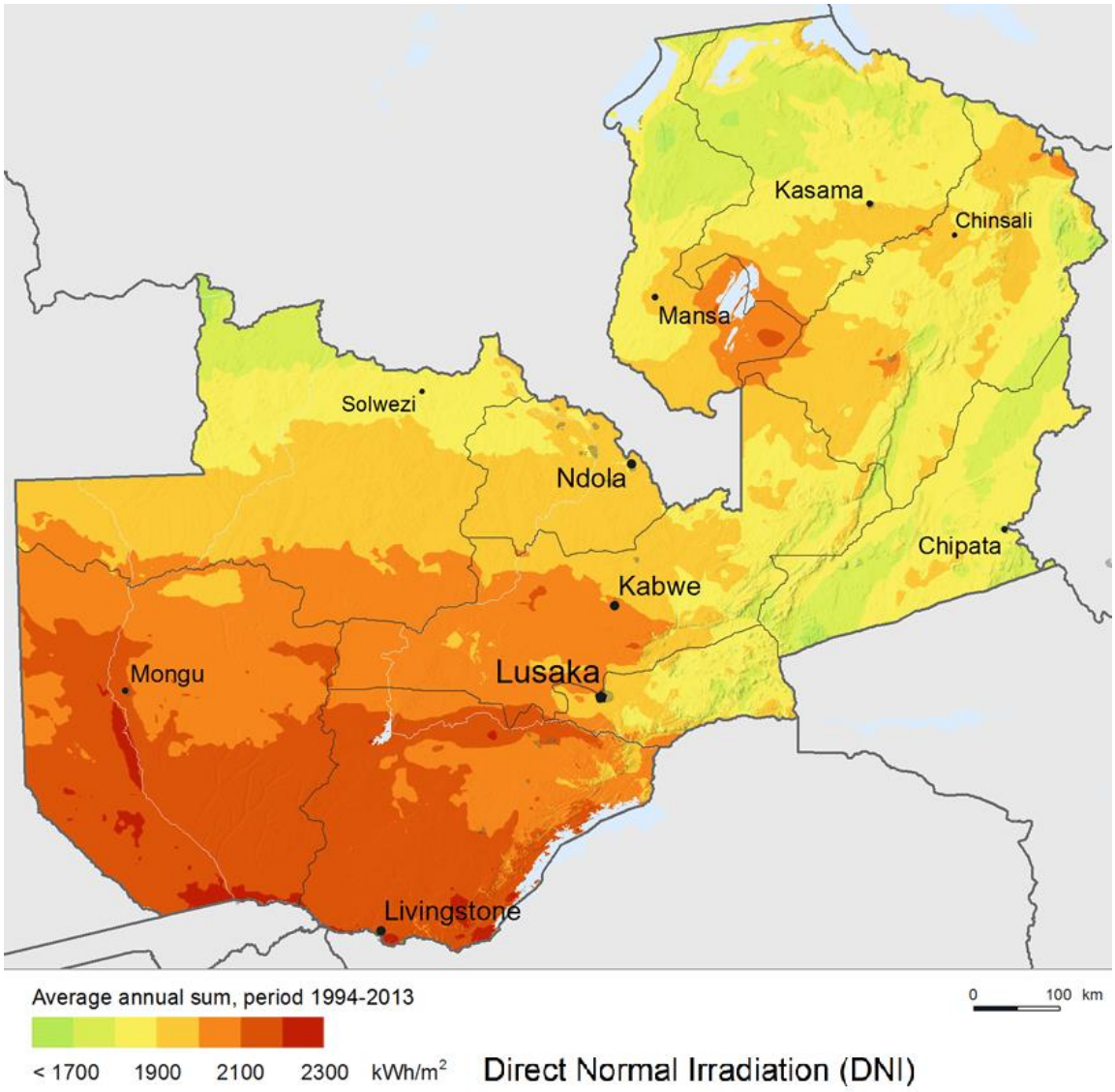

Fig 2: GTI – Global irradiation on tilted surface [kWh/m^2/day] (World Bank, 2014)

Despite the potential cited in Fig 2, Zambia was only able to harness about 117.56GWh of grid-connected Solar PV electricity in the year 2019 (ERB, 2020) in order to scale up the utilization of grid-connected Solar PV power generation, there is a need to fully understand the impacts of such Solar PV integration.

2.2. The Traditional Power System

Traditionally, power system operation is based on the assumption that electricity generation, in the form of thermal power plants, reliably supplied with fossil fuels or hydropower, involves rotating synchronous generators that are fully dispatchable. These rotating machines provide the most critical component in the operation of traditional power systems – Rotational Inertia. The total system rotational inertia is made up of the combined inertia of most of the spinning generation and load connected to the power system (Gonzalez-Longatt et al, 2013). This inertia forms the basis on which power system protection is anchored and therefore is important for frequency dynamics and stability.

The change in kinetic energy provided by the rotating masses in the generators is proportional to the rate of change of frequency (Δf) (Kundur, 1994). In this way, the grid frequency (f) is directly coupled to the rotational speed of a rotating generator and thus to the active power balance. Rotational inertia minimizes Δf in case of frequency deviations depending on the magnitude of the inertia constant H. This renders frequency dynamics much slower, and thus increase the available response time to react to fault events such as line losses, power plant outages or large-scale set-point changes of either generation or load units (Andreas et al, 2014).

The exchange between the power fed into the system and the power consumed by the load is what is referred to as the active power balance and at every instant, the net power should be zero. However, during normal operations, small variations in the power balance occur spontaneously. When large deviations occur, the net effect is damaging vibrations in synchronous machines leading to the protective mechanism of load shedding. This load shedding mechanism can influence the whole power system, in the worst-case ending in fault cascades and consequently, black-outs (Andreas et al, 2014).

Low levels of rotational inertia in a power system, caused in particular by high penetration of renewable energy sources such as wind turbines and Solar PV units that normally do not provide any rotational inertia, have implications on frequency dynamics (Rycroft, 2017). This results in a situation where traditional frequency control schemes tend to be too slow with respect to the disturbance dynamics for preventing large frequency deviations and the resulting consequences.

By integrating more and more renewables in the generation mix, the system inertia drops, and the power system can even become completely inertia-less (Tielens, 2019). The loss of rotational inertia and its increasing time-variance leads to new frequency instability phenomena in power systems at the risk of system stability.

2.3. Power System Stability

Power system stability may be defined as the ability of a power system to remain in a state of operating equilibrium under normal operating conditions and to regain an acceptable state of equilibrium after being subjected to a disturbance (Kundur, 1994). Disturbances could be in the form of faults, load changes, generator outages, line outages, voltage collapse or some combination of these.

In the evaluation of stability, the concern is the behaviour of the power system when subjected to a transient disturbance which may be small or large. Small disturbances are in the form of load changes and take place continually. Large-disturbance stability normally refers to a specified disturbance scenario which results in structural changes as a way to isolate the faulted elements.

Traditional power systems are designed to self-adjust with respect to the changing conditions. The systems are expected to be able to operate satisfactorily under these new conditions and successfully supply the maximum amount of load as previously. The systems are also expected to be capable of surviving numerous disturbances of a severe nature, such as short-circuits on transmission lines, loss of a large generator or load, or loss of a tie between two subsystems. Power system stability can be subdivided as shown in Fig 3.

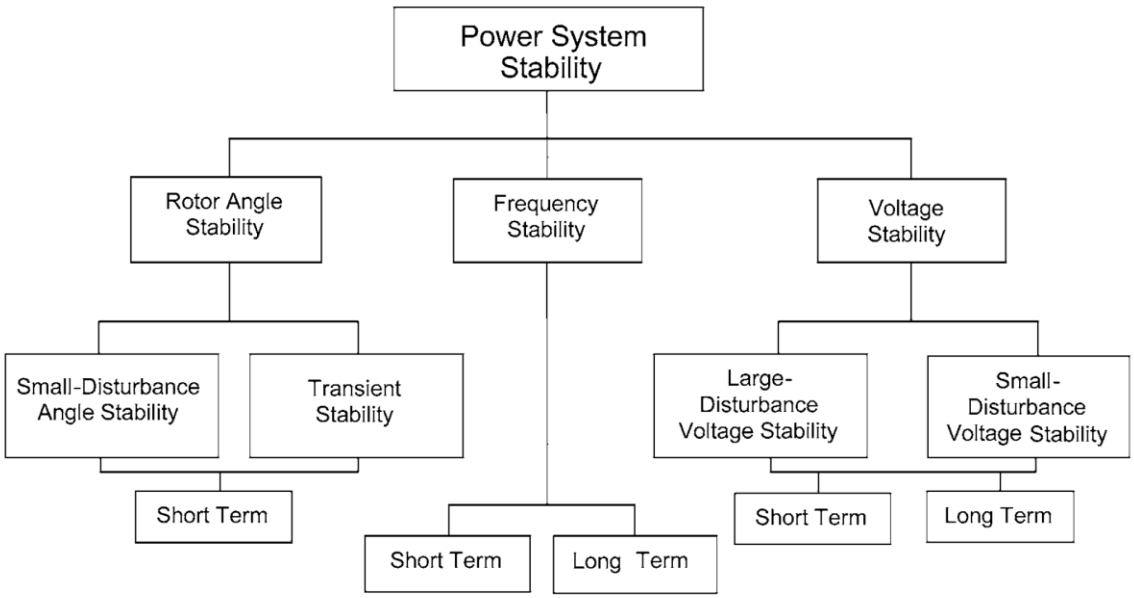

Fig 3: Subdivisions of power system stability (Kundur et al, 2004)

The above classification of power system stability was adapted by the IEEE/CIGRE Joint Task Force on Stability Terms and Definitions (Kundur et al, 2004) based on the considerations by Kundur (1994) and these are:

(i) The physical nature of the resulting mode of instability as indicated by the main system variable in which instability can be observed;
(ii) The size of the disturbance considered, which influences the method of calculation and prediction of stability; and
(iii) The devices, processes, and time span must be taken into consideration in order to assess stability.

Clearly, the classification of power system stability is a matter of convenience since the considerations made above may be revised triggering a revision of the said classifications. Furthermore, it is possible that at a given equilibrium set, a power system may be stable for a given physical disturbance, and unstable for another or there can be a whole combination of stability phenomena.

Nonetheless, the classification of stability given by Kundur et al, (2004) is appropriate for the correct identification of possible instabilities; their causes and the effects thereof. Appropriate techniques and measures can then be derived to address the respective instability phenomenon.

Power systems are continually experiencing fluctuations of small magnitudes. However, for assessing stability when subjected to a specified disturbance, it is usually valid to assume that the system is initially in a true steady-state operating condition (Kundur, 2004). It is impractical and uneconomical to design power systems to be stable for every possible disturbance. The design contingencies are selected on the basis that they have a reasonably high probability of occurrence (Kundur, 2004) or the extent and cost of damage that may result for a given occurrence.

2.3.1. Rotor Angle Stability

Rotor angle stability is the ability of the interconnected synchronous machines of a power system to remain in synchronism. The stability problem here involves the study of the electromechanical oscillations inherent in power systems. A fundamental factor in this problem is the manner in which the power outputs of synchronous machines vary as their rotors oscillate. Rotor angle stability is broken down further into:

1. Small signal stability
   Small-signal or small-disturbance stability is the ability of the power system to maintain synchronism under small disturbances. Such disturbances occur continually on the system because of small variations in loads and generation. The instability that may result in this case can be of two forms: (i) steady increase in rotor angle due to lack of sufficient synchronizing torque, or (ii) rotor oscillations of increasing amplitude due to lack of sufficient damping torque (Kundur, 1994).

2. Transient stability
   Transient stability is the ability of the power system to maintain synchronism when subjected to a severe transient disturbance. The resulting system response involves large excursions of generator rotor angles and is influenced by the nonlinear power-angle relationship. Stability depends on both the initial operating state of the system and the severity of the disturbance. Usually, the system is altered so that the post-disturbance steady-state operation differs from that prior to the disturbance.

   Although dynamic stability is used in place of transient stability only transient stability has to be used (Kumar, 2014), a point also raised by the IEEE Task Force Committee Report by Kundur et al (2004).

The time-domain of interest in the case of large-disturbance as well as small-disturbance angle stability is anywhere between 0.1 – 10s and it is due to this reason that small and large-disturbance angle stability is considered to be short term phenomenon (Kumar, 2014).

The detailed assessment for Rotor Angle Stability for a simplified power system is provided in Appendix 2.

2.3.2. Frequency Stability

Frequency stability refers to the ability of a power system to maintain steady frequency following a severe system upset resulting in a significant imbalance between generation and load (Kundur et al, 2004). It depends on the ability to maintain or restore equilibrium between system generation and load, with minimum unintentional loss of load. The instability that may result occurs in the form of sustained frequency swings leading to tripping of generating units and/or loads (Kumar, 2014).

Severe system upsets generally result in large excursions of frequency, power flows, voltage, and other system variables, thereby invoking the actions of processes, controls, and protections that are not modelled in conventional transient stability (2.3.1 (2)) or voltage stability studies (2.3.3) (Kundur, 1994). These processes may be very slow or only triggered for extreme system conditions, such as Volts/Hertz initiating a trip out of the generators.

Generally, frequency stability problems are associated with inadequacies in equipment responses, poor coordination of control and protection equipment, or insufficient generation reserve (Kundur, 1994). During frequency excursions, voltage magnitudes may change significantly, especially for islanding conditions with under-frequency load shedding that unloads the system. Voltage magnitude changes, which may be higher in percentage than frequency changes, affect the load-generation imbalance.

The detailed assessment for Frequency Stability for a simplified power system is provided in Appendix 2.

2.3.3. Voltage Stability and Voltage Collapse

Voltage stability is the ability of a power system to maintain steady acceptable voltages at all buses in the system under normal operating conditions and after being subjected to a disturbance (Kundur, 1994). A system enters a state of voltage instability when a disturbance, increase in load demand, or change in system condition causes a progressive and uncontrollable drop in voltage. The main factor causing instability is the inability of the power system to meet the demand for reactive power. The heart of the problem is usually the voltage drop that occurs when active power and reactive power flow through inductive reactances associated with the transmission network (IEEE, 1982).

A criterion for voltage stability is that, at a given operating condition for every bus in the system, the bus voltage magnitude increases as the reactive power injection at the same bus is increased (Kundur et al, 2004). A system is voltage unstable if, for at least one bus in the system, the bus voltage magnitude (V) decreases as the reactive power injection (Q) at the same bus is increased. In other words, a system is voltage stable if V-Q sensitivity is positive for every bus and voltage unstable if V-Q sensitivity is negative for at least one bus. Voltage instability is essentially a local phenomenon; however, its consequences may have a widespread impact (Kundur et al, 2004).

Voltage collapse, on the other hand, is more complex than simple voltage instability and is usually the result of a sequence of events accompanying voltage instability leading to a low-voltage profile in a significant part of the power system. In practical power systems, many factors contribute to the process of system collapse because of voltage instability: strength of transmission system; power-transfer levels; load characteristics; generator reactive power capability limits; and characteristics of reactive power compensating devices. In some cases, the problem is compounded by the uncoordinated action of various controls and protective systems (Kundur et al, 2004). For purposes of analysis, it is useful to conveniently classify voltage stability into large and small-disturbance voltage stability:

a. **Large Disturbance Voltage Stability** is concerned with a system's ability to control voltages following large disturbances such as system faults, loss of generation, or circuit contingencies. This ability is determined by the system load characteristics and the interactions of both continuous and discrete controls and protections. A criterion for large-disturbance voltage stability is that, following a given disturbance and following system-control actions, voltages at all buses reach acceptable steady-state levels (Kundur, 1994).

b. **Small Disturbance Voltage Stability** is concerned with a system's ability to control voltages following small perturbations such as incremental changes in system load. This form of stability is determined by the characteristics of the load, continuous controls, and discrete controls at a given instant of time. This concept is useful in determining, at any instant, how the system voltage will respond to small system changes.

The detailed assessment for Voltage Stability for a simplified power system is provided in Appendix 2.

2.3.4. Mutually Exclusivity of Stability Events

Although stability is classified into rotor angle, voltage and frequency stability they need not be independent isolated events (Kumar, 2014). A voltage collapse at a bus can result in large excursions in rotor angle and frequency. Similarly, large frequency deviations can lead to large changes in voltage magnitude.

The analysis of stability in the case of Solar PV integration therefore needs to take a broader perspective encompassing all stability phenomena and then ascertaining the most dominant among them.

This study focused more on voltage stability based on the preliminary findings that indicated that frequency and rotor angle excursions were adequately attenuated by the system dynamic control mechanisms embedded at the major power stations. These control mechanisms are called dynamic controllers. A dynamic controller is basically a model that predicts and initiates

an optimised operating condition of the power system by varying the output parameters of the respective generator and/or ancillary services.

2.4. Variability and Uncertainty of Solar PV Generation

Unlike the traditional generation sources, renewable energy resources such as wind power and photovoltaic (PV) solar power are considered variable generation (VG) in that they have a maximum generation limit that changes with time (variability) and this limit is not known with perfect accuracy (uncertainty) (Ela et al, 2013). Variability of variable generators occurs at multiple timescales, from seconds to minutes to hours, and requires movement of other resources to ensure the balance of generation and load (Mills et al, 2009). This movement of resources is why Solar PV is regarded as a Disruptive Technology since it gives rise to operational challenges that have financial and economic implications on the grid operator. As a consequence, grid operators are inclined to restrain the penetration levels of Solar PV and other renewables on to the grid.

In the recent past, various solar PV plants have been developed and successfully integrated into existing grids. The lessons learned from such developments have been captured by Mills et al (2009) and these include:

2.4.1 Clouds cause significant ramps in solar insolation and Solar PV output

The output of PV plants is necessarily variable simply because the sun changes position throughout the day and throughout the seasons influencing with it the intensity of the solar insolation falling on a given surface. The rising and setting of the sun regularly may lead to 10 – 13% changes in PV output over a period of 15 minutes for single-axis tracking PV plants (Mills et al, 2009).

Clouds, however, are largely responsible for rapid changes in the output of PV plants and are of more concern to grid operators and planners. Changes in solar insolation at a point due to a passing cloud can exceed 60% of the peak insolation in a matter of seconds (Ela et al, 2011). The time it takes for a passing cloud to shade an entire PV system, in contrast, depends on the PV system size, cloud speed and height. For PV systems with a rated capacity of 100 MW or more, the time it takes to shade the system will be in the order of minutes rather than seconds giving ample time to system operators to institute control measures.

2.4.2 Clouds are Diverse

Unlike changes in the position of the sun which affects the output of all PV plants in a nearly uniform, highly correlated way, changes in Solar PV output due to clouds are not driven by a similar uniform process. Clouds move across plants affecting one part of a plant before another or leaving some parts of plants unobstructed as the cloud passes.

Clouds, therefore, cause diverse changes in Solar PV output across plants and between separate plants.

Just as electrical connections are used to aggregate diverse loads and conventional plants, electrical connections aggregate the diverse output of separate Solar PV panels and blocks of Solar PV panels within a plant or between separate Solar PV plants. The degree of diversity between points or plants can be characterized by the correlation of simultaneous changes in the output. This was illustrated by Mills et al (2009) that aggregating the output of several different solar insolation meters reduces the variability of multiple sites relative to a single site. The change in irradiance from one minute to the next is dramatically reduced for multiple sites due to diversity.

2.4.3 Smoothing occurs within Solar PV plants

Diversity, even within a small PV plant, can smooth rapid ramps relative to the expected ramps from just examining solar insolation alone. Comparison between variability observed in insolation meters and the output of larger multi-MW plants exhibits more pronounced reductions in variability (Mills et al, 2009).

2.4.4 Diversity occurs between separate Solar PV plants

While diversity over longer time-scales may be limited within multi-MW PV plants, analysis of a network of several time-synchronized solar insolation measurements of six Solar PV plants in the city of Las Vegas, four PV plants in Arizona, and two PV plants in Colorado Mills et al concluded that smoothing can occur on even longer time-scales between separate plants (2009).

2.4.5 Multiple methods are available for PV forecasting

For economic and operational reasons, forecasts of Solar PV output or any other generator in the system are required for days ahead down to hours and tens-of-minutes ahead. Such Forecasts normally include information about the expected output and the degree of uncertainty in the expected output to indicate particularly volatile periods.

Forecasts are an important method for managing both the variability and the uncertainty of Solar PV and should be incorporated into system planning and operations. Forecast tools include sky imagers that can indicate approaching clouds and predict the impact the clouds will have on Solar PV output. Others are successive satellite images that can yield useful information about the direction and speed of approaching clouds. For longer time scales, numerical weather models can be used to predict solar insolation out to multiple days.

2.4.6 Grid events can impact the Variability of PV

Step changes in PV output can occur from simultaneous inverter trips within the plant. Although inverter trip events are far less common than cloud-induced ramps, the severity and magnitude of trips exceed the observed severity and magnitude of ramps due to clouds. Currently, these trips are normal operation as inverters are designed to shut off when abnormal events occur on the grid and cause voltage or frequency deviations outside of a tolerance envelope. Tripping is presently required by IEEE Standard 1547 for PV and other distributed generation that is embedded in distribution systems. This requirement stems from safety concerns surrounding inadvertent islanding.

In addition to grid events, PV plants are subject to outages due to equipment malfunction or outages inside the plant similar to conventional generators. PV plant outages should be planned for in the normal way that grid operators prepare for grid contingencies.

2.5. Managing Variability and Uncertainty

Variability and uncertainty are inherent characteristics of power systems (Mills et al, 2009). Many of the properties of the power system, including its generation output, load levels, and transmission equipment availability are both variable and unpredictable (Ela et al, 2011).

There are many different ways to manage variability and uncertainty. Enforceable reliability requirements, such as the N – 1 contingency administered through SI No. 79 of 2013 or SAPP requirements, as the case may be, generally focus on minimum performance standards for reliable operation of power systems in a contingency situation. Such reliability requirements do not, however, dictate how to meet many of the other performance requirements. Therefore, system operators and planners use mechanisms such as forecasting, scheduling, economic dispatch, and reserves to ensure performance that satisfies reliability standards in a least-cost manner.

2.5.1. Predictability and Modelling of Fluctuations

Managing variability and uncertainty is easier and less expensive when transmission lines are used to aggregate several diverse sources of variability and uncertainty (Ela and O'Malley, 2012) (Mills et al, 2009). The daily load shape that system operators use to plan for the real-time operation of the grid is dramatically smoother than the daily profile of an individual residential customer, due to the diversity of load usage among customers. Rather than being concerned with the timing and duration of each individual customer appliance, system operators know that the aggregate of all customers will follow a general trend that can be predicted and managed with relative ease (Ela and O'Malley, 2012). Similarly, experience with managing wind energy in several countries with high penetrations of wind indicates that aggregation of several diverse wind farms leads to much smoother wind profiles than would be expected from scaling the output of a single wind turbine (Holttinen et al, 2009).

Fares also observes that as opposed to the thought that high penetration of Solar PV implies destabilising the grid, it turns out that renewable energy actually becomes more predictable as the number of renewable generators connected to the grid increases (2015). The argument by Fares is supported by the effect of geographic diversity as collaborated with the Law of Large Numbers.

The Law of Large Numbers is a probability theorem which states that the aggregate result of a large number of uncertain processes becomes more predictable as the total number of processes increases. Considering the law of large numbers, a combined output of aggregated solar plants connected to the grid should be far less volatile than the output of an individual generator, consistent with the findings by Mills et al (2009). In the United States, data collected through the Atmospheric Radiation Measurement (ARM) Program revealed how aggregating solar resources across a utility territory could significantly reduce second-to-second variations in power output, even when only 20 locations were combined (Perez et al., 2009). Fig 4 below is the depiction of the ARM findings.

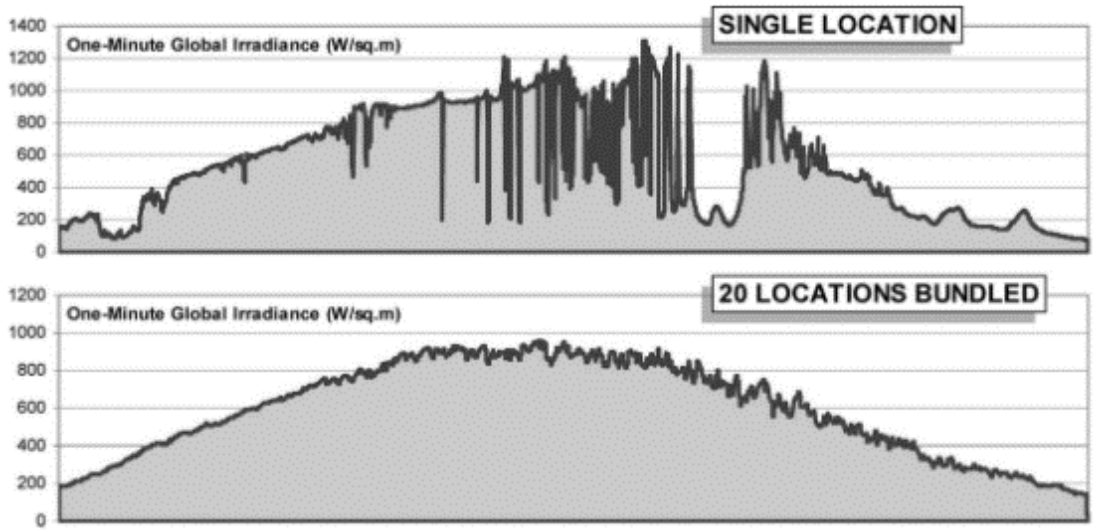

Fig 4: Atmospheric Radiation Measurement (Perez et al., 2009)

The Law of Large Numbers can be coupled with modelling techniques in order to attenuate the effects of large-scale Solar PV deployment; this is because solar depends on natural systems that have been mastered over a long period of time and can be modelled and forecasted with reasonable accuracy.

The general idea of modelling and forecasting an aggregate number of solar photovoltaic systems leads to the superior powers of prediction. Andreas et al (2014) demonstrated two concepts of modelling system dynamics under low rotational Inertia and concluded that with an increased number of solar generators:

1. The rotational inertia becomes heterogeneous

Instead of a global inertia constant (*H)*, there are different (H_i) for the individual areas (*i)* as a function of how much converter-connected units versus conventional units are online.

2. Rotational inertia constants become time-variant [$H_i(t)$]

   This is due to the variability of the power dispatch. Frequency dynamics become thus differently fast in the respective grid areas.

3. Grid frequency instability phenomena are amplified

   Reduced rotational inertia leads to faster frequency dynamics and in turn, causes larger frequency deviations and transient power exchanges over tie-lines in the event of a power fault. This may cause false errors and unexpected tripping of the tie-lines in question by automatic protection devices, in turn further aggravating an already critical situation.

4. Faster primary control emulates a time-variant damping effect [k(t)]

   This is critical for power system stability immediately after a fault event.

Apart from modelling, forecasting and predicting complex renewable energy systems, smart grid mitigation measures can be employed in managing the impacts of variable power generation from renewable energy sources. Smart grid mitigation measures are fully controllable and if expertly configured can contribute to the grid base load.

2.5.2. Smart Grid Mitigation Measures

The increase in the penetration of renewable energy generation increases the risk of undesired operation of protection devices and contributes to a shortage of dynamic immediate response to frequency changes. The following mitigation measures can be used against renewable energy technologies, the so-called low inertial generation technologies:

1. Synthetic inertia from renewable energy devices

   The term synthetic inertia is described by ENTSO-E as the facility provided by a power park module or HVDC system to replace the effect of the inertia of a synchronous power generating module to a prescribed level of performance (2013). Synthetic inertia is achieved by reprogramming power inverters attached to renewable energy generators so that they emulate the behaviour of synchronised spinning masses.

   Supply of synthetic inertia requires energy stored in systems behind power electronic interfaces, such as batteries, rotating masses in wind turbines or even other power systems connected through HVDC connections. To supply synthetic inertia,

supplementary control of these sources is required, as there is usually no direct relation between power output of these sources and the frequency of the system.

Many Solar PV systems are overdesigned today, i.e., the DC power available exceeds the AC power output mostly by a factor in the range of 1.2 – 1.5. They also have a very rapid response time. This could be used to strengthen the network, depending on the circumstances, however, the output is limited by the rating of the inverter.

2. Distributed Energy Storage Systems (DESS)

A Distributed Energy Storage System (DESS) is a packaged solution that stores energy for use at a later time. Energy storage is the main component of any holistic consideration of grids, particularly when incorporating power derived from variable, distributed and renewable energy resources. Coupled with synthetic inertia technologies, DESS has the ability to both absorb and supply energy to the grid mimicking the actions of a synchronous machine.

Storage systems are seen as an important component of the smart grid and are usually installed with the aim of long-term balancing of supply and demand or load shifting in mind. Energy storage is a very expensive approach and is still under research and development. But with the steep shift towards smart grids, the economics around storage needs to be addressed.

Typical distributed energy storage systems may be in the form shown in Table 2.

Table 2: Forms of Energy Storage Systems

No.	**Form**	**Storage Mechanism**
1.	Air	Compressed Air or Liquified Air
2.	Grid Oriented Batteries	Molten-Salt Batteries or Flow Batteries
3.	Electric Vehicles	Vehicle-to-Grid (V2G)
4.	Flywheels	Flywheel storage power system and Flywheel energy storage
5.	Hydrogen	Underground hydrogen storage, Power to Gas or Power-to-Ammonia concept
6.	Hydroelectricity	Water Saving and Pumped Storage
7.	Thermal	Thermal Energy Storage (Hot Water etc)
8.	Superconducting Magnetic Energy	Superconducting Magnetic Energy Storage
9.	Gravitational Potential Energy Storage with Solid Masses	Energy Storage and Solid Mass Gravitational Energy

3. Battery Energy Storage Systems (BESS)

   BESS can absorb energy during periods of high frequency and dispatch energy during periods of low frequency. A fairly complex control algorithm is required to ensure that the BESS is capable of performing either function when required. By using the Small Signal Theory [2.3.1(1)], many papers demonstrated that storage can improve the dynamic response of power systems (Delille, 2013).

   While battery energy storage technologies can cover a wide spectrum of applications, ranging from short-time power quality support to hours-long energy management, the supply of primary control reserve has been identified as the application with the highest value for the owner of the BESS (Oudalov et al, 2007). The focus is on short-duration storage technologies which can be used to assist in primary frequency control. Storage technologies that suit such applications, typically grid-scale batteries, can respond at a much faster rate than the mechanical actions of traditional governor controls and blade pitch or wind turbine speed control mechanisms. However, economic concerns suggest that such storage will be very limited in the amount of power it can provide (De Marco, 2012).

4. Dynamic Frequency Control Support (DFCS)

   The purpose of DFCS is to take advantage of the short response time of DESS to improve the dynamic performances of isolated power systems (Delille et al, 2010). DFCS involves the injection or absorbing of power from the system in the timeframe of hundreds of milliseconds up to seconds after a disturbance so as to support the other generation assets during the activation of their primary reserve (Delille et al, 2010).

   The power is supplied by the DESS for a short period of time in the same manner that power is drawn from the kinetic energy of the rotating masses in a rotational machine. Likewise, during the frequency fall, the storage behaves as virtual inertia from the system point of view. Consequently, it mitigates the rate of change of frequency (ROCOF, Δf_{max}) which makes it a possible solution to the inertia concern in renewable energy generators (Delille et al, 2010).

2.6. Support for Variable Solar PV Power

Solar power is proving to be the energy resource of the future sparking interest from regional bodies, development organisations, financing institutions and climatic change activists. Financing institutions such as the IFC and EPFI and development community such as the UN are advocating for an aggressive transition to renewable energy solutions. Despite these efforts, the shift from conventional fuels to renewables is a subject of much debate in which organisations, countries and the general public have drawn lines between providing various arguments in support for solar power.

For instance, whereas German solar activists have focused heavily on linking decentralized Solar PV to replacing centralized nuclear power, US solar advocates have focused more on climate change and phasing out coal. But even then, focusing on climate change most certainly was an important rallying point for supporters of renewables in the US, but, due to the political success of climate change deniers, this argument has alienated key parts of the American public (Franke, 2016).

On the more technical front, Fares (2015) argues that while the fact that wind and solar don't produce energy around the clock is certainly a major disadvantage, the problems associated with the intermittent nature of many renewables are often exaggerated, and rarely discussed from a practical perspective, a position supported by Mills et al (2009).

Fares (2015) asserts that keeping the lights on is a utility's core responsibility and any innovations that threaten that reliability metric simply won't be allowed onto the grid. He further states that if the grid can't be made flexible, new technologies won't make it into the picture" (Fares, 2015). For this reason, it is incumbent on the respective Governments to spearhead the development of the so-termed disruptive power generation innovations. In Zambia, this has been demonstrated through policy directives and strategies such as the RE-FiT Strategy and the Renewable Energy Strategy.

2.7. Solar PV Power Developments

2.7.1. Global Solar Power Generation

Despite the perceived inadequacies of Solar PV technologies, solar power installations have been on the rise world over. Table 3 below shows historical developments of solar in terms of the installed capacity.

Table 3: Timeline of the largest PV power stations in the world (Wikipedia, 2019)

Year	Name of PV power station	Country	Capacity (MW)
1982	Lugo	United States	1
1985	Carrisa Plain	United States	5.6
2005	Bavaria Solarpark (Mühlhausen)	Germany	6.3
2006	Erlasee Solar Park	Germany	11.4
2008	Olmedilla Photovoltaic Park	Spain	60
2010	Sarnia Photovoltaic Power Plant	Canada	97
2011	Huanghe Hydropower Golmud Solar Park	China	200
2012	Agua Caliente Solar Project	United States	290
2014	Topaz Solar Farm	United States	550
2015	Longyangxia Dam Solar Park	China	850
2016	Tengger Desert Solar Park	China	1547

2.7.2. Solar PV Power Developments in Zambia

Solar PV generation is still at the development stage in Zambia. However, the commitment of the Zambian Government to scaling up of Solar PV power generation has been affirmed through the various policy directives and strategies that have been promogulated in the recent past. The national energy policy introduced in 2019 emphasised the scaling up of utility-scale solar power and other renewable developments. The National Energy Policy 2019 has since ushered in the revision of the Electricity Act and Energy Regulation Act to respond to emerging issues in the energy sector that were no conceived during the design of the existing national grid.

Some programs aimed at facilitating the development of Solar and other renewable energy technologies are:

1. RE-FiT Strategy

   Under this program, the Government through the energy regulator has developed an incentive mechanism that enhances the financial viability of renewable energy projects by making a part payment on the tariff payable by the national utility. This funding is called Viability Gap Funding considering that in the current regulated electricity market, renewable energy developments may not be viable.

2. Scaling Solar Zambia

   Another instrument instituted by the Zambian government is the Scaling Solar Zambia program. The program is being undertaken by the Industrial Development Corporation and since commissioned a combined 86 MW of Solar PV power in Lusaka. Prior to the commissioning of the Solar PV plants, the program undertook a Grid Integration Study that confirmed 600 MW could be integrated into the Zambian Grid. However, the details of the report were not made available to the public.

   The Scaling Solar Zambia program was aimed at realizing about 600 MW of utility-scale renewable power. Under the Scaling Solar Zambia program, viability incentives included partial risk guarantees and free-issued land. Other incentives granted include a waiver of some provisions contained in Statutory Instrument No. 79 of 2013. the national grid code to accommodate renewable energy technologies on to a grid designed for rotational hydroelectric power generators.

3. RE4Africa: Integration of Variable Renewable Energy Sources in The National Electric System of Zambia

   The objective of the RE4Africa study was to address the integration of variable renewable energy sources into the Zambian Grid. Considering the inadequacies of Solar

PV as discussed above, the RE4Africa study concluded that the optimal renewable energy integration for the Zambia grid would result from about 1,176 MW of Solar PV and 1,200 MW of wind capacities in the year 2025 and from 1,376 MW PV and 1,400 MW wind capacities in 2030 considering that all rotational power generation plants are commissioned by the respective years (RES4Africa, 2020).

3. METHODOLOGY

This chapter provides an overview of the methods and methodologies that were employed in the execution of this study.

3.1. Study Design

This study was undertaken through theoretical analyses of power systems coupled with applied approaches in developing representative models of the Zambian national grid for simulation. Simulation activities included steady-state analysis and dynamic stability cases.

3.2. Data collection

Key to the development of this study was the acquisition of data. Various avenues were employed in acquiring data and these include:

3.2.1. Site visits

Visits were undertaken to the IDC solar Power plants during construction and commissioning. Other visits were conducted on projects sites for the GET FiT Solar Power Projects, Globeleq Leopards Hill Solar PV, Proposed Nalolo Solar PV Power Plant, Proposed Muwezwa Solar PV project Site in Mumbwa. Site visits were also undertaken on various ZESCO installations, and projects sites, that makeup part of the Zambia national grid e.g., Kasama 330 kV Substation, Kabwe Stepdown, Kafue Gorge, Kariba etc.

3.2.2. Participation in Solar PV development Work Groups

1. RES4Africa – Integration of Variable Renewable Energy Sources in The National Electric System of Zambia; and

2. GET FiT Evaluation Team – Included Interim Rapid Grid Assessment;

3.2.3. Review of Secondary Sources

Because renewable energy gives a promise to resolve the imminent global energy crisis, numerous works have been conducted on how the novice technologies can be seamlessly integrated into existing energy systems and how the best renewable energy can fit in the supply and demand matrix.

From the above, knowledge and data was acquired on the current trends in renewable energy deployment and the technical considerations thereof.

3.3. Modelling of the Zambia National Grid

A review of the Zambian grid was undertaken and then an old case file of the Zambian national grid was updated to include the new power plants and transmission lines that had been commissioned up-to 2017.

The tool used in modelling the Zambian National Grid is PowerFactory DIgSILENT, a commercially available simulation software packaged.

3.3.1. PowerFactory DIgSILENT

PowerFactory DIgSILENT is a computer-aided engineering tool for the analysis of transmission, distribution, and industrial electrical power systems. The term DIgSILENT is an acronym for DIgital SImuLation of Electrical NeTworks and DIgSILENT Version 7 was the world's first power system analysis software with an integrated graphical single-line interface. The software does not require advanced software programming skills due to its enhanced graphical user interface (GUI).

DIgSILENT has been designed as an advanced integrated and interactive software package dedicated to the electrical power system and control analysis in order to achieve the main objectives of planning and operation optimisation. It is easy to use and fully compatible with Windows platforms and can be integrated with other packages to meet the requirements of all power system analysis applications.

There are many other power system simulation software such as, PSSE, MATLAB, ETAP, PSCAD, PSAT, PowerWorld Simulator, ASPEN and others. Apart from being a robust software best fitted for this study, DIgSILENT was chosen because the ZESCO national grid is built and operated based on PowerFactory DIgSILENT. CEC which until recently operated on ETAP are considering the transition to DIgSILENT. Equally, SAPP has adopted DIgSILENT as a software of choice and the EAPP is slowly transitioning from PSSE to DIgSILENT in awe of the planned merger of the SAPP and the EAPP.

Karlsson (2013) makes a comparison between PSSE and DIgSILENT and concludes that it is possible to have identical load flows and dynamic simulations in PSSE and DIgSILENT if the correct set-up is made. Karlsson notes that generators for the two software use different modelling and can be tested in a step response. By tuning the generator parameters according to the step responses, a positive impact on the dynamic simulation results may be achieved (2013).

Provided the system is properly and accordingly modelled, system performance is expected to be the same irrespective of the software package used.

3.3.2. Modelling of the Zambian Power System

The Zambian power system is maintained and operated under a vertically integrated utility ZESCO Limited, which is responsible for the generation, transmission, distribution and supply of electricity in Zambia.

1. Generation Resources

   In the study, the total installed generation capacity was set at around 2800 MW dominated by 'high inertia' hydroelectric power plants and a thermal coal-fired power plant. Table 4 shows a list of power plants considered in the study model and their respective status.

Table 4: List of generation plants in the Model

No.	Station	Type	Units	Installed Capacity
1.	Kariba North	Hydro	6 x 120 MW	1080MW
2.	Kafue Gorge	Hydro	6 x 120 MW	990MW
3.	Maamba Coal	Coal Fired	2 x 108 MW	300MW
4.	Itezhi Tezhi	Hydro	2 x 54 MW	120MW
5.	Victoria Falls	Hydro	2 x 0.9 MW 2 x 3 MW 6 x 9.9 MW 4 x 5.73 MW	108MW
6.	Lunsemfwa	Hydro	3 x 5.1 MW	18MW
7.	Mulungushi	Hydro	1 x 2.125 MW 2 x 5.3125 MW 1 x 6.8 MW	24MW
8.	Lusiwasi	Hydro	4 x 2.8 MW	12MW
9.	Chishimba Falls	Hydro	4 x 1.044 MW	5MW
10.	Musonda Falls	Hydro	1 x 10 MW	10 MW
	Total		**1914 MW**	**2667 MW**

2. Transmission Infrastructure

The transmission system was characterised as follows:

- Standard transmission voltage levels of 330 kV, 220 kV, 132 kV, 88 kV and 66 kV which are further stepped-down to 33 kV and 11 kV for distribution at substations;
- 330kV transmission lines forming the backbone of the transmission network;

- 220kV transmission lines forming much of the network in the mining areas of the Copperbelt province. The Copperbelt network is mainly operated by Copperbelt Energy Corporation. Other 220kV lines run between Kafue and Victoria Falls, and Victoria Falls and Sesheke;

- 132kV for regional power supply;

- 88kV and 66kV transmission lines for local supply;

- Interconnection with neighbouring countries as part of the Southern African Power Pool (SAPP).

- Zambia is currently developing an interconnection with Tanzania which will ultimately connect the East African Network with the Southern Africa Network. The model was simulated with Zambia operating in island mode.

- Expansion projects commissioned such as:

  - 132kV Kabompo – Mumbezhi Line;

  - 330kV Chipata West – Msoro Line;

  - 132/33kV Mumbezhi Substation;

  - 132kV Zambezi – Chavuma Line;

  - 330/132kV Kafue Town GIS; and

  - Upgrade of Musonda Falls Generators 6 and 7.

Single line diagrams of the Zambian Power System under ZESCO Ltd and CEC are shown in Fig 5 and Fig 6.

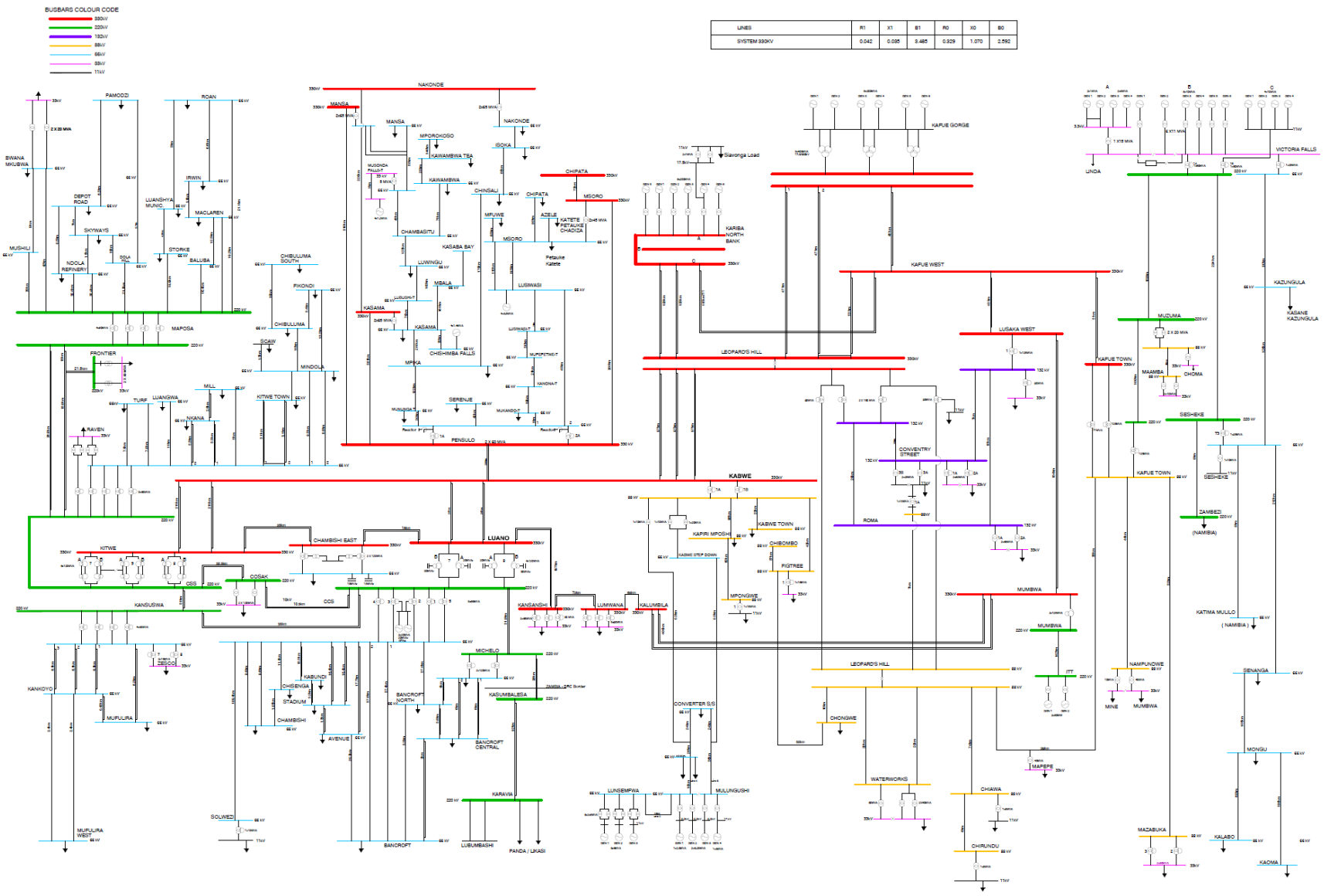

Fig 5: SLD of the ZESCO Power System

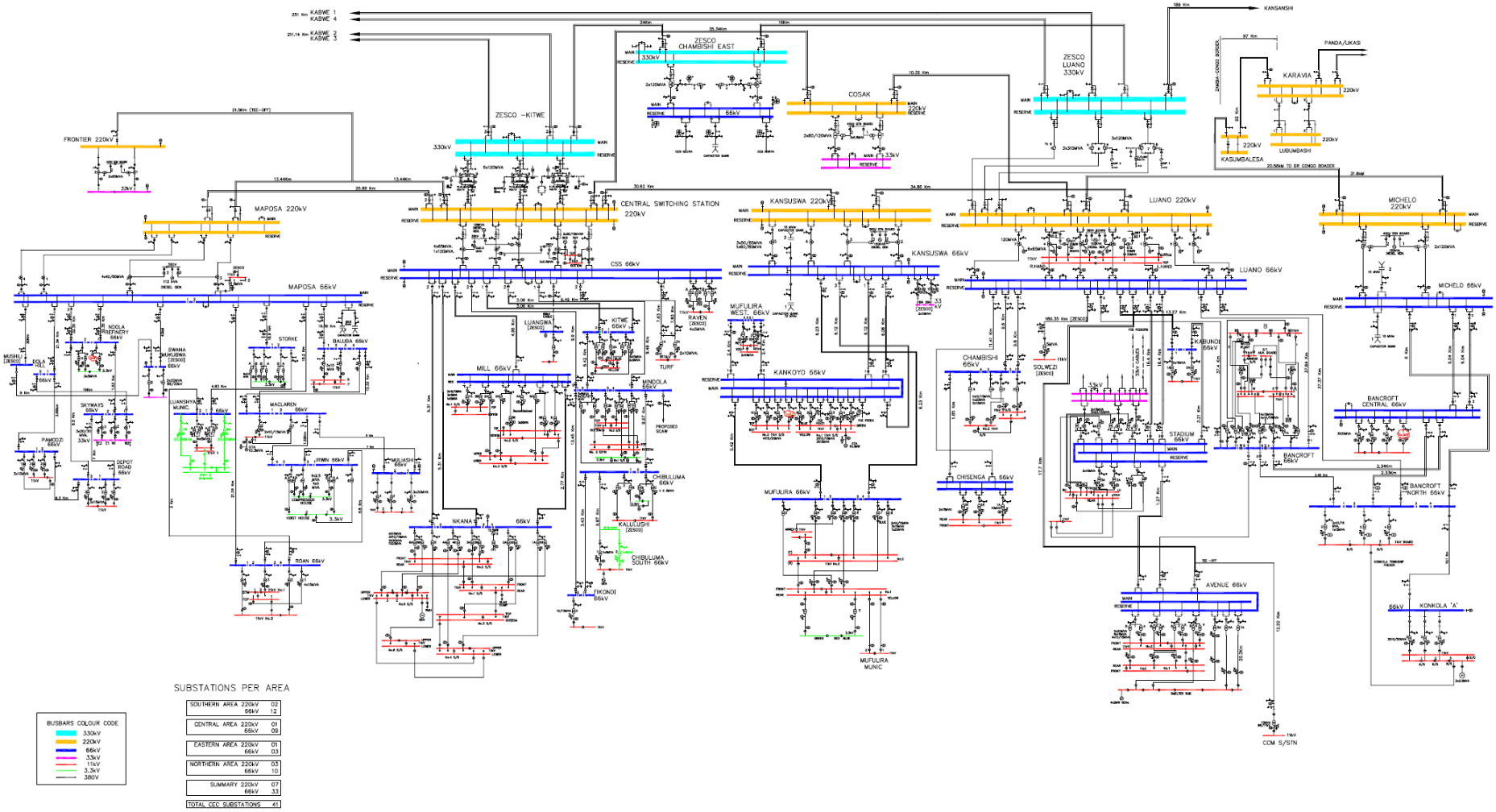

Fig 6:SLD of the CEC Power System

For the purpose of the study, the Zambian Grid was modelled as shown in Fig 7 below:

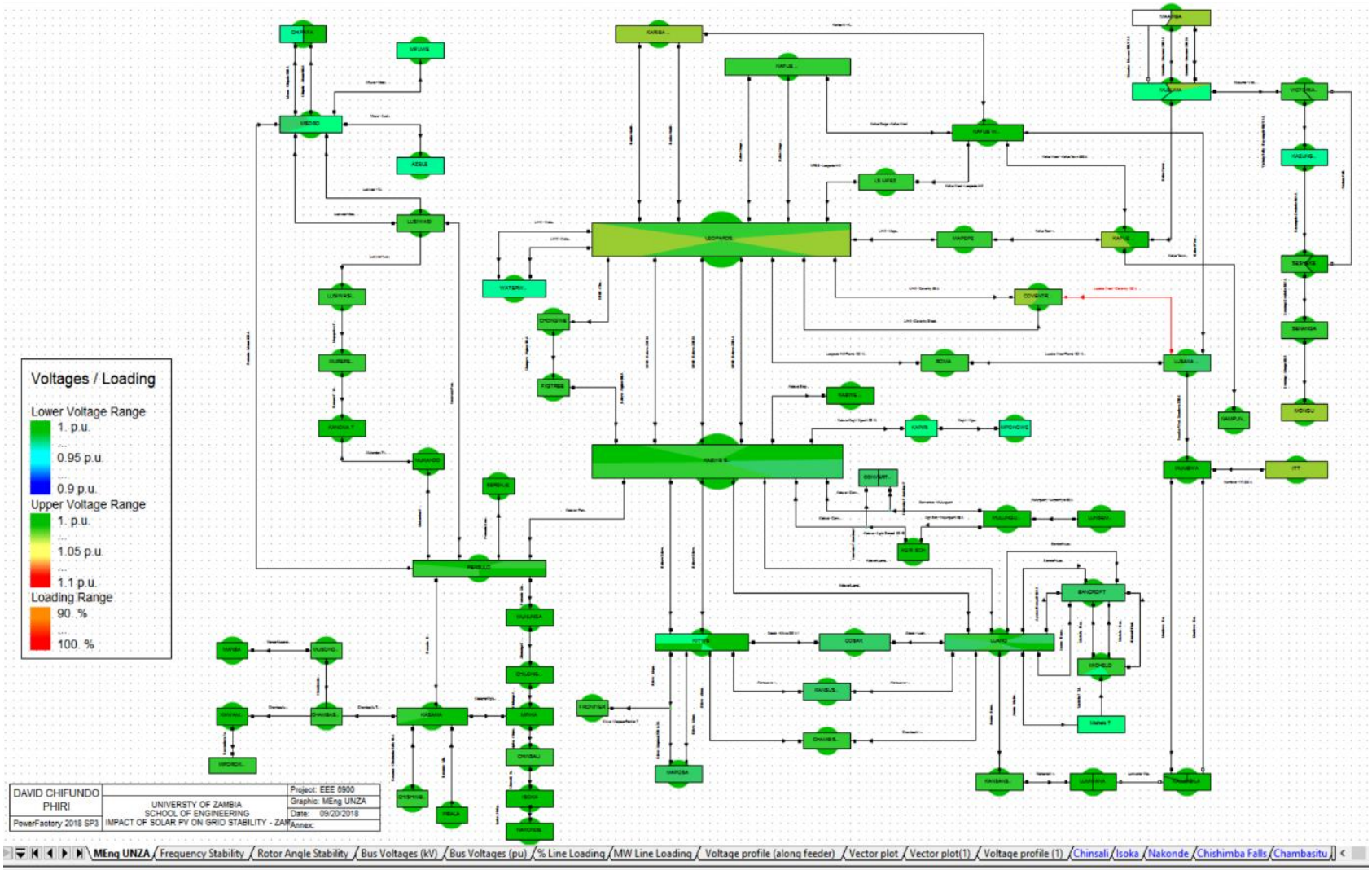

Fig 7:Depiction of the model of the Zambia National Grid

3.3.3. Modelling of a PV System in PowerFactory DIgSILENT

In DIgSILENT the photovoltaic system element (ElmPvsys) is based on the static generator element (ElmGenstat). The PV model represents an array of photovoltaic panels, connected to the grid through a single inverter. However, the PV system differs from the static generator in that the former provides an option to automatically estimate the active power set-point, given the geographical location, date and time. Fig 8 below shows the functional diagram for a Solar PV power generator.

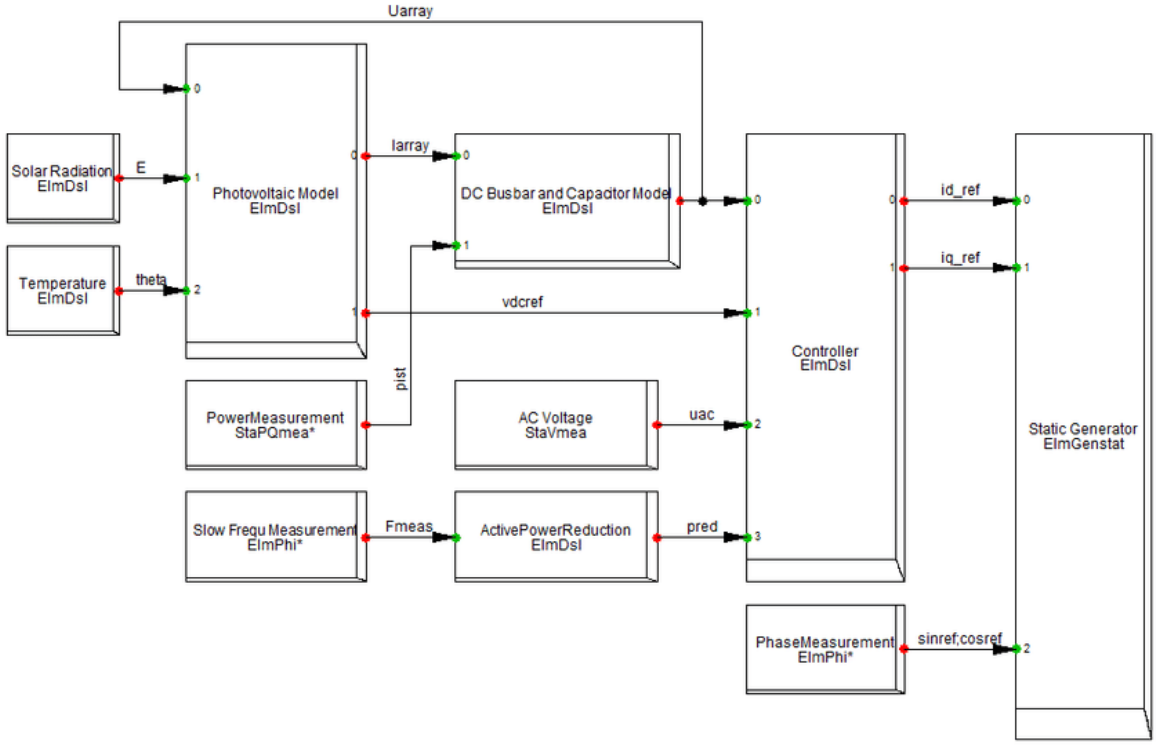

Fig 8:Functional Diagram of the PV plant (DIgSILENT, 2018)

The generic Solar PV model gives the basic understanding of the operation of the PV system with basic control and measurement systems such as solar radiation, temperature, power measurement and frequency measurements. Many deficiencies exist in this model that needs to be addressed.

The generic model has PV panel models with many assumptions and approximations and it does not have any MPPT control to ensure the PV system always operate on maximum power. There is only one type of reactive power control available based upon voltage deviation and there is no AC voltage and active power regulation available. A detailed discussion of the standard DIgSILENT PV model is given in Appendix 4.

3.4. Simulations in Power factory DIgSILENT

Investigation on the impact of Solar PV integration on the Zambian National grid was undertaken by modelling of the national grid and then undertaking contingency simulations in DIgSILENT PowerFactory. The contingency was simulated as a loss of power generation from a Solar PV power plant at a given injection point.

3.4.1. Simulation Packages in PowerFactory DIgSILENT

PowerFactory DIgSILENT comes with in-built packages that would enable steady-state and transient stability analysis to be carried out. The following is a description of some of the packages used in DIgSILENT.

1. **Quasi-Dynamic Simulation**

   Quasi-dynamic simulations are mainly used for medium to long-term system analyses. In a Solar PV System, quasi-dynamic simulations will include appropriate functionality like: estimation of solar irradiance based on GPS coordinates, PV panel model using datasheet parameters, different mounting options, including single/dual axis MPP trackers, various steady-state voltage/reactive power control options applied either locally or in coordination with other units etc.

2. **RMS Stability**

   The RMS stability dynamic simulation tool is used for short term analyses and for analysing the fault ride-through behaviour of PV units, voltage and frequency stability of the power system stability in a micro-grid system. For grid-connected studies, PowerFactory provides a number of PV templates modelled such as to represent short-time transients correctly.

3. **EMT simulation**

   For very fast transients the EMT simulation package is used. PV system disconnection from the grid depicts such fast transients, and for this reason, the EMT simulation package was used during the study.

   In EMT only a minimum set of controllers and auxiliary elements need to be modelled e.g., for switching/islanding transients the fast-reacting over-current protection, over/under voltage/frequency protection and a couple of other fast-acting blocks are needed. In such an analysis, solar models (where the power is calculated based on irradiance), MPPT models, slow-acting voltage regulators with relatively large time constants are typically not needed.

3.4.2. Study Criteria

The focus of the study was to analyse the impact of integrating utility-scale Solar PV on an existing grid. The purpose of the study criteria was therefore to screen penetration levels of Solar PV technology that would influence the behaviour of the grid. Since the ZESCO grid is part of the SAPP system, the SAPP planning criteria was adopted as the study criteria in this study.

The SAPP system is designed to satisfy the NERC N-1 criteria. Using the NERC N-1 criterion and in conformity with the IEEE 1453-2004 standard, the Zambian system is therefore designed to uphold the following:

1. Following the tripping of any network component (overhead lines, transformers, generators);
    - No overload must appear on any of the remaining components;
    - Thermal ratings of equipment should not be exceeded during the outage. Whatever the situation, operational limits must be respected;

2. In normal condition;
    - The flows must be kept below the thermal rating of each network element;
    - The voltage at each bus bar must be kept within 95% and 105% of its nominal value.
    - The generators must operate within their reactive capabilities (generation and absorption).

3. In emergency situation (outage of one element);
    - The thermal rating of any equipment should not be exceeded;
    - The voltage should be kept within 95% and 105% of its nominal value;
    - A 15% over-voltage will be acceptable during 5 s and a 20 % over-voltage will be acceptable during 1s or 2s;

4. In transient state;
    - The power system must remain stable following a three-phase fault cleared within 100 ms. This time includes the current transformer errors, protection relay response and the breaker operating time.

5. Spinning reserve
   Spinning or primary reserve corresponds to the power delivered by generators due to the action of their speed governor following a decline of the system frequency (when there is a deficit of power to satisfy the load).

All the units may participate in the primary reserve. The primary reserve for the Zambian system in island mode is around 180 MW, corresponding to the loss of one large unit at Kariba North Bank or Kafue Gorge power stations.

6. Under frequency load shedding

   The following under frequency load shedding settings were used.

Table 5: Frequency load shedding settings

Stage	Under Frequency Settings (Hz)	Time Delay (ms)
1	48.75	700
2	48.5	1000
3	48	1200
4	47.75	2000

3.4.3. The choice of study areas – Leopards Hill and Lusaka West Substations

This study was aimed at understanding the behaviour of the interconnected power system when Solar PV technology is injected into the system. Critical to this understanding is the precise point at which the Solar PV is introduced and the operating conditions. Various points on the Zambian system were identified for the purposes of the study based on various factors. The following characteristics became of importance to the study:

i. The behaviour of the system when Solar PV is injected at a highly congested substation; and

ii. The behaviour of the system when Solar PV is injected at a lightly loaded substation (transit point).

Due to the suitability and ease of access to the substations, Leopards Hill and Lusaka West Substations were picked as the best fit for the above selection criteria.

Leopards Hill is currently the most highly congested substation in Zambia followed by Kabwe Stepdown. In the case of Leopards Hill, power from the major generation stations is aggregated at this substation in transit to the major load centres on the Copperbelt and for distribution to service the bulk of the load in Lusaka.

Despite the grid around Leopards Hill being stiff, the substation poses a significant risk to the security of the national grid. Any uncontrolled behaviour at Leopards Hill will most likely result in a nationwide blackout. Under the Zambian Government's medium to long term planning, future transmission lines or generation will have to bypass the Leopards Hill substation.

Lusaka West, on the other hand, is currently just a transit point for power coming from the south en route to the mining areas in the Northwestern Province. The substation was constructed as part of the measures to service future mining loads at Lumwana and Kalumbila. The demand projected through the Ministry of Energy-JICA power systems development master plant may have been too optimistic on the economic activities that would have come about due to the new mining activities in Kalumbila and Lumwana (GRZ, 2010). This then implies that the Lusaka West substation may be subjected to lower loading than expected. This position makes Lusaka West the second candidate for this study. A description of the Leopards Hill and Lusaka West substations is provided below:

1. Leopards Hill Substation

   Leopards Hill Substation is located 27 km East of Lusaka City CBD and is accessible using Leopards Hill Road (D152). The substation is feed by five (05) 330 kV transmission lines. Two (02) lines come directly from the 1080 MW Kariba North Power Station, and two (02) lines come directly from the 950 MW Kafue Gorge Power Station. The fifth 330 kV line is an interconnector with Kafue West via the Solar PV 330 kV Substation at LS MFEZ. Kafue West is fed from Kafue Gorge, Kariba North and Victoria Falls via the GIS Kafue Town Substation.

   At 330 kV voltage level, Leopards Hill has a double busbar arrangement delivering power to the Kabwe Stepdown Substation via three (03) 330 kV lines. The 330 kV Leopards Hill busbar also feeds one (01) 132kV single busbar via 2 x 150 MVA three-winding transformers within Leopards Hill Substation. Further, there are two (02) 90 MVA three-winding transformers connected to Leopards Hill 330kV busbar that feed an 88kV double busbar. The 11 kV bus at Leopards Hill is feed from the axillary windings of the three-winding transformer.

2. Lusaka West Substation

   The 330 kV Lusaka West Substation is located 12 km West of Lusaka City CBD and is accessible using Mumbwa Road (M9). It does not have a direct feed from a power station; however, it is connected to Kafue West Substation and Nambala Substation via 43 km and 134 km of 330 kV transmission lines respectively.

   The 330 kV Lusaka West busbar feeds a 132kV single busbar through two (02) 125MVA two-winding transformers. The 132 kV Lusaka West busbar is interconnected to the 132 kV busbars at Coventry Street and Roma substations via 7 km and 15 km tie lines, respectively.

3. Pensulo Substation

   After undertaking various simulations at Leopards Hill and Lusaka West, interesting behaviour was observed on the Kabwe-Pensulo 330 kV line. Therefore, the 66kV Pensulo

busbar was adopted as a third injection point just to understand system behaviour if the low rotation power plant was injected at the terminal point of the 298 km line.

The Pensulo Substation is composed of one (01) 330 kV single busbar coupled to one (01) 66 kV double busbar via two (02) 60 MVA two-winding transformers. The 66 kV busbar has a 30 MVAr reactor connected to it for voltage regulation.

The Pensulo Substation is the major distributor connecting the 330 kV Mpika Substation and the 330 kV Msoro substations to the backbone network of the Zambian grid. There are five (05) provinces that are supplied from the Pensulo Substation and these are Central, Muchinga, Eastern, Luapula and Northern Provinces making it the third (3^{rd}) most critical substation in Zambia after Leopards Hill and Kabwe Stepdown. Future generation and transmission developments are planned to bypass the Pensulo Substation with the creation of an intermediary substation around the district of Mkushi.

3.4.4. Simulation Flow Process

For purposes of this study, a model of the Zambian grid was developed in DIgSILENT and then a model Solar PV plant was adopted and integrated into the model Zambian grid for simulation for the impacts of integrating variable generation Solar PV power onto the Grid. The system study simulation flow chart is shown in Fig 9 below.

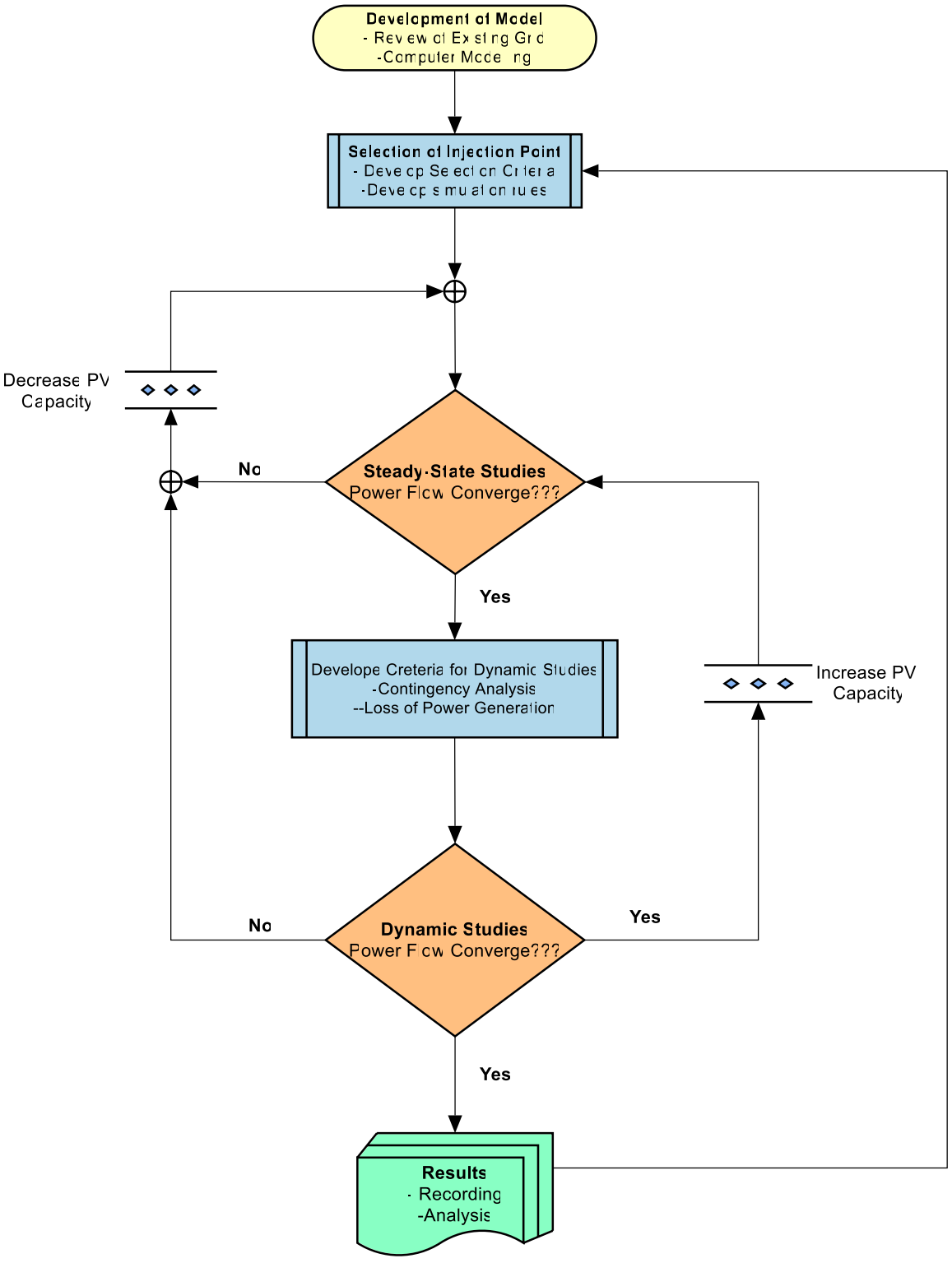

Fig 9: Study Flow Chart

3.5. Data Analysis

Using the inbuilt tools in DIgSILENT, the modelled Zambian Power System was analysed for instabilities when various conditions of Solar PV generation prevailed. The results were expressed in terms of graphs and tables as provided in Chapter 4.

3.6. Comparison of Results with Other Studies Conducted by Other Researchers

The results obtained were later compared with findings from other studies. Learning points were shared with other programs and projects. Of these the following are notable:

1. CEC 1MW Solar PV plant at the Copperbelt University (Commissioned)
   Copperbelt Energy Corporation has constructed and commissioned a 1 MW grid-tied Solar PV power plant in Kitwe. The plant was developed as a demonstration project for industrial purposes as well as academic training for Copperbelt University.

   The 1 MW CEC plant was commissioned in 2018 and since then no adverse impacts have been recorded as a result of the power plant. CEC operations have remained normal and power quality obligation to its customers remain fulfilled.

2. 86 MW Scaling Solar at LS MFEZ (Commissioned);
   The 86 MW Solar PV power plant under the scaling solar power projects is made up of two (02) Solar PV power plants located south of Lusaka at the LS MFEZ. Both power plants are fed through the 330 kV LS MFEZ Substation cutting into 330 kV tie line between Kafue West and Leopards Hill Substation.

   The plants were commissioned in 2019 and since then no adverse grid impacts have been recorded as a result of the power plants.

3. Globeleq 200 MW at Leopards Hill Substation (feasibility study)
   A feasibility study has been developed for the project in which a grid impact study confirms that 200 MW of Solar PV can be injected at the 330 kV Leopards Hills Substation without adversely affecting the integrity of the grid;

4. Access 130MW Wind power (feasibility study);
   A feasibility study has been developed for the project in which a grid impact study confirms that 130 MW of wind power generation Solar PV can be injected at the 330 kV Pensulo Substation without adversely affecting the integrity of the grid;

5. 100MW RE – FiT/GET FiT projects across the country (feasibility study)
   Rapid Grid Impact Studies undertaken on various renewable energy projects. The results show that a disaggregated number of renewable energy power plants can be integrated on the grid without adversely affecting the reliability of the grid.

4. RESULTS AND DISCUSSIONS

This chapter provides an overview of the results and findings of the research.

4.1. Overview

Chapter 3 above notes that three (03) injection points on the national grid were identified for which different simulation scenarios were undertaken. For each of the injection points, both steady-state and dynamic stability assessments were undertaken. The simulated scenarios were categorised as:

1. **Base Case**;
   A base case was aimed at capturing the normal system operating conditions prior to Solar PV injection.

2. **Solar PV Injection**; and
   Various penetration levels of solar photovoltaic analysed.

3. **Equivalent Hydropower Model**
   An equivalent hydropower model was used to contextualise the performance of an equivalent rotational power plant at the selected given injection point.

The findings of the investigation of the impact of Solar PV on the system stability of the Zambia National Grid are outlined as follows:

4.2. Base Case

The base case involved the simulation of the model with no Solar PV injection. The voltage magnitude and line loading of some selected busbars and lines respectively were observed.

Fig 10 shows the per unit voltage level for selected busbars on the Zambian grid while Fig 11 shows the line loading for some selected lines and feeders. The selection of the busbars and feeders was based on critical loads associated with the elements. The associated line loading and line losses were summarised as shown in Table 6.

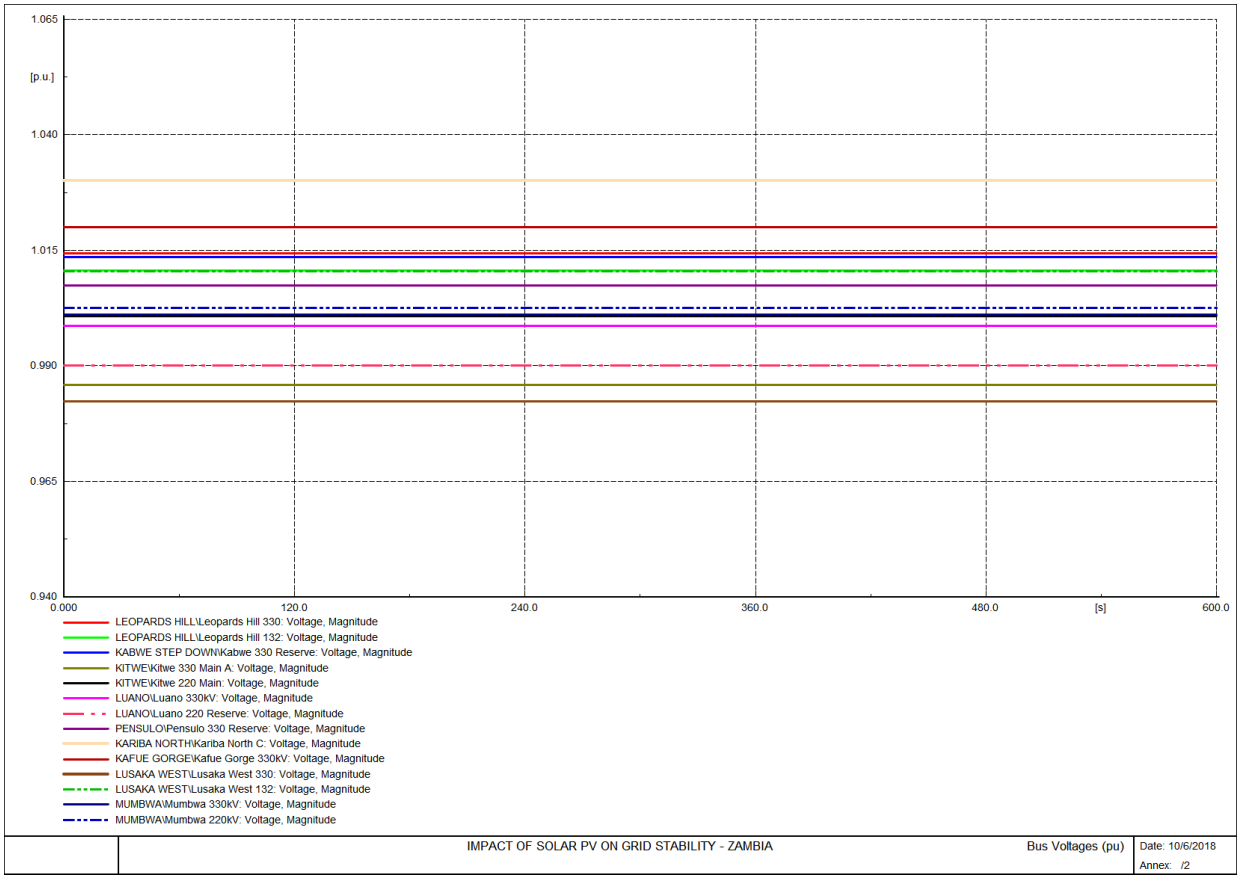

Fig 10: Voltage level (pu) with no solar injection on the power grid (base case)

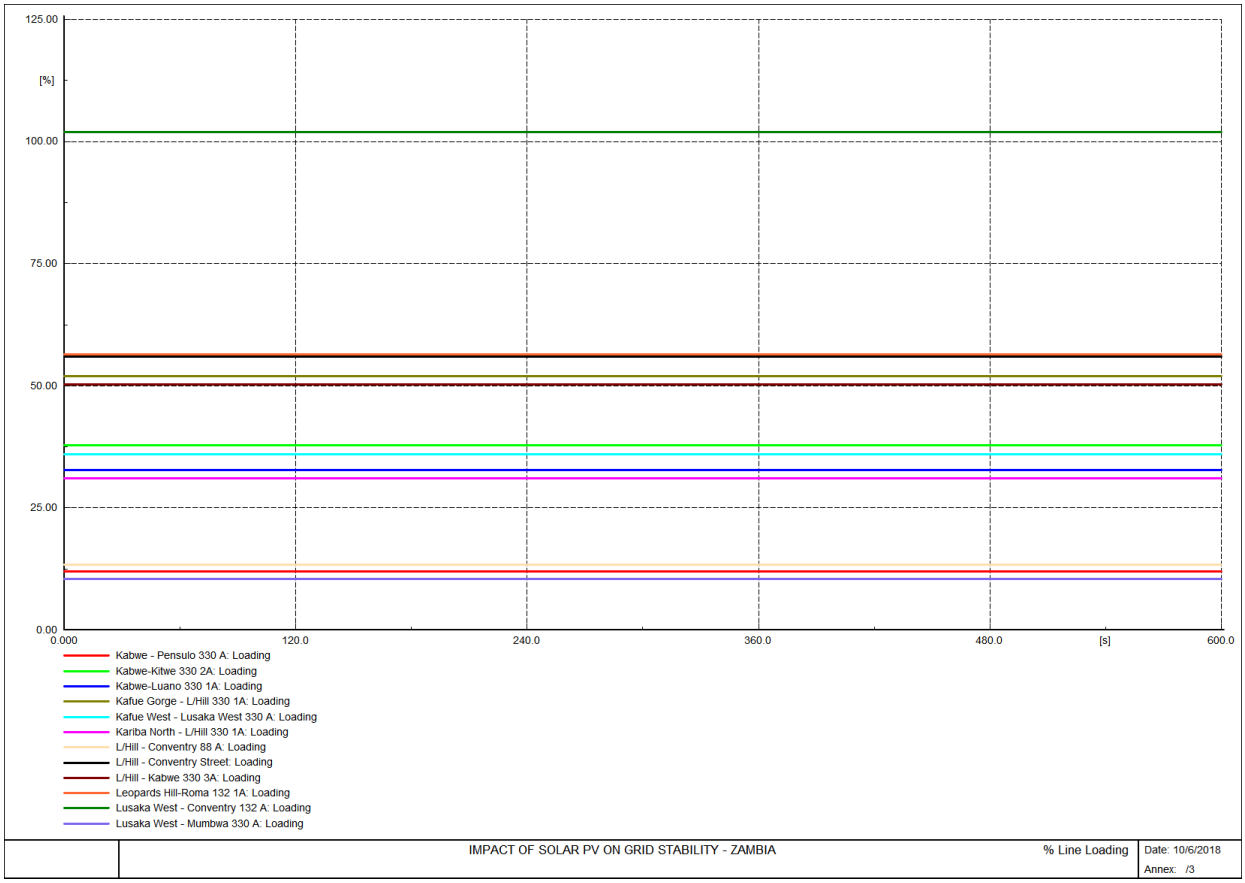

Fig 11: % Line Loading with no solar injection on the power grid (base case)

Table 6: Transmission Line Parameters

Line ID	Transmission Line	Conductor Type	Length (km)	% Line Loading	(MW) Line Losses
1.	330 kV Kabwe – Pensulo	2xBison	298	12.1	0.4
2.	330 kV Kabwe – Kitwe	2xBison	211	37.9	5.1
3.	330 kV Kabwe – Luano	2xBison	247	32.8	4.5
4.	330 kV Kafue Gorge – Leopards Hill	2xBison	47	51.9	2.1
5.	330 kV Kafue West – Lusaka West	2xBison	43	36.0	0.9
6.	330 kV Kariba North – Leopards Hill	2xBison	123	31.0	2.0
7.	88 kV Leopards Hill – Coventry Street	Wolf	7	13.5	0.0
8.	132 kV Leopards Hill – Coventry Street	Wolf	28	56.0	1.1
9.	330kV Leopards Hill – Kabwe Step Down	2xBison	97	50.2	4.2
10.	132 kV Leopards Hill – Roma	Wolf	28	56.4	1.0
11.	132 kV Lusaka West – Coventry Street	Wolf	7	102	0.9
12.	330 kV Lusaka West – Mumbwa	2xBison	134	10.4	0.1

4.3. Impact of Solar PV on the stability of the Zambia National Grid

The impacts of integrating Solar PV power on the system stability of the Zambia National Grid are as presented below:

4.3.1. Injection of Solar PV at the 132 kV Leopards Hill Substation

The system at Leopards Hill substation was modelled as shown in Fig 12 below:

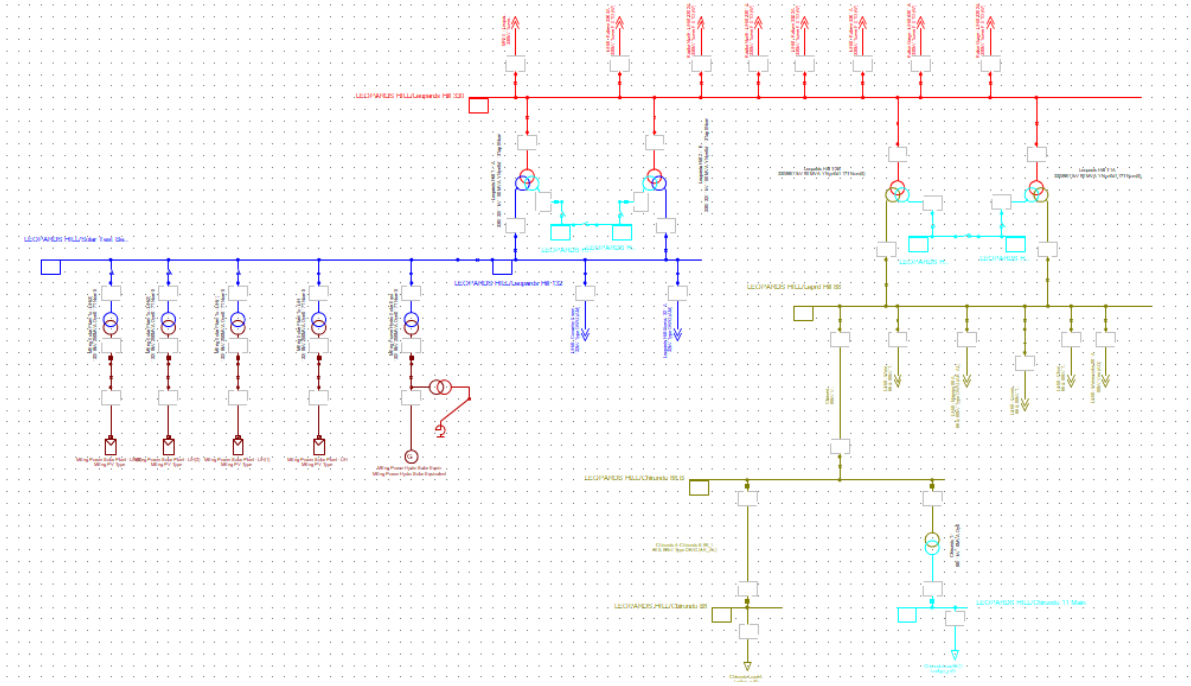

Fig 12: DIgSILENT model of the Leopards Hill Substation

When 200 MW of Solar PV was injected at the 132 kV Leopards Hill bus bar, the system exhibited high magnitude oscillatory behaviour until after 102 seconds when a total system collapse occurred. The collapse was due to the loss of synchronising torque. Causes of system collapse in PowerFactory DIgSILENT or indeed in functional power systems are further explained in Appendix 5 below:

The 200 MW Solar PV injected at the 132 kV Leopards Hill busbar resulted in 59 % additional loading on the 132 kV bus bar but a reduction in the loading at the 330 kV busbar by 11% was observed. Fig 13 below depicts system behaviour when 200 MW of Solar PV is injected into the 132 kV Leopards Hill busbar in terms of line voltages.

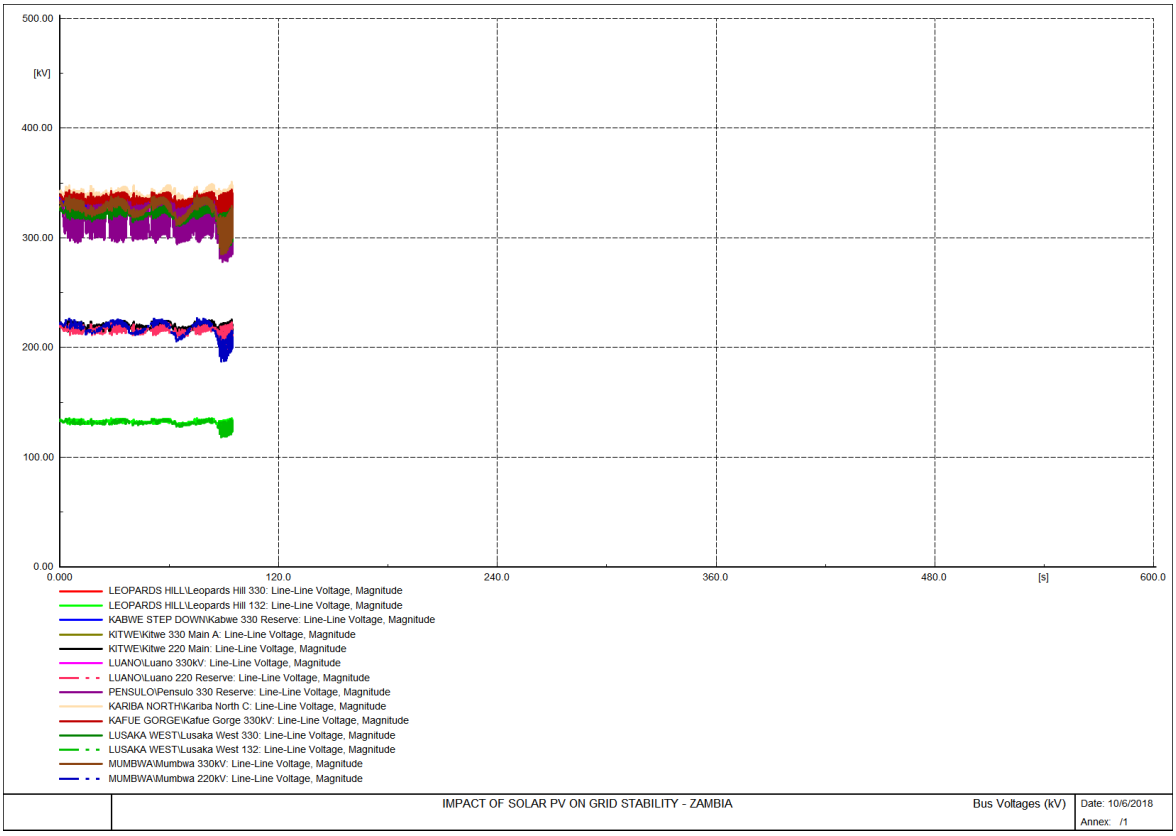

Fig 13: System collapse with 200 MW of Solar PV at 132 kV Leopards Hill Substation

Following the system collapse due to the 200 MW Solar PV injection at the 132 kV Leopards Hill substation, decreasing quantities of solar injection, as provided in 3.4.4 above, were investigated. The system was observed to have a self-stabilising capability with an injection level of 123 MW at the 132 kV Leopards Hills Busbar representing an additional loading of 26 % at the 132 kV bus and a corresponding 7 % reduction in the loading on the 330 kV bus. Fig 14 below shows the per-unit voltage levels for the system when 26 % Solar PV is injected at the 132 kV Leopards Hill Substation.

When a total loss of generation from the 123 MW Solar PV power plant at Leopards Hill was investigated, oscillatory behaviour leading to total system collapse was observed. Fig 15 below shows the system the per unit voltage levels for selected bus bars on the Zambian grid when a total loss of the 123 MW Solar PV plant at the 132 kV Leopards Hill bus bar was simulated.

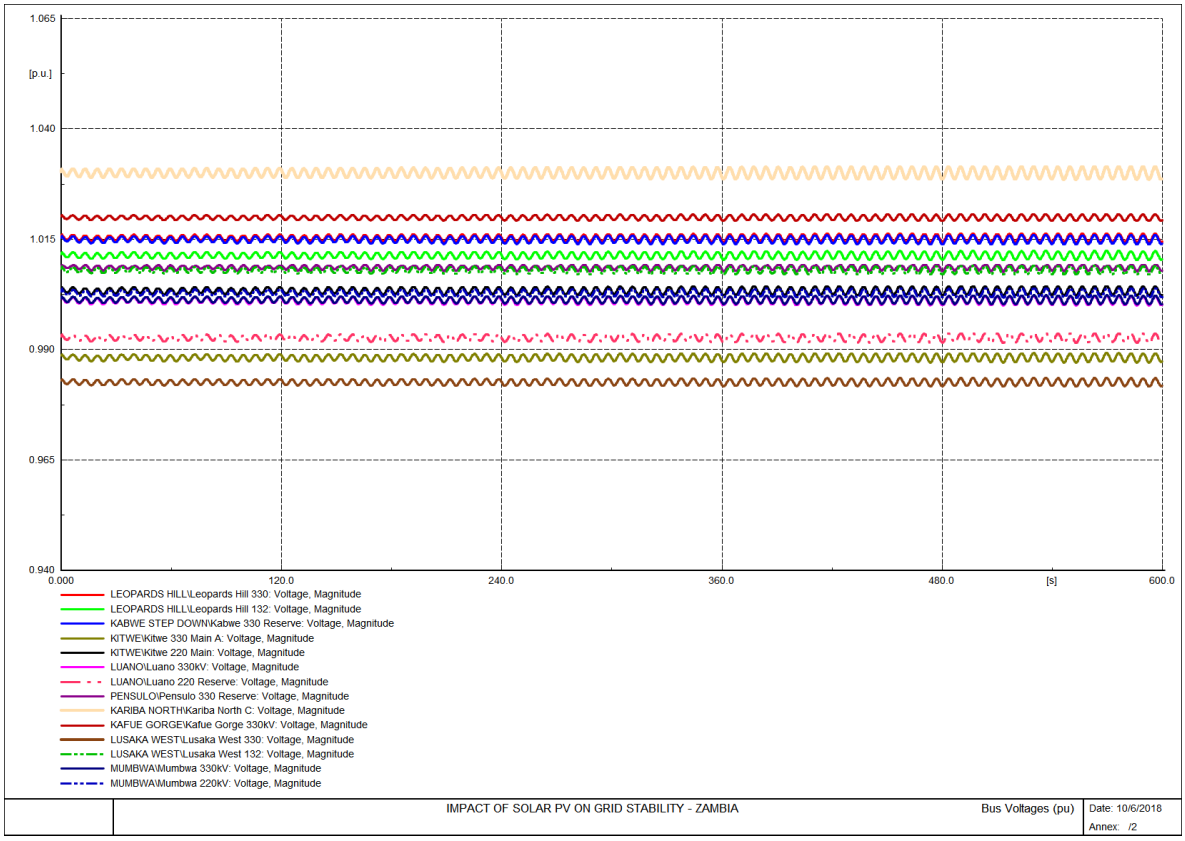

Fig 14: Voltage Level (pu) for self-stabilizing capability at 132 kV L/Hill

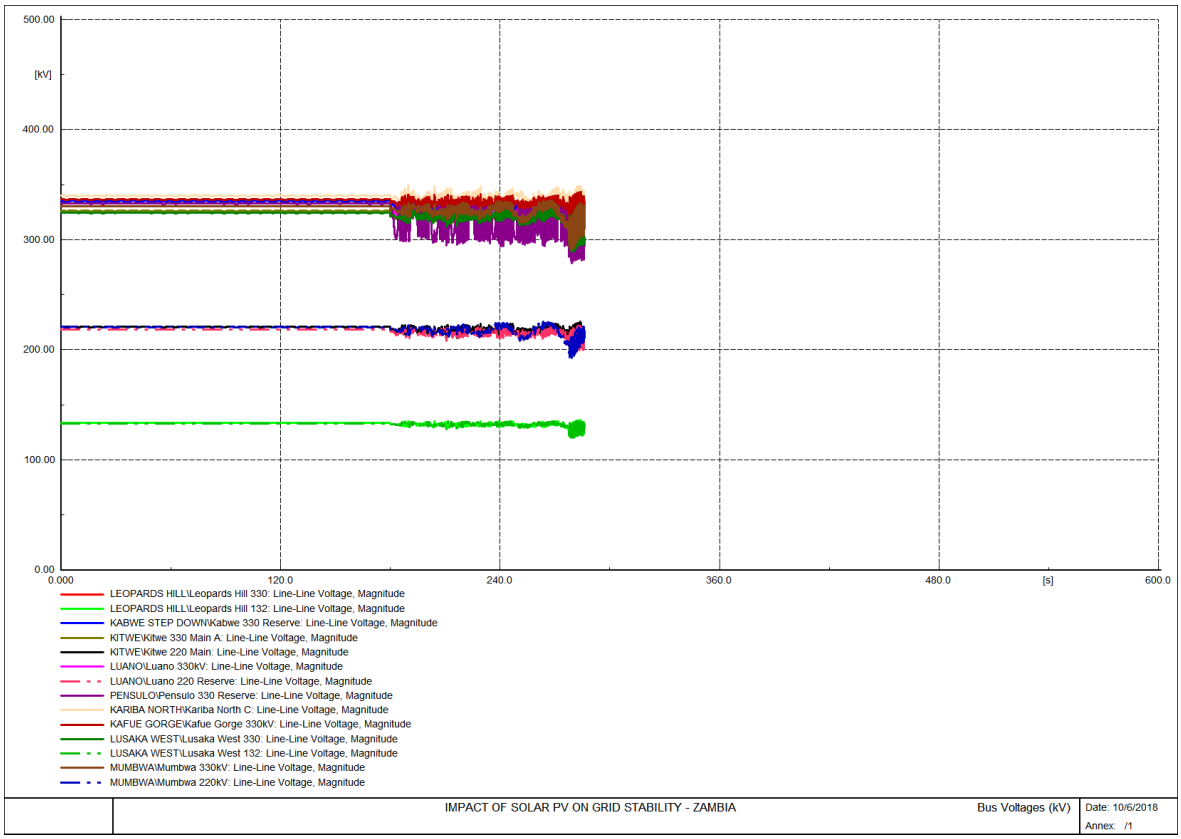

Fig 15: Voltage Level (pu) for loss of 123 MW Solar PV generation at 132 kV L/Hill

After several iterations, system stability was observed only with a loss of generation of 43.6 MW at the 132 kV Leopards Hill Busbar. This represents an additional loading of 9.2% on the 132 kV busbar with a corresponding 2.5% reduction in the loading on the 330 kV busbar. System behaviour resulting from a loss of 43.6 MW of Solar PV at 132 kV Leopards Hill Substation is shown in Fig 16 below while the corresponding line loading is shown in Fig 17:

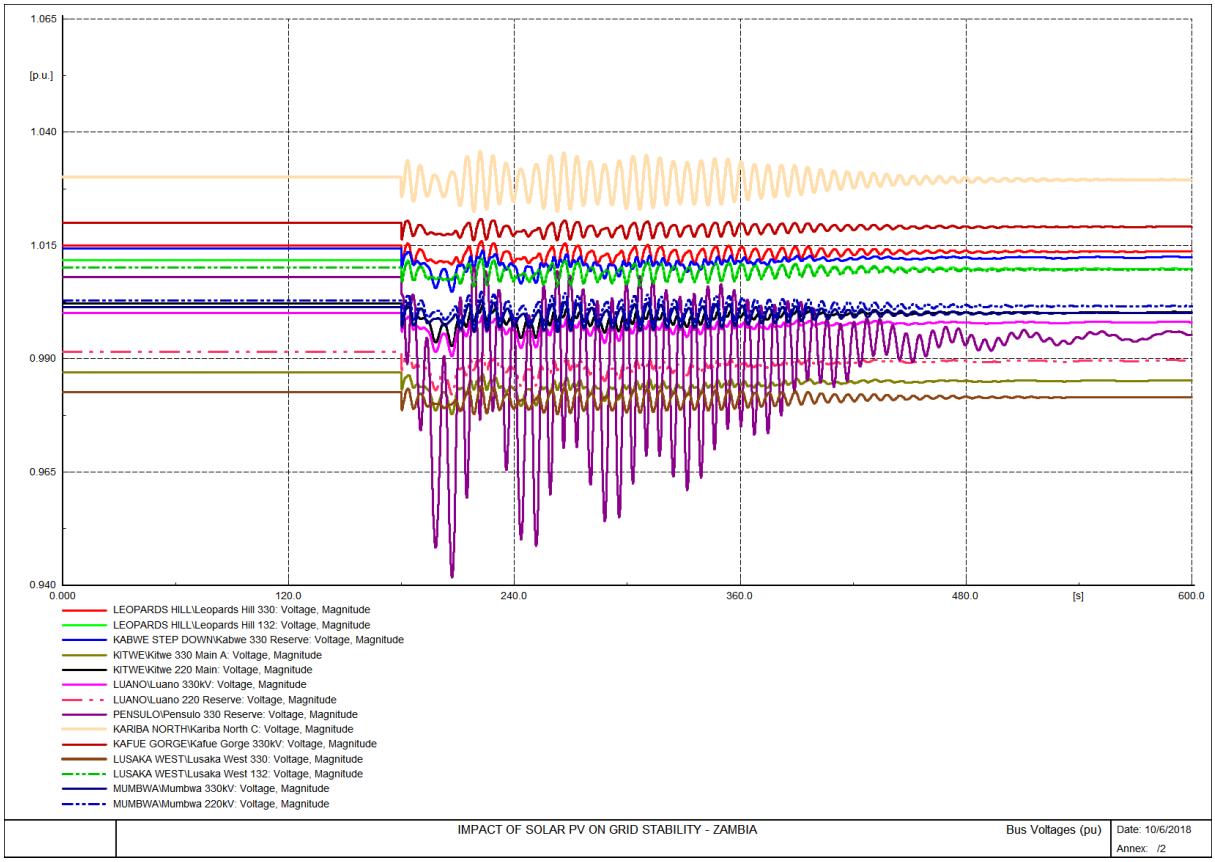

Fig 16: Voltage Level (pu) for loss of 43.6MW of Solar PV generation at 132 kV L/Hill

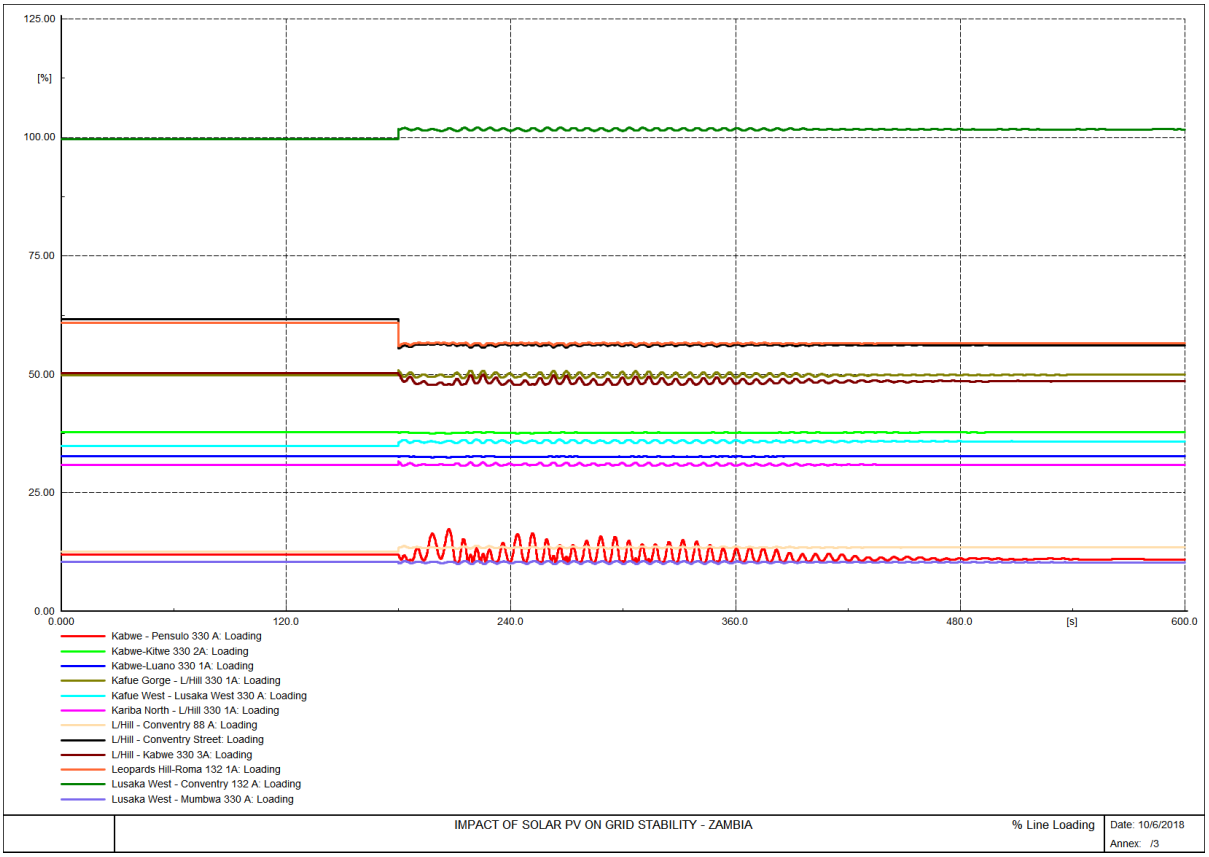

Fig 17: % Line Loading for 43.6 MW Switch Off at 132 kV Leopards Hill

Fig 16 above shows system operation where at t=0s, the full 43.6 MW is already on the grid until the 43.6 MW is switched off at t = 180s simulating a total loss of generation. From t = 180s to t = 540s, the system was observed to undergo deep oscillations that decreasingly subsided at t = 540s thereafter restoring system stability. Table 8 shows a list of some of the voltage levels obtained during the simulation of a Solar PV generating plant at the 132 kV Leopards Hill bus bar. The results may be presented as shown in Fig 18.

Table 7: Per Unit Voltage for Selected Busbars for Solar PV Injection at Leopards Hill

S/N	Busbar	Voltage (pu)		
		Base	123MW	43.6MW
1	330kV Leopards Hill	1.01	1.02	1.01
2	132kV Leopards Hill	1.01	1.01	1.01
3	330kV Kabwe Step Down	1.01	1.01	1.01
4	330kV Kitwe	0.98	0.99	0.99
5	220kV Kitwe	1.00	1.00	1.00
6	330kV Luano	1.00	1.00	1.00
7	220kV Luano	0.99	0.99	0.99
8	330kV Pensulo	1.00	1.01	1.00
9	330kV Kariba North	1.03	1.03	1.03
10	330kV Kafue Gorge	1.02	1.02	1.02
11	330kV Lusaka West	0.98	0.98	0.98
12	132kV Lusaka West	1.01	1.01	1.01
13	330kV Mumbwa	1.00	1.00	1.00
14	220kV Mumbwa	1.00	1.00	1.00

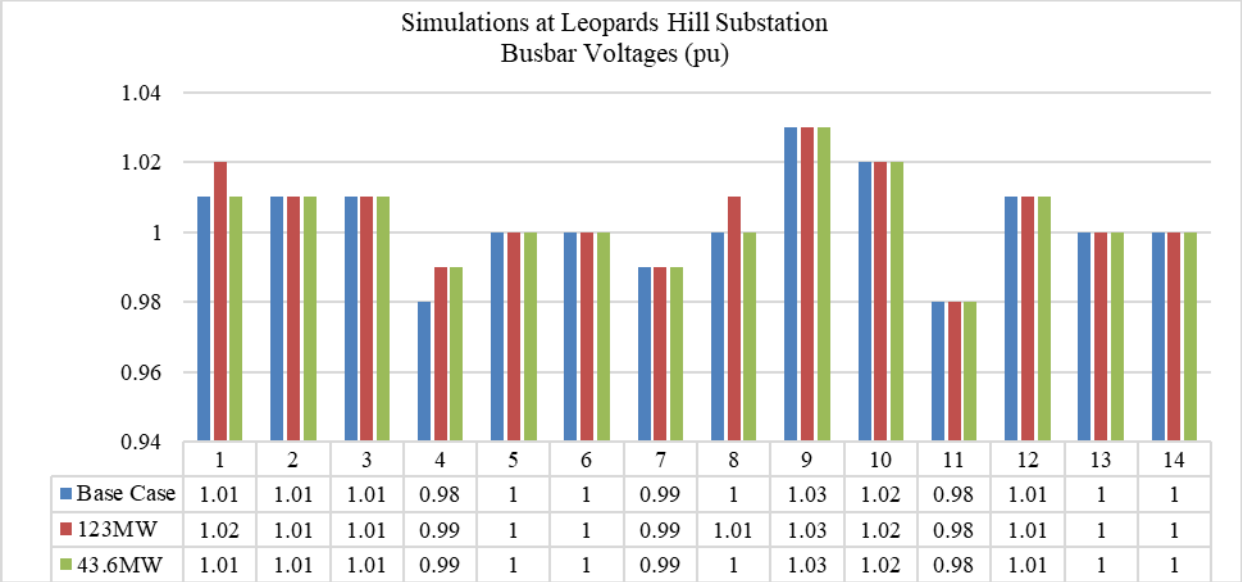

Fig 18: Per Unit Voltage Level for Selected Bus bars Solar injection at Leopards Hill

Table 8 shows a summary of some of the parameters for selected transmission lines while Fig 19 and Fig 20 shows the graphical representation of the results.

Table 8: Transmission Line parameters at steady state at Leopards Hill

Line ID	Line	Conductor Type	Length (km)	Line Loading %			Line Losses (MW)		
				Base	123MW	43.6MW	Base	123MW	43.6MW
1.	330kV Kabwe – Pensulo	2xBison	298	12.1	12.0	12.0	0.4	0.4	0.4
2.	330kV Kabwe – Kitwe	2xBison	211	37.9	37.8	37.9	5.1	5.1	5.1
3.	330kV Kabwe – Luano	2xBison	247	32.8	32.8	32.8	4.5	4.5	4.5
4.	330kV Kafue Gorge – Leopards Hill	2xBison	47	51.9	45.8	49.7	2.1	1.7	2.0
5.	330kV Kafue West – Lusaka West	2xBison	43	36.0	33.2	34.9	0.9	0.8	0.9
6.	330kV Kariba North – Leopards Hill	2xBison	123	31.0	30.8	30.9	2.0	2.0	2.0
7.	88kV Leopards Hill – Coventry Street	Wolf	7	13.5	11.1	12.6	0.0	0.0	0.1
8.	132kV Leopards Hill – Coventry Street	Wolf	28	56.0	72.3	61.7	1.1	1.7	1.3
9.	330kV Leopards Hill – Kabwe Step Down	2xBison	97	50.2	50.1	50.1	4.2	4.2	4.1
10.	132kV Leopards Hill – Roma	Wolf	28	56.4	69.2	60.9	1.0	1.6	1.2
11.	132kV Lusaka West – Coventry Street	Wolf	7	102	96.8	99.6	0.9	0.8	0.9
12.	330kV Lusaka West – Mumbwa	2xBison	134	10.4	10.4	10.4	0.1	0.1	0.1

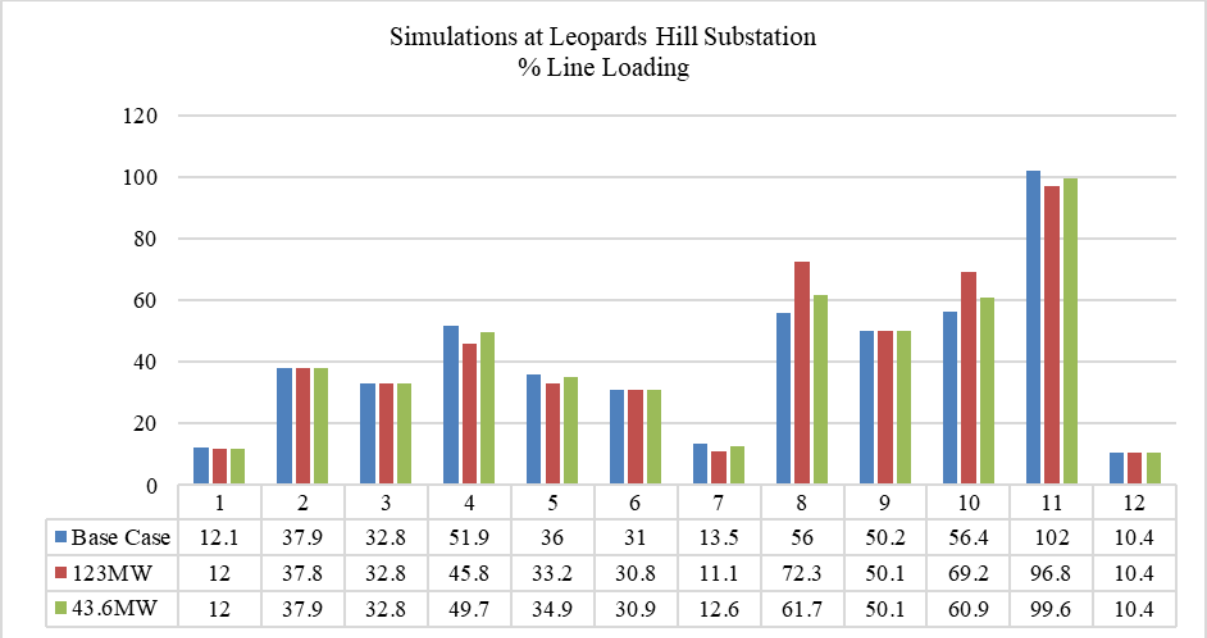

	1	2	3	4	5	6	7	8	9	10	11	12
Base Case	12.1	37.9	32.8	51.9	36	31	13.5	56	50.2	56.4	102	10.4
123MW	12	37.8	32.8	45.8	33.2	30.8	11.1	72.3	50.1	69.2	96.8	10.4
43.6MW	12	37.9	32.8	49.7	34.9	30.9	12.6	61.7	50.1	60.9	99.6	10.4

Fig 19: % Line Loading for Solar injection at Leopards Hill

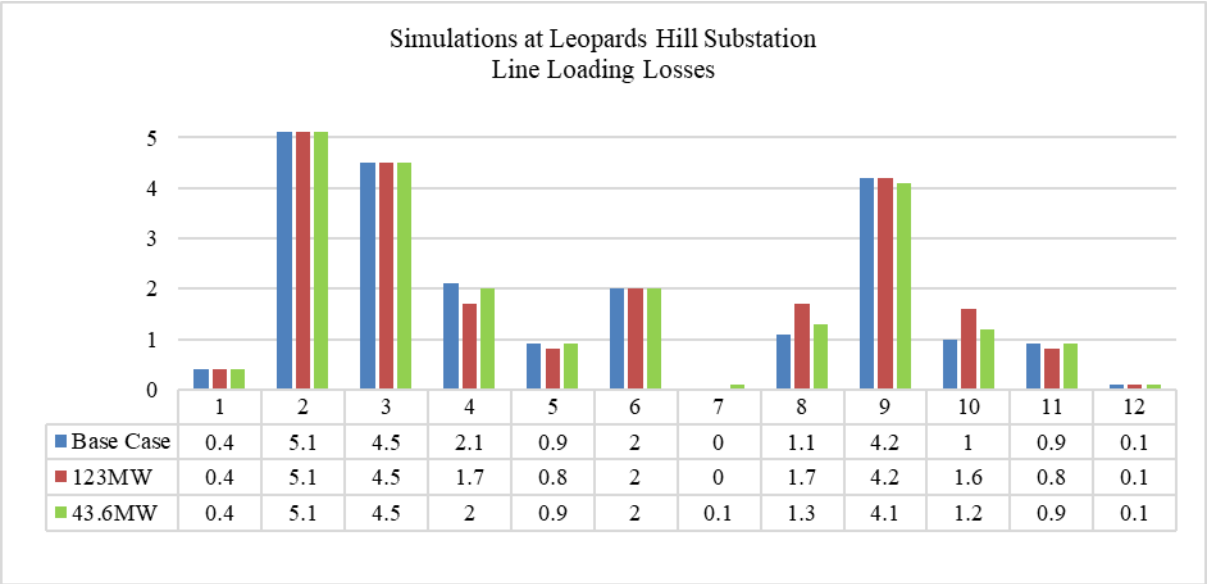

	1	2	3	4	5	6	7	8	9	10	11	12
Base Case	0.4	5.1	4.5	2.1	0.9	2	0	1.1	4.2	1	0.9	0.1
123MW	0.4	5.1	4.5	1.7	0.8	2	0	1.7	4.2	1.6	0.8	0.1
43.6MW	0.4	5.1	4.5	2	0.9	2	0.1	1.3	4.1	1.2	0.9	0.1

Fig 20: Line Losses for Solar injection at Leopards Hill

4.3.2. Injection of Solar PV at the 132 kV Lusaka West Hill Substation

At Lusaka West, investigations for the impact of Solar PV power generation on the interconnected grid was undertaken at the 132 kV bus bar. The same steps and methodologies applied during the simulations at Leopards Hill in 4.3.1 above were applied for the simulations at the Lusaka West Substation. The system at the Lusaka West substation was modelled as shown in Fig 21.

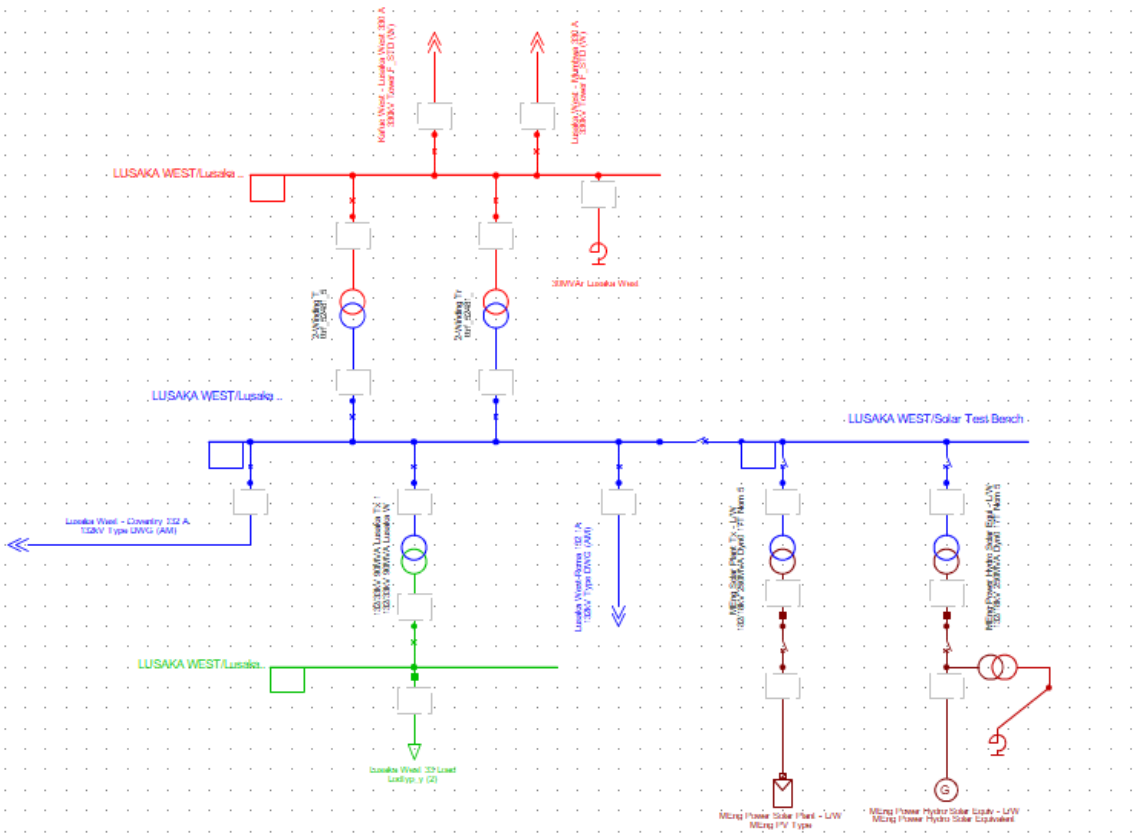

Fig 21: DIgSILENT model of the Lusaka West Substation

In the case of Lusaka West, the maximum Solar PV plant that could be connected to the 132 kV busbar had a capacity of 121 MW beyond which the system could not retain stability. The injection of 121 MW Solar PV power on the 132 kV Lusaka West busbar represented 31.5 % additional loading on the 132 kV bus bar and 36.4 % load reduction on the 330 kV bus bar.

The injection of 121 MW Solar PV power on the 132 kV Lusaka West busbar resulted in system collapse when a total loss of generation from the Solar PV plant was simulated. Stability in both voltage and power flow following a total loss of generation from a Solar PV power plant at the 132 kV Lusaka West Busbar could only be reached with Solar PV injection of 11.5 % representing 43.6 MW of additional loading as a result of the Solar PV plant. The corresponding reduction of load on the 330 kV Lusaka West busbar was 13 %.

Fig 22 shows the per unit voltage levels when a loss of generation from the 43.6 MW Solar PV power plant at the 132 kV Lusaka West busbar was simulated.

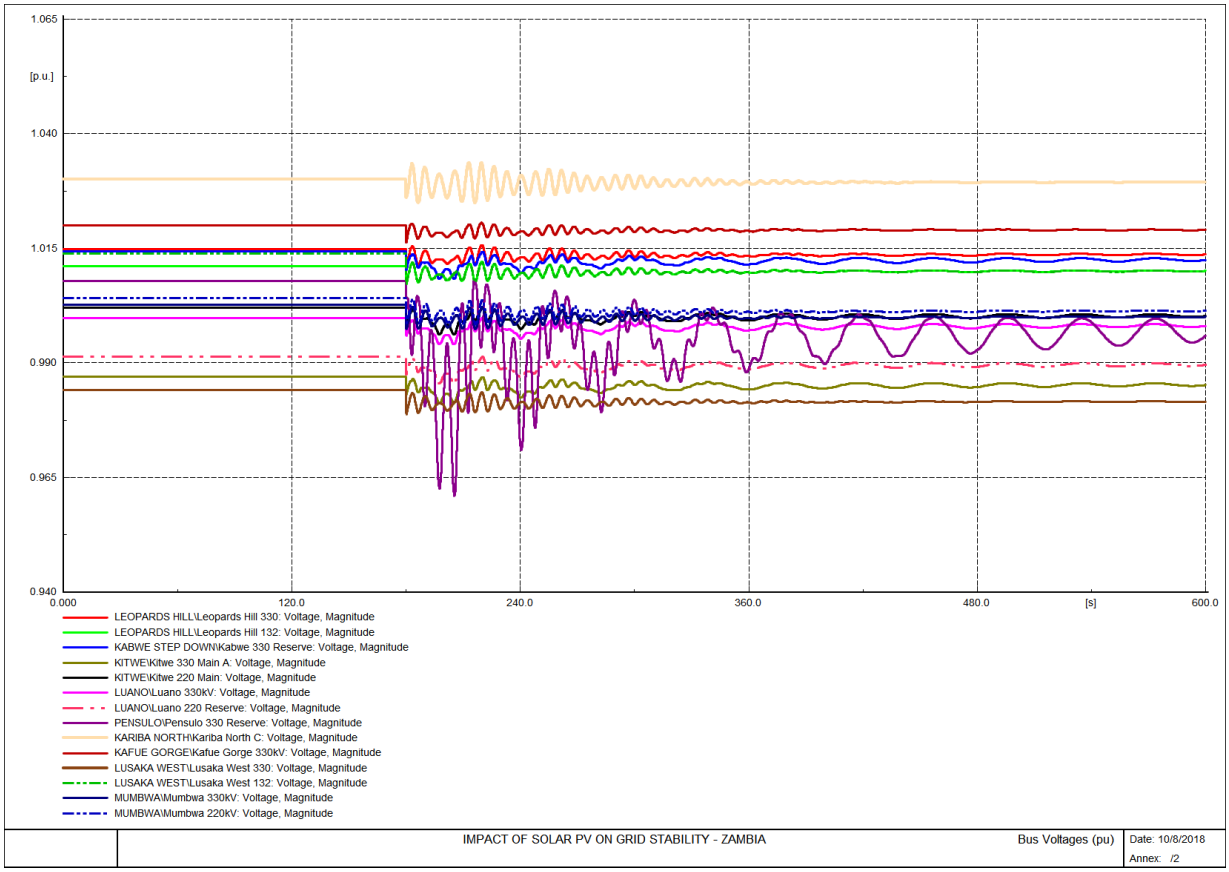

Fig 22: Voltage Level (pu) for loss of 43.6 MW Solar Plant Switch Off at L/West 132 kV

Table 9 below shows a list of some of the voltage levels obtained during the simulation of a Solar PV generating plant at the 132 kV Lusaka West bus bar. The results may be presented as shown in Fig 23.

Table 9: Per Unit Voltage for Selected Busbars for Solar PV Injection at Lusaka West

S/N	Busbar	Voltage (pu)		
		Base	121MW	43.6MW
1	330kV Leopards Hill	1.01	1.02	1.01
2	132kV Leopards Hill	1.01	1.01	1.01
3	330kV Kabwe Step Down	1.01	1.01	1.01
4	330kV Kitwe	0.98	0.99	0.99
5	220kV Kitwe	1.00	1.00	1.00
6	330kV Luano	1.00	1.00	1.00
7	220kV Luano	0.99	0.99	0.99
8	330kV Pensulo	1.00	1.01	1.00
9	330kV Kariba North	1.03	1.03	1.03
10	330kV Kafue Gorge	1.02	1.02	1.02
11	330kV Lusaka West	0.98	0.98	0.98
12	132kV Lusaka West	1.01	1.01	1.01
13	330kV Mumbwa	1.00	1.00	1.00
14	220kV Mumbwa	1.00	1.00	1.00

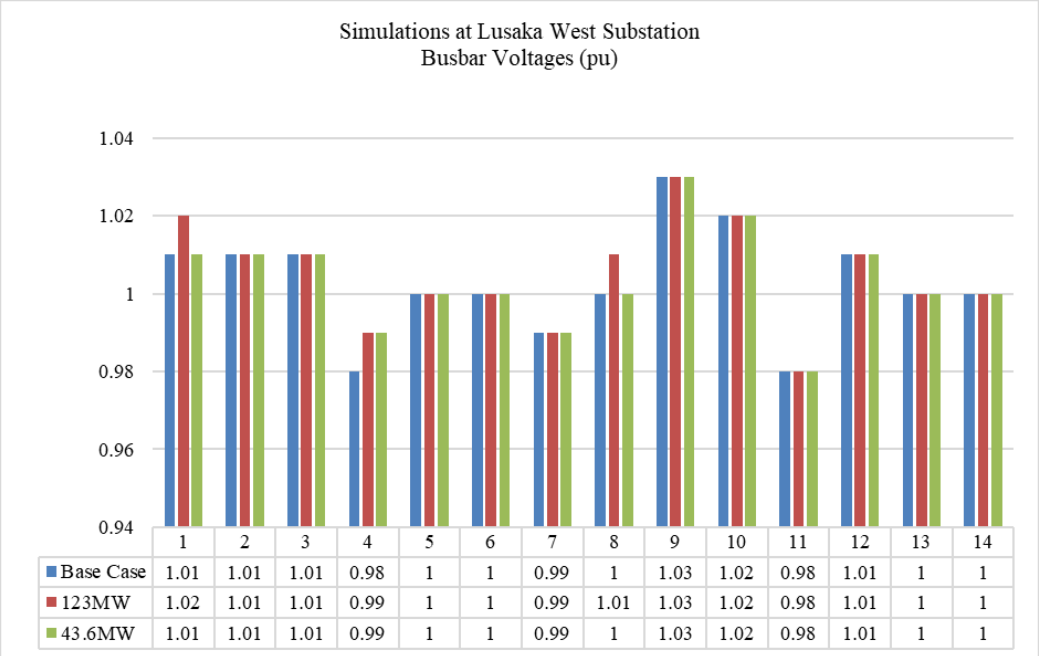

	1	2	3	4	5	6	7	8	9	10	11	12	13	14
Base Case	1.01	1.01	1.01	0.98	1	1	0.99	1	1.03	1.02	0.98	1.01	1	1
123MW	1.02	1.01	1.01	0.99	1	1	0.99	1.01	1.03	1.02	0.98	1.01	1	1
43.6MW	1.01	1.01	1.01	0.99	1	1	0.99	1	1.03	1.02	0.98	1.01	1	1

Fig 23: Per Unit Voltage Level for Selected Bus bars Solar injection at Lusaka West

Table 10 shows a summary of some of the parameters for selected transmission lines while Fig 24 and Fig 25 shows the graphical representation of the results.

Table 10: Transmission Line parameters at steady state for Lusaka West

Line ID	Line	Conductor Type	Length (km)	Line Loading (%)			Line Losses (MW)		
				Base	121MW	43.6MW	Base	121MW	43.6MW
1.	330kV Kabwe – Pensulo	2xBison	298	12.1	12.0	12.0	0.4	0.4	0.4
2.	330kV Kabwe – Kitwe	2xBison	211	37.9	37.8	37.9	5.1	5.1	5.1
3.	330kV Kabwe – Luano	2xBison	247	32.8	32.8	32.8	4.5	4.5	4.5
4.	330kV Kafue Gorge – Leopards Hill	2xBison	47	51.9	46.8	50.0	2.1	1.7	2.0
5.	330kV Kafue West – Lusaka West	2xBison	43	36.0	28.0	32.8	0.9	0.5	0.7
6.	330kV Kariba North – Leopards Hill	2xBison	123	31.0	31.2	31.1	2.0	2.0	2.0
7.	88kV Leopards Hill – Coventry Street	Wolf	7	13.5	9.7	12.1	0.0	0.0	0.0
8.	132kV Leopards Hill – Coventry Street	Wolf	28	56.0	31.1	46.7	1.1	0.3	0.8
9.	330kV Leopards Hill – Kabwe Step Down	2xBison	97	50.2	50.1	50.1	4.2	4.1	4.1
10.	132kV Leopards Hill – Roma	Wolf	28	56.4	35.8	48.7	1.0	0.4	0.8
11.	132kV Lusaka West – Coventry Street	Wolf	7	102	119.3	108	0.9	1.2	1.0
12.	330kV Lusaka West – Mumbwa	2xBison	134	10.4	10.4	10.4	0.1	0.1	0.1

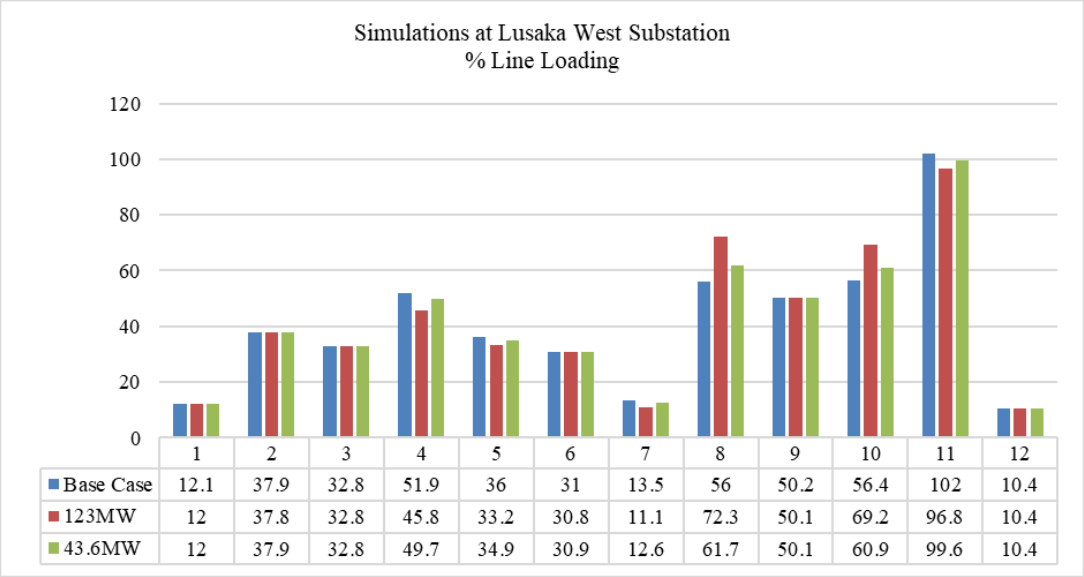

	1	2	3	4	5	6	7	8	9	10	11	12
Base Case	12.1	37.9	32.8	51.9	36	31	13.5	56	50.2	56.4	102	10.4
123MW	12	37.8	32.8	45.8	33.2	30.8	11.1	72.3	50.1	69.2	96.8	10.4
43.6MW	12	37.9	32.8	49.7	34.9	30.9	12.6	61.7	50.1	60.9	99.6	10.4

Fig 24: % Line Loading for solar injection at Lusaka West

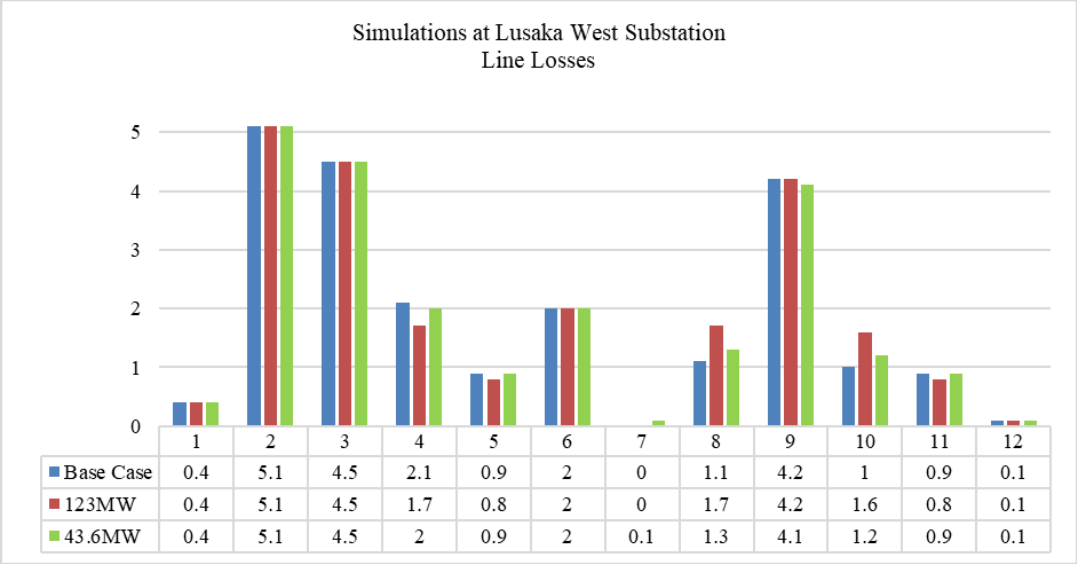

	1	2	3	4	5	6	7	8	9	10	11	12
Base Case	0.4	5.1	4.5	2.1	0.9	2	0	1.1	4.2	1	0.9	0.1
123MW	0.4	5.1	4.5	1.7	0.8	2	0	1.7	4.2	1.6	0.8	0.1
43.6MW	0.4	5.1	4.5	2	0.9	2	0.1	1.3	4.1	1.2	0.9	0.1

Fig 25: % Line Losses for Solar Injection at Lusaka West Substation

4.3.3. Injection of Solar PV at the 66 kV Pensulo Substation

Arising from the studies conducted at Leopards Hill and Lusaka West Substations, the 298 km 330 kV transmission line between Kabwe and Pensulo was identified to manifest more oscillatory amplitudes even when other feeders had attained voltage and power flow stability.

Fig 26 shows the voltages oscillations characteristic of the Kabwe – Pensulo 330 kV transmission.

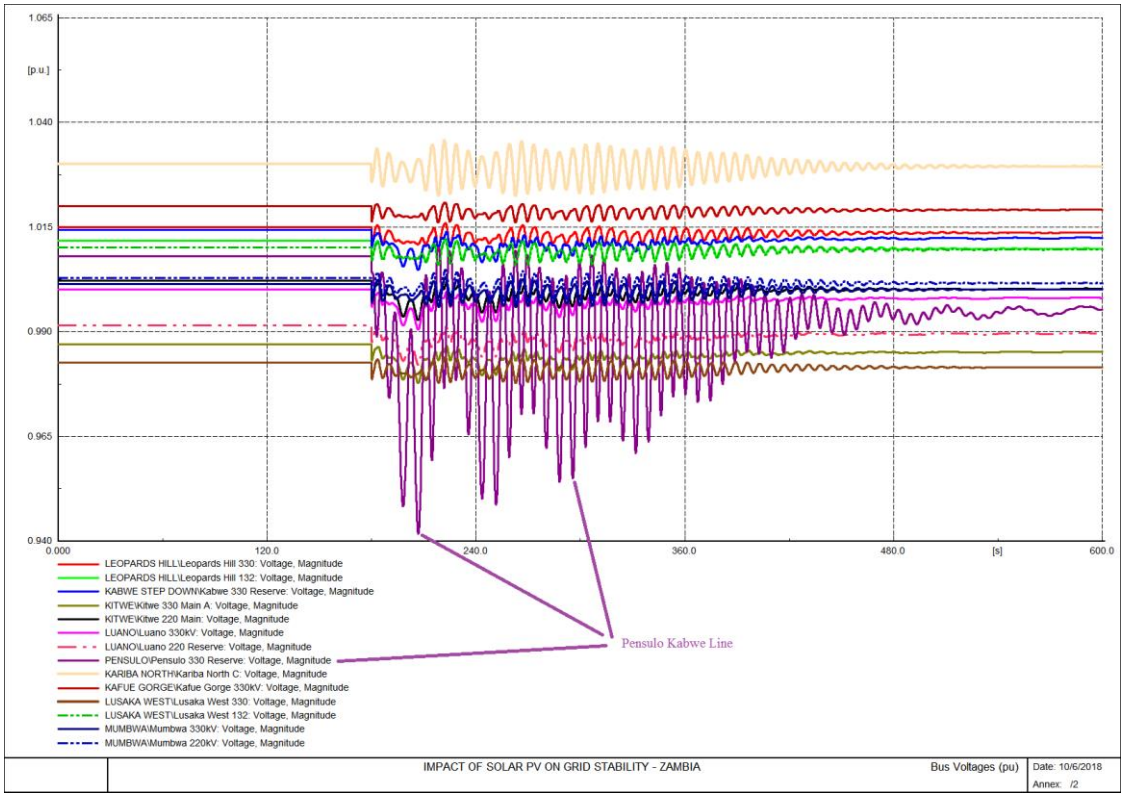

Fig 26: Voltage Oscillations on the 330 kV Kabwe – Pensulo Transmission line

Arising from the findings in Fig 26, the Pensulo substation became a point of interest for the injection of a Solar PV power plant. Other than the characteristic oscillations manifested on the Kabwe – Pensulo line, there are a number of renewable power projects that have been proposed near Pensulo that may impact on the stability of the grid. Further, the Government of Zambia has plans to construct an additional 330 kV line from Pensulo towards Mansa through the proposed Mumbotuta Hydroelectric Power Projects on the Luapula River. Thus, Pensulo substation proved to be node worth investigating. The system at Pensulo substation was modelled as shown in Fig 27.

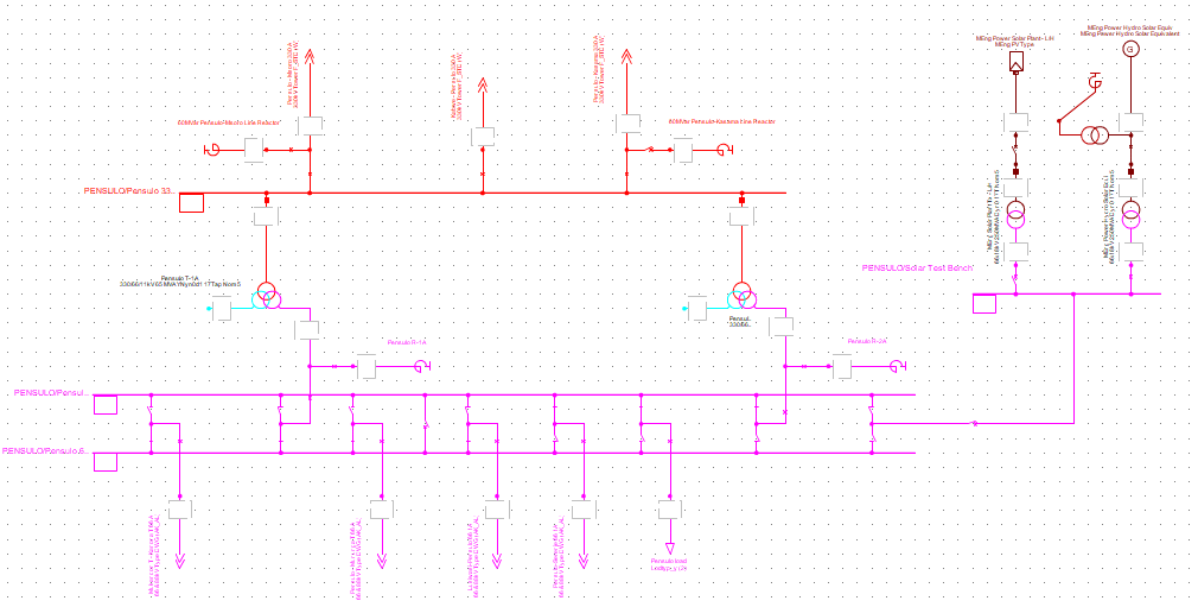

Fig 27: DIgSILENT model of the Pensulo Substation

In the case of Pensulo substation, the maximum Solar PV plant was found to be 130 MW representing a 240 % addition loading on the 66 kV busbar and a corresponding 30 % additional loading on the 330 kV busbar. The simulation of 130 MW on the 66 kV Pensulo substation resulted in reversed power flows of about 73.8 MW towards Kabwe. Fig 28 shows the reverse power flows on the Kabwe - Pensulo line.

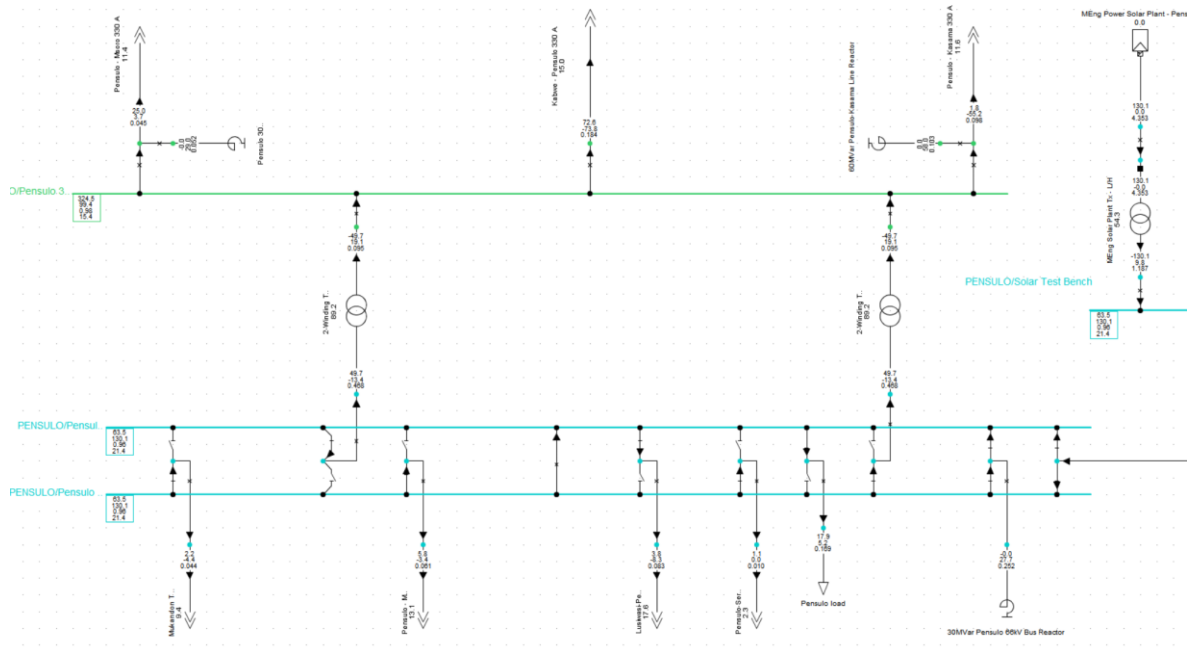

Fig 28: Reversed power flows on the 330 kV Kabwe Pensulo Line

When a total loss of generation for a Solar PV power plant at the 66 kV Pensulo Substation was simulated, system stability was achieved at 49.6 MW which is 51.3 % of additional loading on the 66 kV busbar and 11 % reduction in the load on the 330 kV busbar.

Table 11shows some of the voltage levels obtained during the simulation of a Solar PV generating plant at the 66 kV Pensulo bus bar. The results may be presented graphically as shown in Fig 29.

Table 11: Per Unit Voltage for Selected Busbars for Solar PV Injection at Pensulo

S/N	Busbar	Voltage (pu)		
		Base	130MW	43.6MW
1	330kV Leopards Hill	1.01	1.02	1.01
2	132kV Leopards Hill	1.01	1.01	1.01
3	330kV Kabwe Step Down	1.01	1.01	1.01
4	330kV Kitwe	0.98	0.99	0.99
5	220kV Kitwe	1.00	1.00	1.00
6	330kV Luano	1.00	1.00	1.00
7	220kV Luano	0.99	0.99	0.99
8	330kV Pensulo	1.00	1.01	1.00
9	330kV Kariba North	1.03	1.03	1.03
10	330kV Kafue Gorge	1.02	1.02	1.02
11	330kV Lusaka West	0.98	0.98	0.98
12	132kV Lusaka West	1.01	1.01	1.01
13	330kV Mumbwa	1.00	1.00	1.00
14	220kV Mumbwa	1.00	1.00	1.00

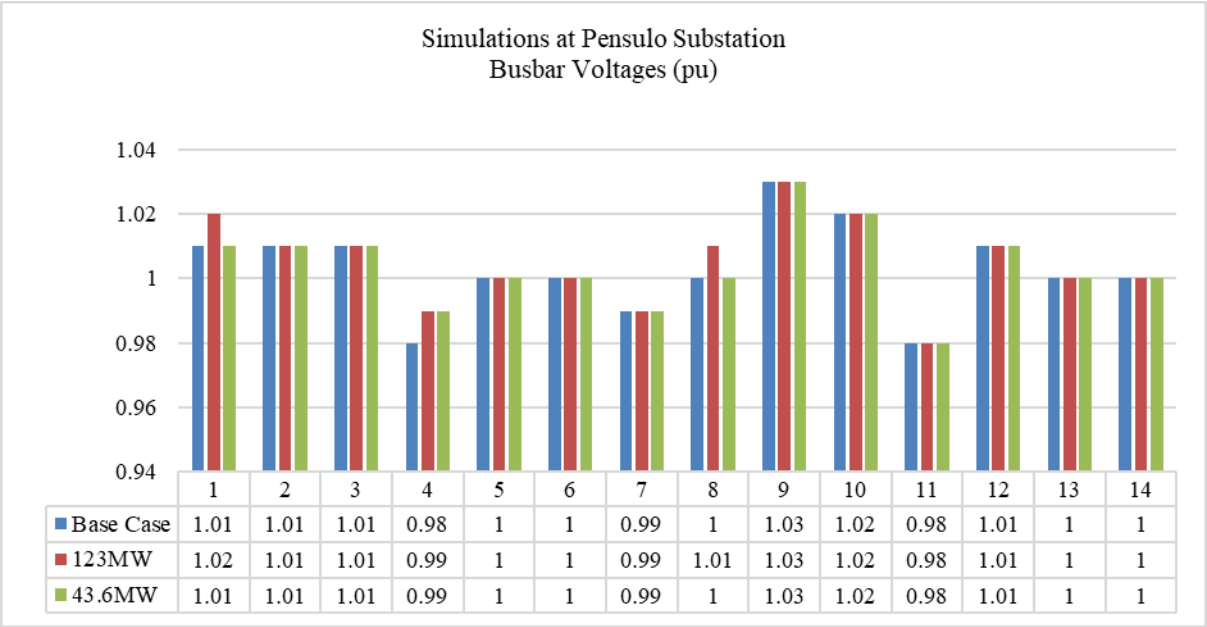

	1	2	3	4	5	6	7	8	9	10	11	12	13	14
Base Case	1.01	1.01	1.01	0.98	1	1	0.99	1	1.03	1.02	0.98	1.01	1	1
123MW	1.02	1.01	1.01	0.99	1	1	0.99	1.01	1.03	1.02	0.98	1.01	1	1
43.6MW	1.01	1.01	1.01	0.99	1	1	0.99	1	1.03	1.02	0.98	1.01	1	1

Fig 29: Per Unit Voltage Level for Selected Bus bars Solar injection at Pensulo

Table 12 shows a summary of some of the parameters for selected transmission lines while Fig 30 and Fig 31 shows the graphical representation of the results.

Table 12: Steady state transmission line parameters for solar injection at Pensulo

Line ID	Line	Conductor Type	Length (km)	Line Loading %			Line Losses (MW)		
				Base	130MW	49.5MW	Base	130MW	49.5MW
1.	330kV Kabwe – Pensulo	2xBison	298	12.1	14.3	8.7	0.4	0.5	0.0
2.	330kV Kabwe – Kitwe	2xBison	211	37.9	37.6	37.6	5.1	5.0	5.0
3.	330kV Kabwe – Luano	2xBison	247	32.8	32.7	32.7	4.5	4.4	4.4
4.	330kV Kafue Gorge – Leopards Hill	2xBison	47	51.9	44.5	49.0	2.1	1.6	2.0
5.	330kV Kafue West – Lusaka West	2xBison	43	36.0	35.6	35.8	0.9	0.9	0.9
6.	330kV Kariba North – Leopards Hill	2xBison	123	31.0	30.5	30.7	2.0	1.9	2.0
7.	88kV Leopards Hill – Coventry Street	Wolf	7	13.5	13.7	13.5	0.0	0.0	0.0
8.	132kV Leopards Hill – Coventry Street	Wolf	28	56.0	57.0	56.3	1.1	1.1	1.1
9.	330kV Leopards Hill – Kabwe Step Down	2xBison	97	50.2	44.1	47.9	4.2	3.2	3.8
10.	132kV Leopards Hill – Roma	Wolf	28	56.4	57.3	56.7	1.0	1.1	1.1
11.	132kV Lusaka West – Coventry Street	Wolf	7	102	100.9	101.4	0.9	0.9	0.8
12.	330kV Lusaka West – Mumbwa	2xBison	134	10.4	10.4	10.4	0.1	0.1	0.1

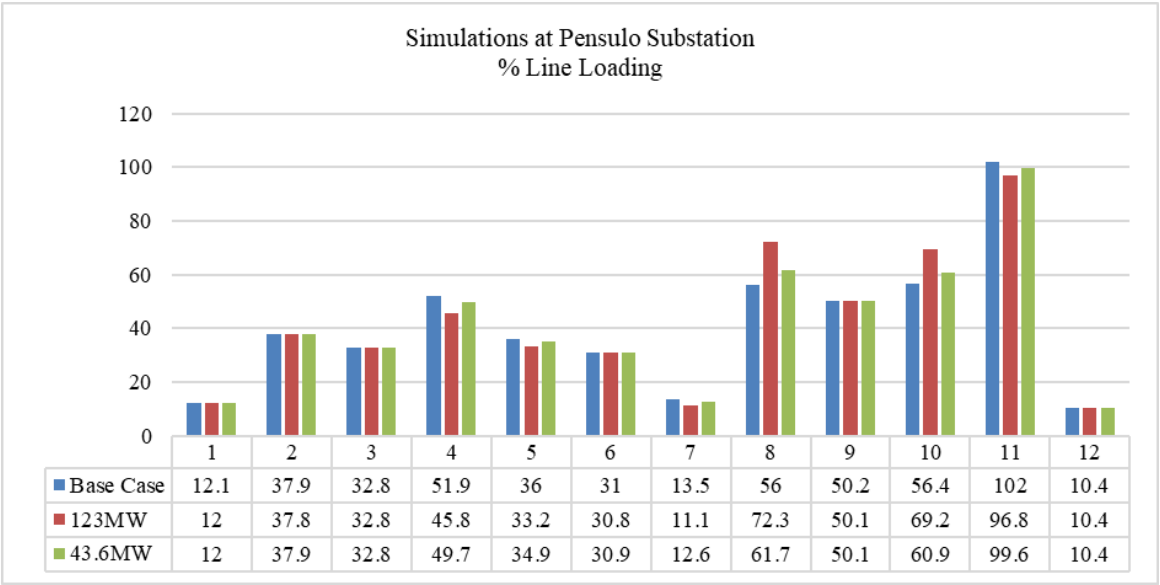

	1	2	3	4	5	6	7	8	9	10	11	12
Base Case	12.1	37.9	32.8	51.9	36	31	13.5	56	50.2	56.4	102	10.4
123MW	12	37.8	32.8	45.8	33.2	30.8	11.1	72.3	50.1	69.2	96.8	10.4
43.6MW	12	37.9	32.8	49.7	34.9	30.9	12.6	61.7	50.1	60.9	99.6	10.4

Fig 30: % Line Loading for solar injection at Pensulo Substation

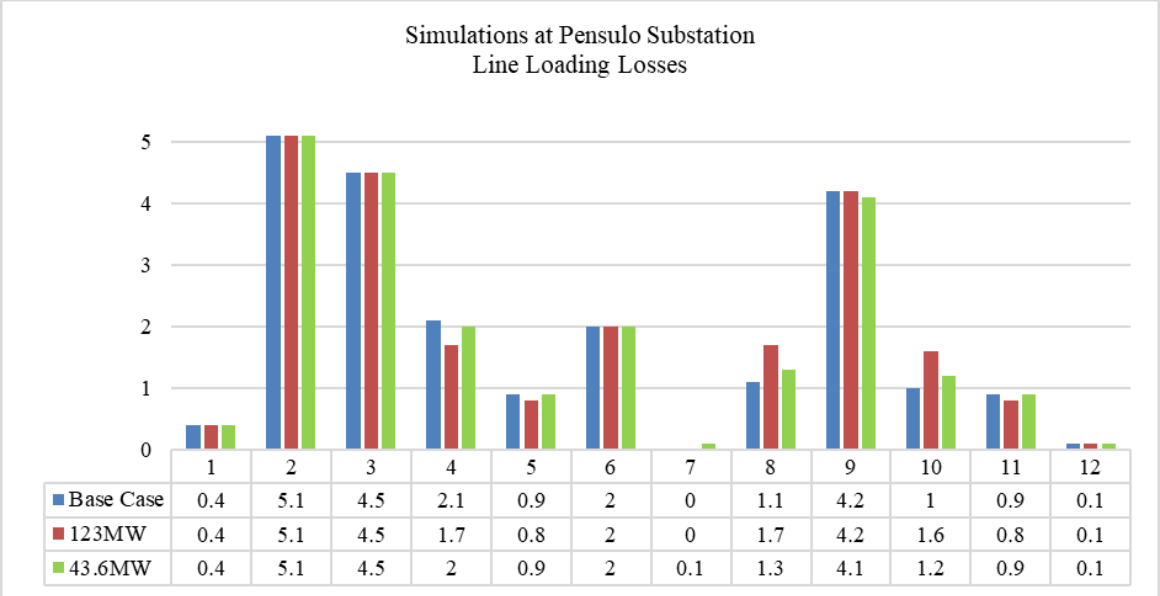

	1	2	3	4	5	6	7	8	9	10	11	12
Base Case	0.4	5.1	4.5	2.1	0.9	2	0	1.1	4.2	1	0.9	0.1
123MW	0.4	5.1	4.5	1.7	0.8	2	0	1.7	4.2	1.6	0.8	0.1
43.6MW	0.4	5.1	4.5	2	0.9	2	0.1	1.3	4.1	1.2	0.9	0.1

Fig 31: Line Losses for Solar injection at Pensulo Substation

4.4. Comparison of Solar PV Plant with Equivalent Rotational Plant

The simulations provided in 4.3 were repeated with a hydro equivalent plant. This was done in order to ascertain the performance of a conventional power plant considering similar conditions of operation as were under solar generation.

4.4.1. Hydro Equivalent Plant at the 132 kV Leopards Hill Busbar

On the Leopards Hill 132 kV busbar, voltage and power flow stability was achieved at around 120 MW of hydroelectric generation representing a 24.6 % of additional MVA loading on the 132 kV busbar and a 7.2 % reduction on the 330 kV busbar. This is depicted in Fig 32.

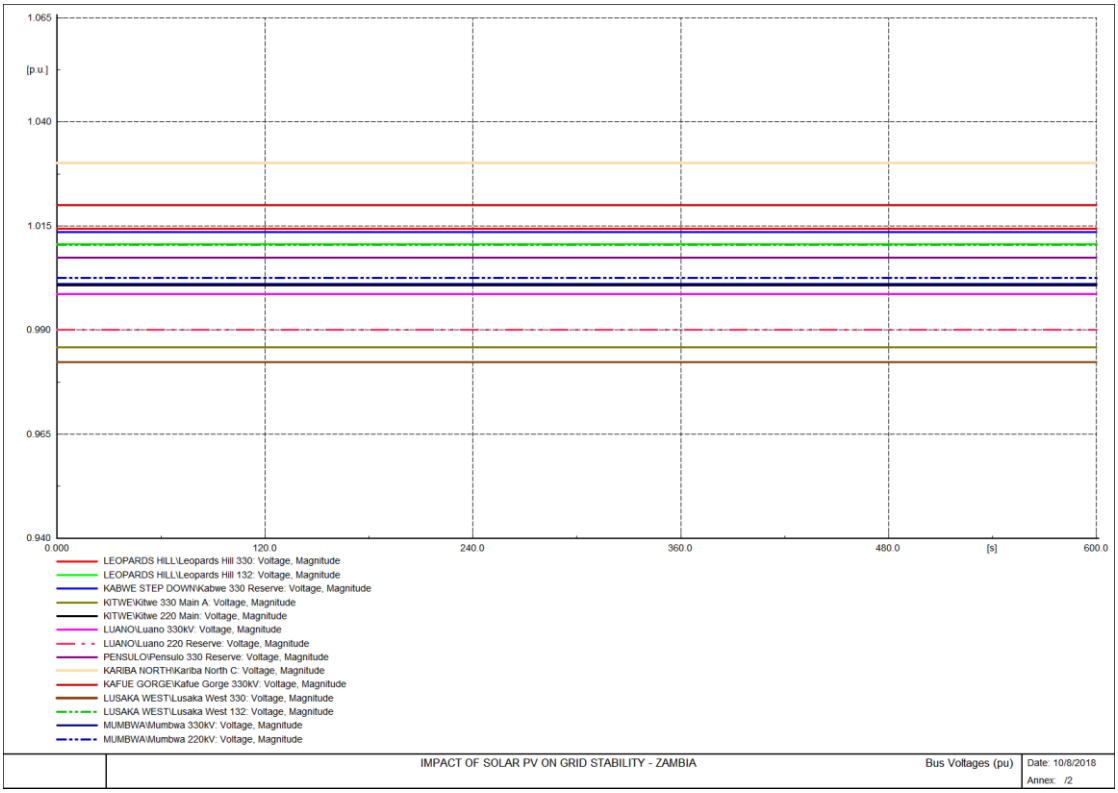

Fig 32: Voltage Levels (pu) for 120 MW Hydro Equivalent at L/Hill 132 kV

The simulation of a total loss of 43.6 MW power generation resulted in system collapse after 108s. Normally, 108s is sufficient time for system operators to institute measures to return stability of a hydroelectric plant, however, for purposes of this study, set operation boundaries of the system were prioritised. It should be noted that under the solar simulation, the system was able to retain voltage and power flow stability with a loss of 43.6 MW.

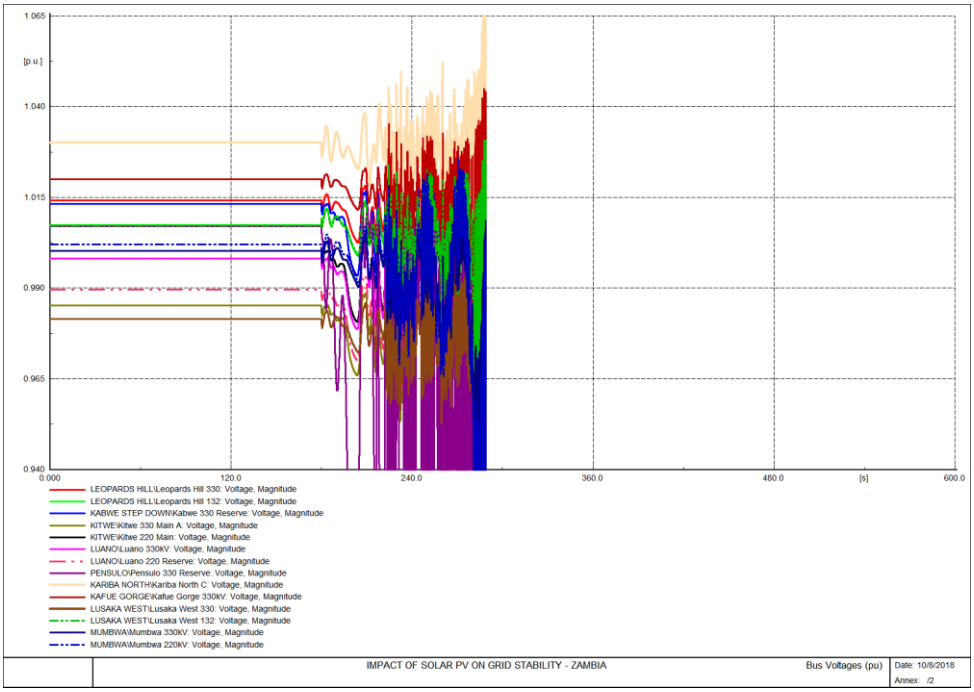

Fig 33: Voltage Level (pu) for 43.6MW Hydro Equivalent Switch off at L/Hill 132 kV

Further iterations of lower capacity hydroelectric power plants revealed that the system was able to return voltage and power flow stability only with a total loss of generation of 36 MW representing a 7.3 % of additional MVA loading on the 132 kV busbar and a 2.1 % reduction on the 330 kV busbar. Fig 34 illustrates system performance under 36 MW loss of hydro generation at the 132 kV Leopards Hill Substation.

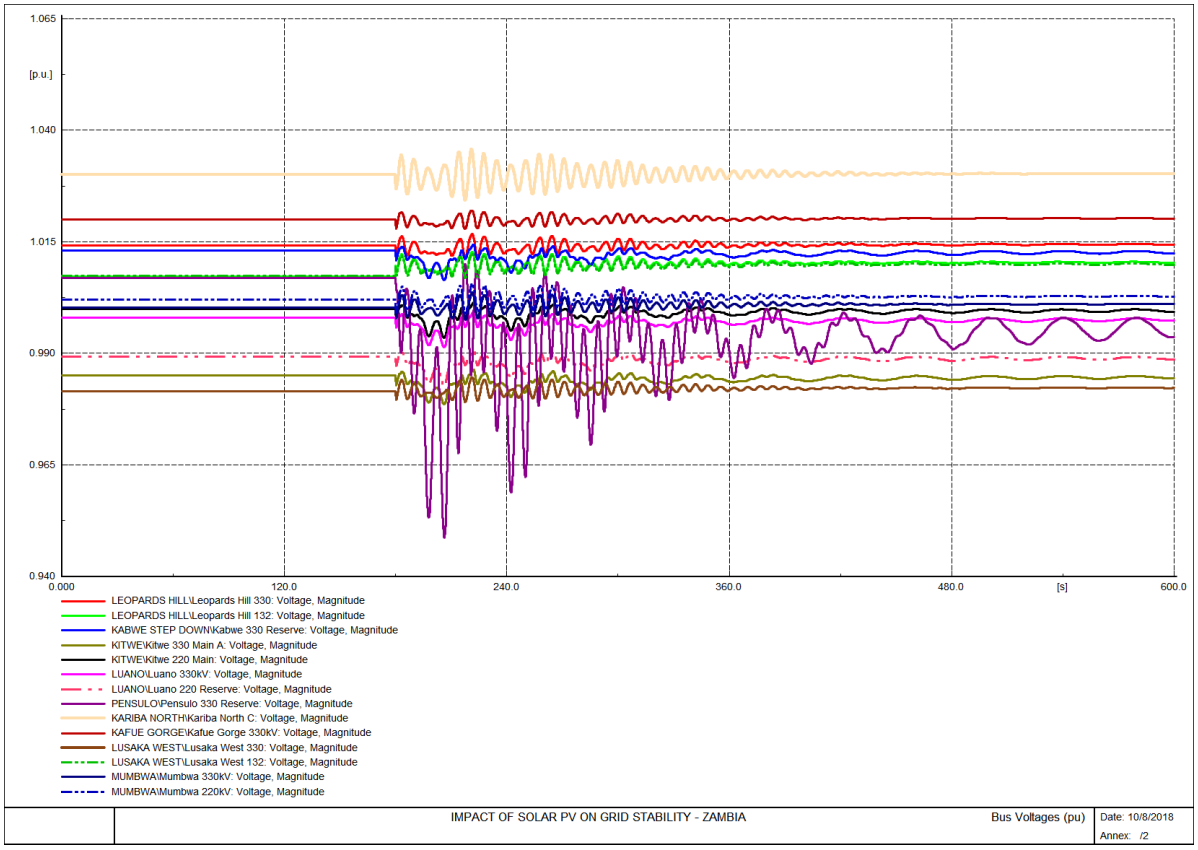

Fig 34: Voltage Level (pu) for 36MW Hydro Equivalent Switch off at L/Hill 132 kV

For the same conditions at the 132 kV Leopards Hill bus bar, the Solar PV power plant could deliver up to 123 MW (26 % maximum additional loading) and 43.6 MW (9.2 % for system stability as loss of power generation) in comparison with the hydro plant that could deliver 120 MW (24.6 % maximum additional loading) and 36 MW (7.3 % for system stability at loss of power generation).

The per unit busbar volage, line loading and line losses for the hydro-equivalent model compared to the Solar PV inject at Leopards Hill are shown in Fig 35, Fig 36 and Fig 37 respectively.

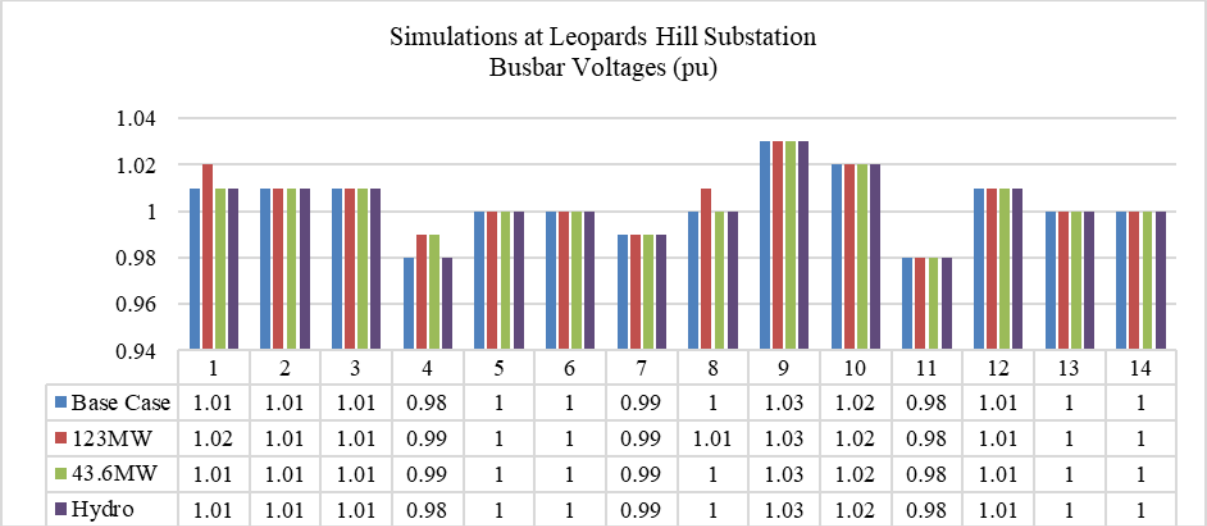

	1	2	3	4	5	6	7	8	9	10	11	12	13	14
Base Case	1.01	1.01	1.01	0.98	1	1	0.99	1	1.03	1.02	0.98	1.01	1	1
123MW	1.02	1.01	1.01	0.99	1	1	0.99	1.01	1.03	1.02	0.98	1.01	1	1
43.6MW	1.01	1.01	1.01	0.99	1	1	0.99	1	1.03	1.02	0.98	1.01	1	1
Hydro	1.01	1.01	1.01	0.98	1	1	0.99	1	1.03	1.02	0.98	1.01	1	1

Fig 35: Per Unit Voltage Level for Selected Bus bars with hydro-equivalent model

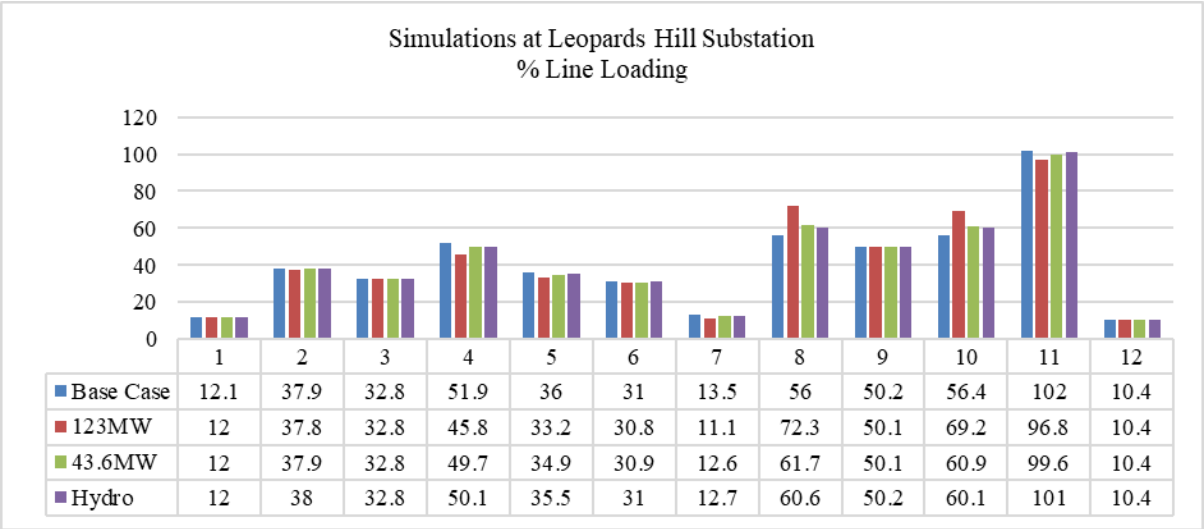

	1	2	3	4	5	6	7	8	9	10	11	12
Base Case	12.1	37.9	32.8	51.9	36	31	13.5	56	50.2	56.4	102	10.4
123MW	12	37.8	32.8	45.8	33.2	30.8	11.1	72.3	50.1	69.2	96.8	10.4
43.6MW	12	37.9	32.8	49.7	34.9	30.9	12.6	61.7	50.1	60.9	99.6	10.4
Hydro	12	38	32.8	50.1	35.5	31	12.7	60.6	50.2	60.1	101	10.4

Fig 36: % Line Loading for Selected Lines with hydro-equivalent model

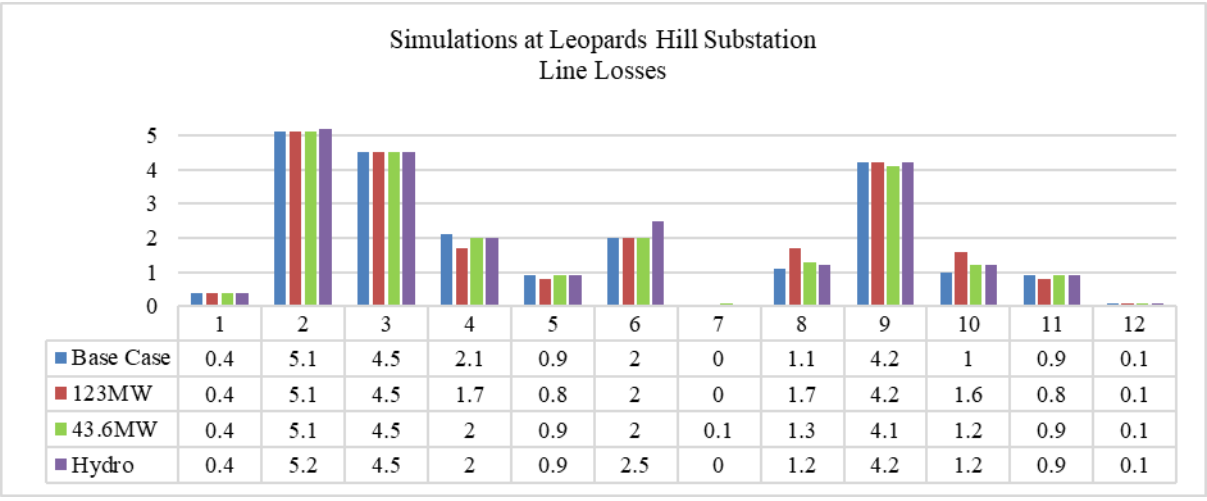

	1	2	3	4	5	6	7	8	9	10	11	12
Base Case	0.4	5.1	4.5	2.1	0.9	2	0	1.1	4.2	1	0.9	0.1
123MW	0.4	5.1	4.5	1.7	0.8	2	0	1.7	4.2	1.6	0.8	0.1
43.6MW	0.4	5.1	4.5	2	0.9	2	0.1	1.3	4.1	1.2	0.9	0.1
Hydro	0.4	5.2	4.5	2	0.9	2.5	0	1.2	4.2	1.2	0.9	0.1

Fig 37: MW Line Losses for Selected Lines with hydro-equivalent model

4.4.2. Hydro equivalent plant at the 132 kV Lusaka West Busbar

On the 132 kV Lusaka West busbar, voltage and power flow stability were achieved at around 123 MW representing a 14 % of additional MVA loading on the 132 kV busbar and a 21 % reduction on the 330 kV busbar. This is depicted in Fig 38.

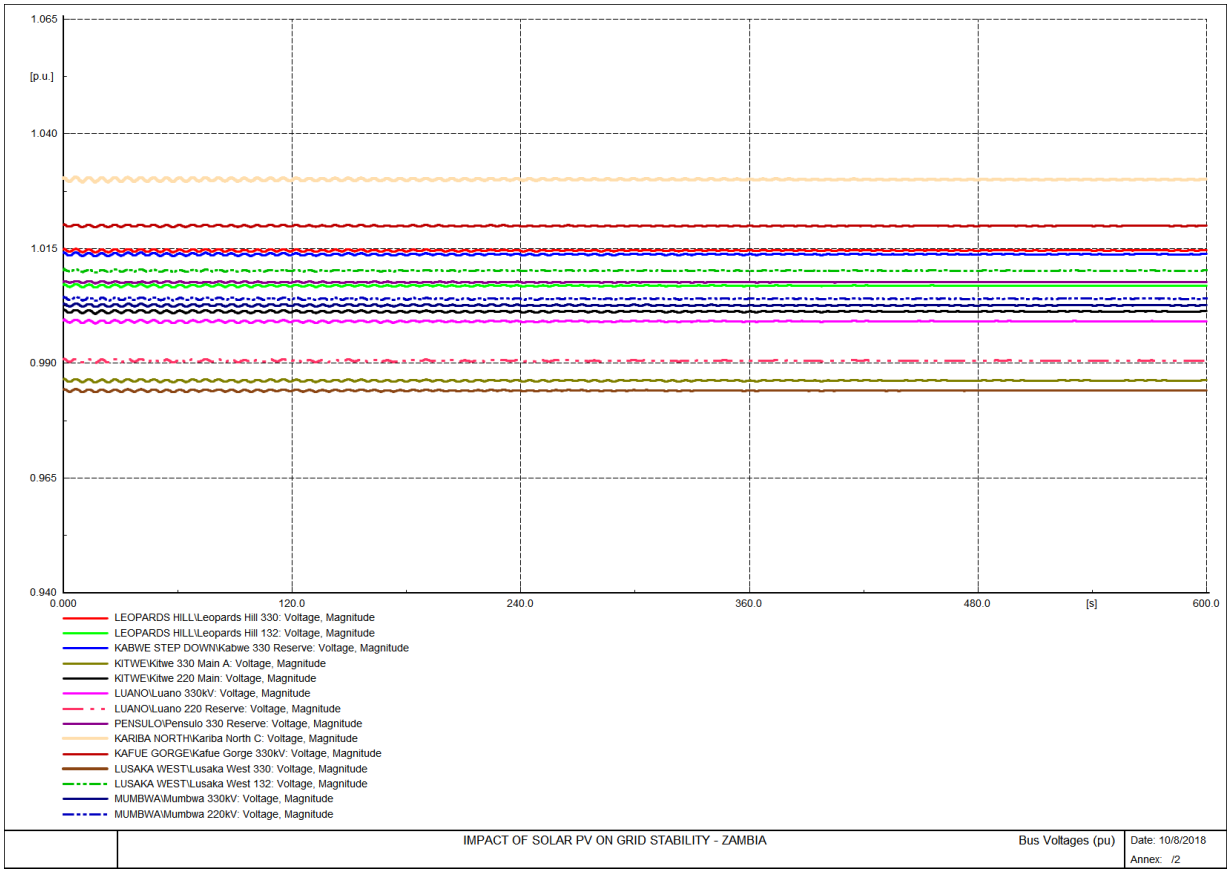

Fig 38: Voltage levels (pu) for 123MW Hydro Equivalent at Lusaka West 132 kV

For a 123 MW hydro plant at the 132 kV Lusaka West busbar, a total loss of generation resulted in high amplitude oscillations leading to total system blackout.

Further iterations of lower capacity hydroelectric power plants revealed that the system was able to return stability with a total loss of hydro generation of up to 36 MW representing about 4 % of additional MVA loading on the 132 kV busbar and about 7 % reduction on the 330 kV busbar. The system behaviour for a 36 MW loss of hydroelectric power generation at the 66 kV Lusaka West is illustrated in Fig 39.

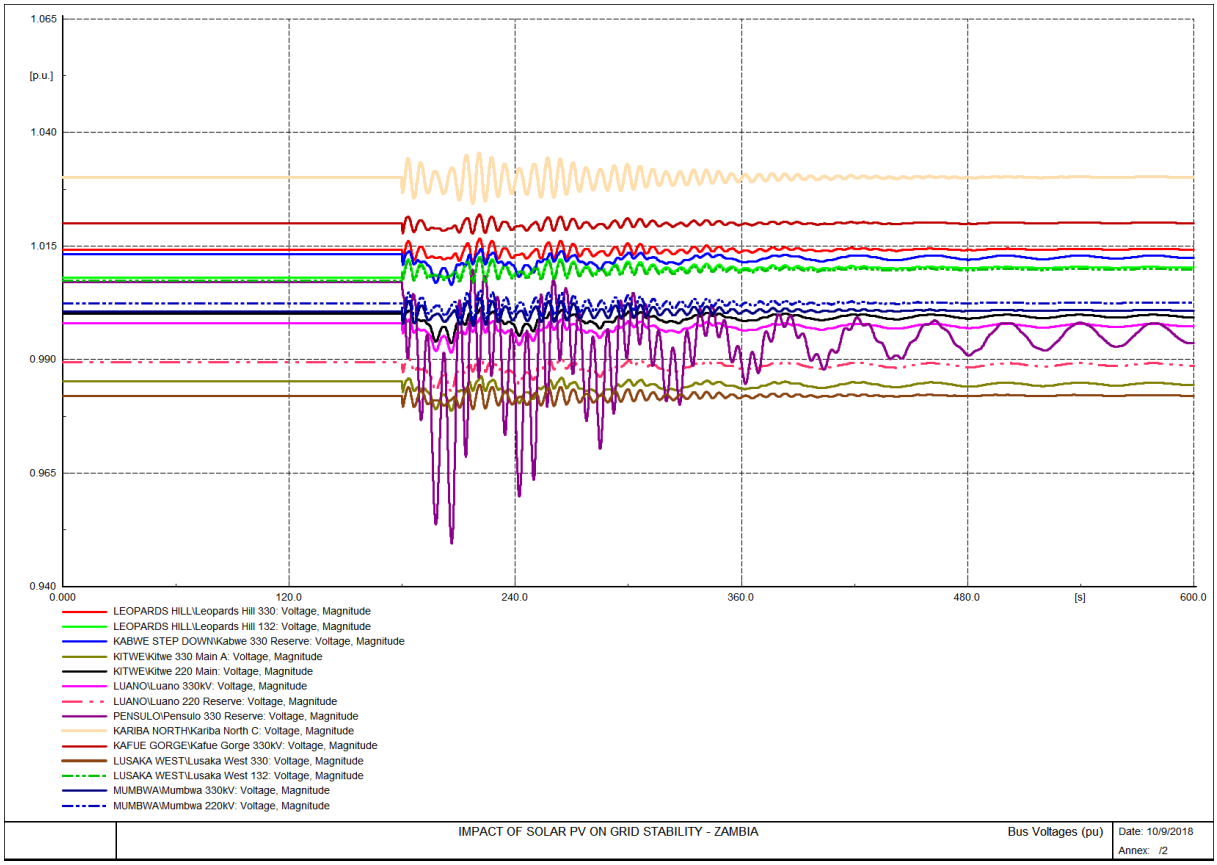

Fig 39: Voltage Level (pu) for 36 MW Hydro Equivalent Switch off at LW 132 kV

For the same conditions at the 132 kV Lusaka West bus bar, the Solar PV power plant could deliver up to 121 MW (31.5 % maximum additional loading) and 43.6 MW (11.5 % for system stability as loss of power generation) in comparison with the hydroelectric plant that could deliver 123 (31.5 % maximum additional loading) and 43.6 MW (11.5 % for system stability as loss of power generation).

The per unit busbar voltage, line loading and line losses for the hydro-equivalent model compared to the Solar PV inject at Lusaka West are shown in Fig 40, Fig 41 and Fig 42 respectively.

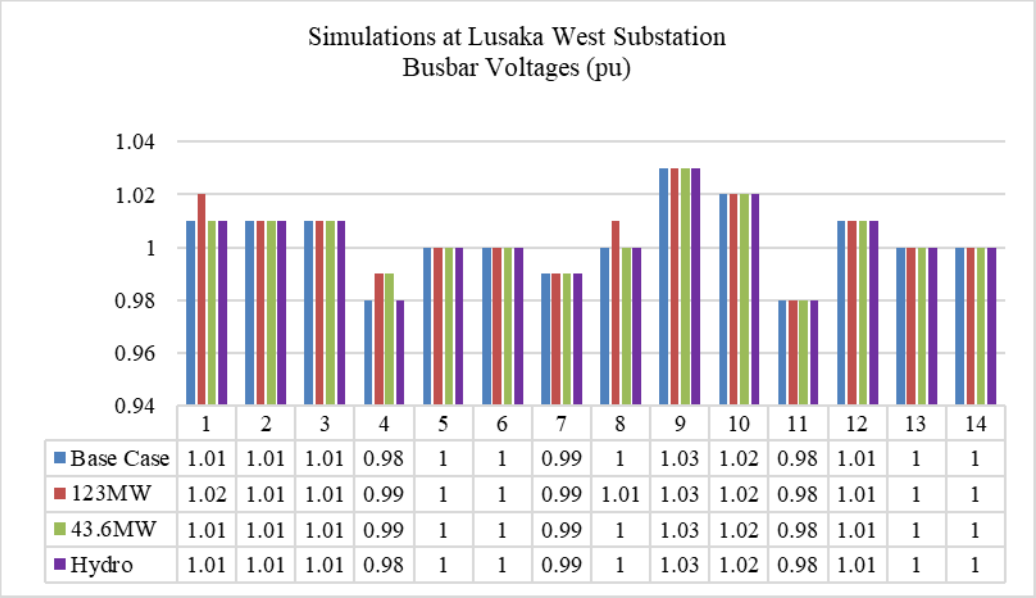

	1	2	3	4	5	6	7	8	9	10	11	12	13	14
Base Case	1.01	1.01	1.01	0.98	1	1	0.99	1	1.03	1.02	0.98	1.01	1	1
123MW	1.02	1.01	1.01	0.99	1	1	0.99	1.01	1.03	1.02	0.98	1.01	1	1
43.6MW	1.01	1.01	1.01	0.99	1	1	0.99	1	1.03	1.02	0.98	1.01	1	1
Hydro	1.01	1.01	1.01	0.98	1	1	0.99	1	1.03	1.02	0.98	1.01	1	1

Fig 40: Per Unit Voltage Level for Selected Bus bars with hydro-equivalent model

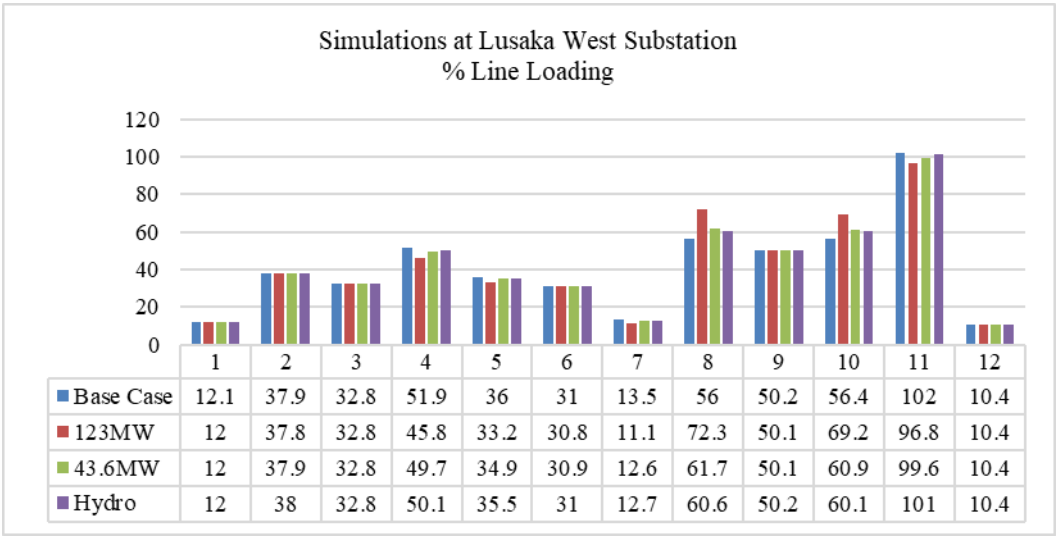

	1	2	3	4	5	6	7	8	9	10	11	12
Base Case	12.1	37.9	32.8	51.9	36	31	13.5	56	50.2	56.4	102	10.4
123MW	12	37.8	32.8	45.8	33.2	30.8	11.1	72.3	50.1	69.2	96.8	10.4
43.6MW	12	37.9	32.8	49.7	34.9	30.9	12.6	61.7	50.1	60.9	99.6	10.4
Hydro	12	38	32.8	50.1	35.5	31	12.7	60.6	50.2	60.1	101	10.4

Fig 41: % Line Loading for Selected Lines with hydro-equivalent model

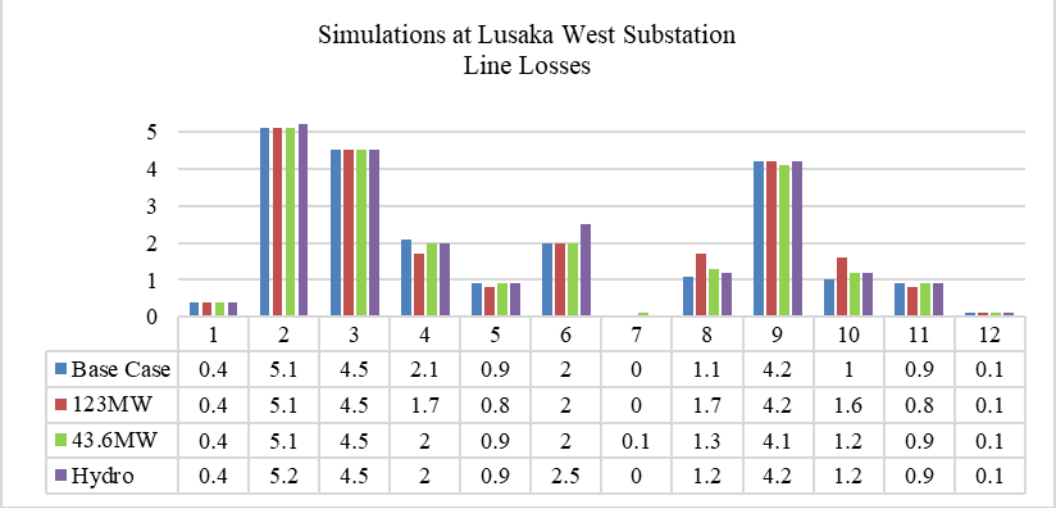

	1	2	3	4	5	6	7	8	9	10	11	12
Base Case	0.4	5.1	4.5	2.1	0.9	2	0	1.1	4.2	1	0.9	0.1
123MW	0.4	5.1	4.5	1.7	0.8	2	0	1.7	4.2	1.6	0.8	0.1
43.6MW	0.4	5.1	4.5	2	0.9	2	0.1	1.3	4.1	1.2	0.9	0.1
Hydro	0.4	5.2	4.5	2	0.9	2.5	0	1.2	4.2	1.2	0.9	0.1

Fig 42: MW Line Losses for Selected Lines with hydro-equivalent model

4.4.3. Hydro equivalent plant at the 66 kV Pensulo Busbar

On the 66 kV busbar at Pensulo busbar, voltage and power flow stability were achieved at around 130 MW as the maximum for an equivalent hydroelectric power plant. This is depicted in Fig 43.

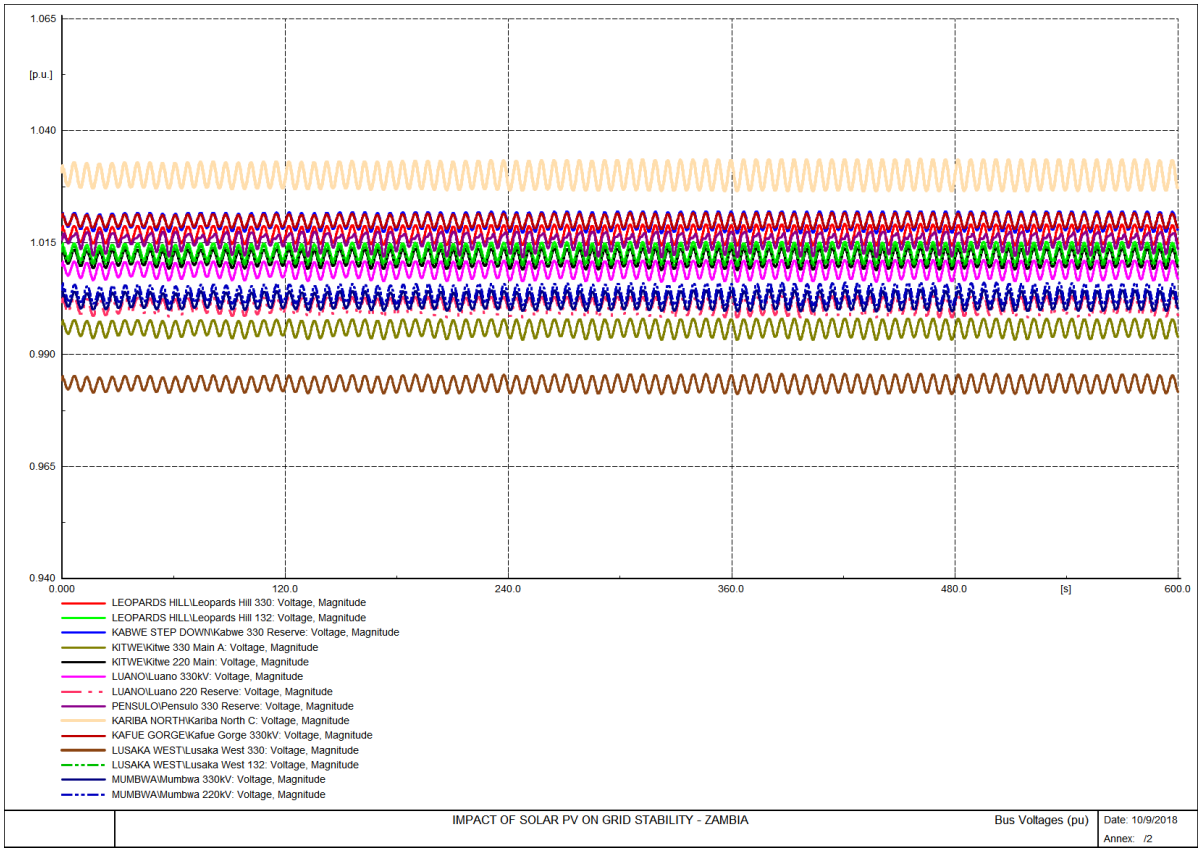

Fig 43: Voltage Level (pu) for 130 MW Hydro Equivalent at Pensulo 66 kV

The injection of a 130 MW hydroelectric power plant at the 66 kV Pensulo busbar resulted in 240 % of additional MVA loading on the 66 kV busbar and a 40 % additional load on the 330 kV Pensulo busbar. As in the case of the Solar PV plant in Fig 28, the simulation of 130 MW of hydroelectric plant on the 66 kV Pensulo substation resulted in reversed power flows of about 72.7 MW towards Kabwe.

The simulation of a total loss of the 130 MW hydroelectric power plant at the 66 kV Pensulo busbar resulted in system collapse as given in Fig 44.

Further iterations of lower capacity hydroelectric power plants revealed that the system was able to return voltage and power flow stability only with a total loss of generation of 50 MW representing a 35 % of additional MVA loading on the 66 kV Pensulo busbar and a 40 % reduction on the 330 kV busbar. The graphical representation of the performance of the system under a 50 MW loss of hydro generation at the 66 kV Pensulo busbar is shown in Fig 45.

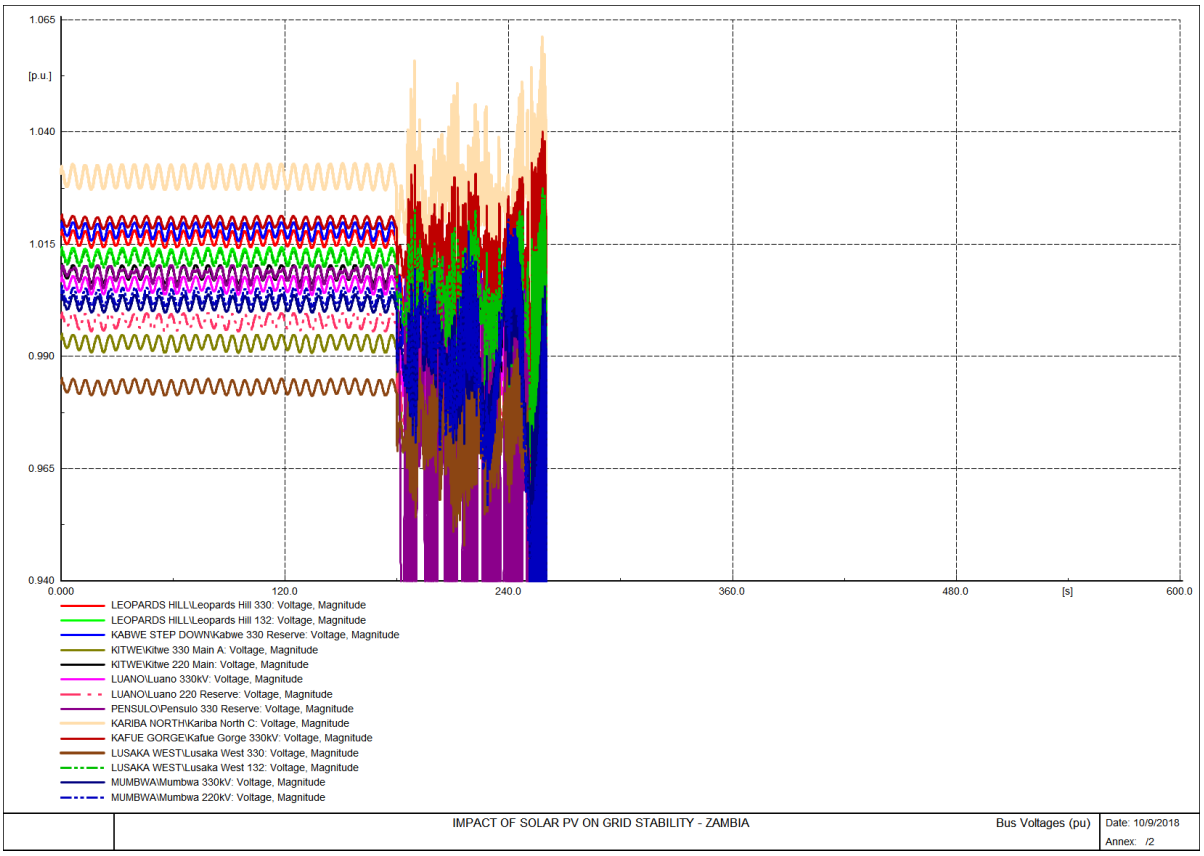

Fig 44: Voltage Level (pu) for 130MW Solar PV Plant Switch off at Pensulo 66kV

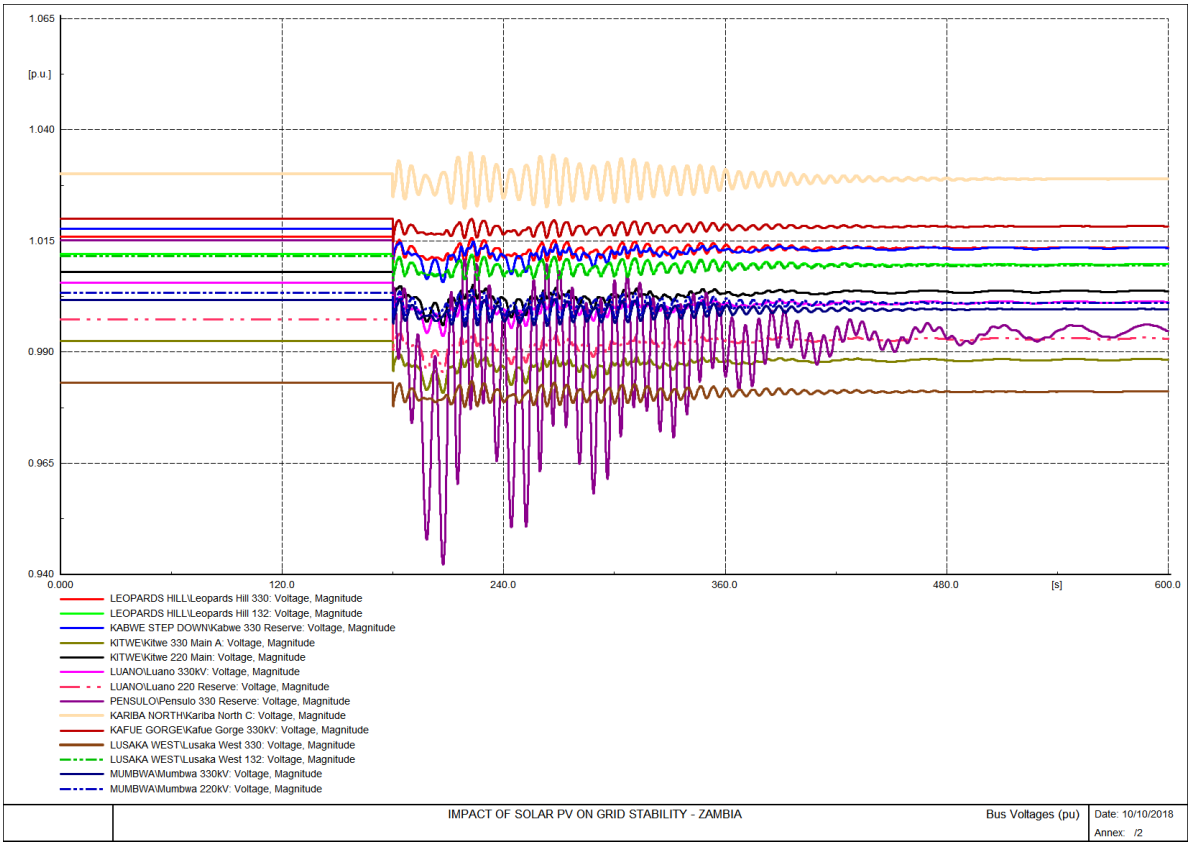

Fig 45: Voltage Level (pu) for 50MW Hydro Equivalent Plant Switch off at Pensulo

For the same conditions at the 66 kV Leopards Hill bus bar, both the Solar PV power plant and the hydroelectric power plant could deliver up to 130 MW (240% maximum additional loading) while for system stability with loss of generation, the Solar PV power plant could deliver 49.6 MW compared to 50 MW from the hydroelectric plant.

4.5. Summary of Results

A summary of the results can be given as in Table 13, Table 14 and Table 15 below:

Table 13: Per Unit Voltage Results at Selected Busbars

S/N	Busbar	Base case	Leopards Hill - Voltage (pu)			Lusaka West - Voltage (pu)			Pensulo - Voltage (pu)		
			123MW	43.6MW	Hydro	121MW	43.6MW	Hydro	130MW	43.6MW	Hydro
1	330kV Leopards Hill	1.01	1.02	1.01	1.01	1.02	1.01	1.01	1.02	1.01	1.01
2	132kV Leopards Hill	1.01	1.01	1.01	1.01	1.01	1.01	1.01	1.01	1.01	1.01
3	330kV Kabwe	1.01	1.01	1.01	1.01	1.01	1.01	1.01	1.01	1.01	1.01
4	330kV Kitwe	0.98	0.99	0.99	0.98	0.99	0.99	0.98	0.99	0.99	0.98
5	220kV Kitwe	1.00	1.00	1.00	1.00	1.00	1.00	1.00	1.00	1.00	1.00
6	330kV Luano	1.00	1.00	1.00	1.00	1.00	1.00	1.00	1.00	1.00	1.00
7	220kV Luano	0.99	0.99	0.99	0.99	0.99	0.99	0.99	0.99	0.99	0.99
8	330kV Pensulo	1.00	1.01	1.00	1.00	1.01	1.00	1.00	1.01	1.00	1.00
9	330kV Kariba North	1.03	1.03	1.03	1.03	1.03	1.03	1.03	1.03	1.03	1.03
10	330kV Kafue Gorge	1.02	1.02	1.02	1.02	1.02	1.02	1.02	1.02	1.02	1.02
11	330kV Lusaka West	0.98	0.98	0.98	0.98	0.98	0.98	0.98	0.98	0.98	0.98
12	132kV Lusaka West	1.01	1.01	1.01	1.01	1.01	1.01	1.01	1.01	1.01	1.01
13	330kV Mumbwa	1.00	1.00	1.00	1.00	1.00	1.00	1.00	1.00	1.00	1.00
14	220kV Mumbwa	1.00	1.00	1.00	1.00	1.00	1.00	1.00	1.00	1.00	1.00

Maximum Voltage Recorded	1.03	Recorded on the 330 kV Kariba North busbar, this is the set Voltage at the Busbar
Minimum Voltage Recorded	0.98	Recorded on the 330 kV Lusaka West Substation, this is the pre-existing voltage level.

Table 14: Penetration Level at the Busbars

No.	**Injection Point**	**Maximum Injection**		**Injection for System Self Stability**	
		Solar PV	Hydro	Solar PV	Hydro
1.	132 kV Leopards Hill	123 MW	126 MW	43.6 MW	36 MW
		25.5%	24.6%	9.2%	7.3%
2.	132 kV Lusaka West	121 MW	123.1 MW	43.6 MW	36 MW
		31.5%	14.0%	11.5%	4.0%
3.	66 kV Pensulo	130 MW	132 MW	49.5 MW	50 MW
		240%	240%	51.3%	35%

Maximum injection for system stability: 51.3% of Solar PV on the 66 kV Pensulo Busbar.

Minimum injection for system stability: 7.3% of Hydro on the 132 kV Leopards Hill busbar.

Table 15: Per Unit Voltage Results at Selected Busbars

S/N	Line	Conductor Type	Length (km)	Base case	Leopards Hill (MW)			Lusaka West (MW)			Pensulo (MW)		
					123MW	43.6MW	Hydro	123MW	43.6MW	Hydro	130MW	49.5MW	Hydro
1	330kV Kabwe – Pensulo	2xBison	298	0.4	0.4	0.4	0.4	0.4	0.4	0.4	0.4	0.4	0.4
2	330kV Kabwe – Kitwe	2xBison	211	5.1	5.1	5.1	5.2	5.1	5.1	5.2	5.1	5.1	5.2
3	330kV Kabwe – Luano	2xBison	247	4.5	4.5	4.5	4.5	4.5	4.5	4.5	4.5	4.5	4.5
4	330kV Kafue Gorge – Leopards Hill	2xBison	47	2.1	1.7	2.0	2.0	1.7	2.0	2.0	1.7	2.0	2.0
5	330kV Kafue West – Lusaka West	2xBison	43	0.9	0.8	0.9	0.9	0.8	0.9	0.9	0.8	0.9	0.9
6	330kV Kariba North – Leopards Hill	2xBison	123	2.0	2.0	2.0	2.5	2.0	2.0	2.5	2.0	2.0	2.5
7	88kV Leopards Hill – Coventry Street	Wolf	7.0	0.0	0.0	0.1	0.0	0.0	0.1	0.0	0.0	0.1	0.0
8	132kV Leopards Hill – Coventry Street	Wolf	28	1.1	1.7	1.3	1.2	1.7	1.3	1.2	1.7	1.3	1.2
9	330kV Leopards Hill – Kabwe Step Down	2xBison	97	4.2	4.2	4.1	4.2	4.2	4.1	4.2	4.2	4.1	4.2
10	132kV Leopards Hill – Roma	Wolf	28	1.0	1.6	1.2	1.2	1.6	1.2	1.2	1.6	1.2	1.2
11	132kV Lusaka West – Coventry Street	Wolf	7.0	0.9	0.8	0.9	0.9	0.8	0.9	0.9	0.8	0.9	0.9
12	330kV Lusaka West – Mumbwa	2xBison	134	0.1	0.1	0.1	0.1	0.1	0.1	0.1	0.1	0.1	0.1

Maximum additional losses at system self-stability operating point: +0.5 MW on 330 kV Leopards Hill Kariba line for hydrogeneration on any of the three injection points

5. CONCLUSIONS AND RECOMMENDATIONS

This chapter provides the conclusion and recommendations arising from the study. The chapter also gives insights on further research to be undertaken in order to fully scale up the integration of utility-scale renewable energy power plants on to the Zambia National Grid.

5.1. Conclusions

The investigation for the impact of Solar PV power generation on the system stability of the Zambia National Grid was carried out and the conclusions and contributions arising from this investigation are outlined below:

5.1.1. Impact on the Stability of the Zambia National Grid

The injection of Solar PV power onto the national grid results in oscillatory behaviour depending on (1) the quantity (MW) of the injected solar power, (2) the nature of the injection point with respect to its location in the grid (electrical characteristics, geographical dispersion) and (3) the operating conditions of the injection point at the time of injecting the Solar PV power; and

The spontaneous loss of generation from a Solar PV power plant has more impacts than the switching on of the same power plant. Mostly because in functional grids, a startup may be carried out following a controlled or standard startup operational procedure whereas a loss of generation may be triggered by weather conditions or system faults which are out of human control and are normally too fast for legacy control systems to respond.

5.1.2. Solar PV Power Injected at Specific Points on The Zambian Grid

The study observed that:

1. It is possible to inject Solar PV power generation of about 123 MW represents 26% additional loading on the 132 kV Leopards Hill busbar and 121 MW representing 31.5% of additional loading on the 132 kV Lusaka West busbar. The Pensulo substation is able to take in about 130 MW of variable power generation representing 240% additional loading on the 66 kV Pensulo busbar.

   These penetration levels may need to be supported by additional equipment to provide ancillary services for frequency control, spinning reserves and operating reserves.to ensure grid stability. This then proposes additional costs in the implementation of Solar PV power projects.

2. A complete loss of generation of the scale of Solar PV plants presented in (1) above would result in both voltage and power flow instabilities on the respective busbars and

transmission lines leading to the total collapse of the entire system in each non-cumulative case, where ancillary services are not provided.

3. The Zambia National Grid is able to autonomously retain stability following a complete loss of smaller quantities of Solar PV generation. For both the 132 kV Leopards and 132 kV Lusaka West busbars, this value of Solar PV generation that would result in such system stability is limited at around 43.6 MW representing a 24.6% and 14% additional loading on the respective busbars. For the 66 kV Pensulo busbar, system stability is attained at 49.5 MW solar generation representing 35% additional loading on the busbar.

   The reduced levels of Solar PV penetration in the magnitude of 50 MW per plant have minimal impacts on the interconnected Zambian Grid provided the total loss of power generation does not occur simultaneously.

   The results obtained for Leopards Hill and Lusaka West may not be surprising considering that the substations are in close proximity to each other. For the magnitude and scale of the Zambian grid, the two substations may be considered as identical point electrically and therefore the difference in the results between the two should be minimal.

4. The injection of Solar PV power at a given point on the grid influences the transmission loss depending on the prevailing direction of flow for power. Were the injection of Solar PV increases the loading of a given line, it follows then that the losses on that line would increase. Were the Solar PV plant unloads a given line, then the losses on such a line will reduce.

   The maximum additional loading recorded in the study was +0.6 MW when Solar PV power above 120 MW was injected at any of the three study points for the Leopards Hill Coventry 132 kV line. However, for system stability, the additional loading was recorded at +0.5 MW for the Kariba North – Leopards Hill 330 kV line.

5.1.3. Comparison of Solar PV Plant with Equivalent Rotational Plant

1. The study observed that Solar PV power had comparable stability characteristics with that of a rotational power plant. With either Solar PV or equivalent hydro generation. The pu voltage for selected busbars experienced marginal variations from the base case scenario.

   Voltage variation in the magnitude of ±0.01pu was observed with the highest voltage level recorded on the 330 kV busbar Kariba North Bank with 1.03pu and the lowest voltage level recorded on the 330 kV busbar at Lusaka West with 0.98pu. From the study model and indeed from normal operations by ZESCO, the 330 kV busbar at

Kariba North is intentionally kept at 1.03pu voltage while the Kafue Gorge is set at 1.02pu for purposes of power transfer.

The 0.98pu recorded on the 330 kV bus at Lusaka West was pre-existing and therefore may not be influenced by either generation technologies except in an instance where the ancillary services are installed to make the busbar at the desired voltage.

Secondly, the two-generation technologies have marginal differences in percentage loading that retains system stability in either case. Fig 46 shows a comparison of the system loading with Solar PV and hydropower generation.

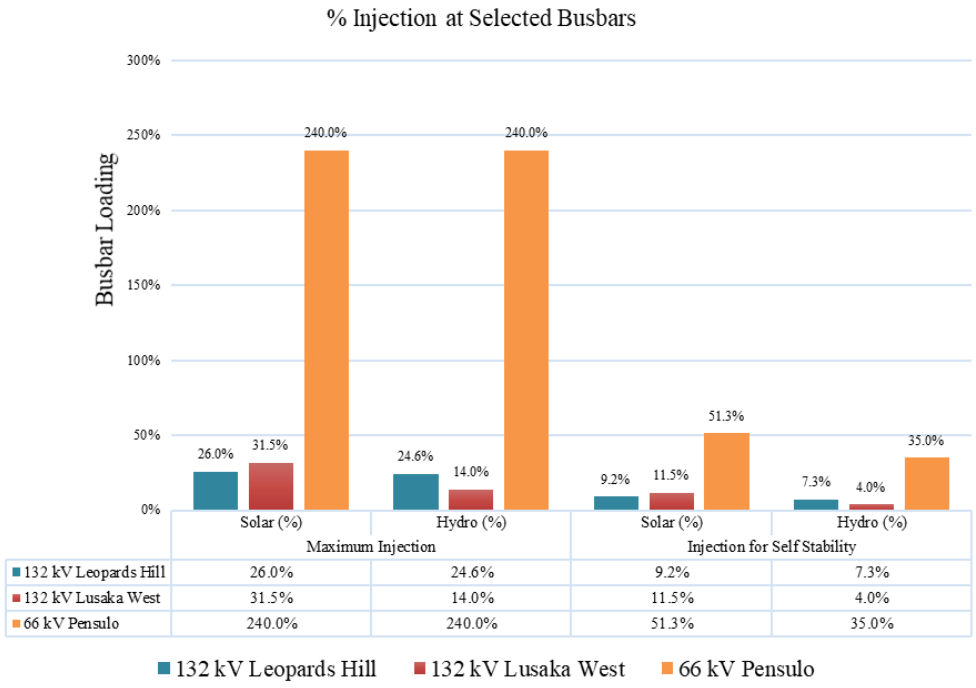

Fig 46: summary of % injection levels on identified busbars

Thirdly, the differences in the system losses attributed to either Solar PV generation or hydropower generation were minimal.

2. The major challenge and common to both Solar PV and hydropower technologies is the requirement for replacement power to sustain existing loads. This replacement power is normally required at very fast rates at which conventional system protection and control mechanism are unable to operate. The protection and control mechanisms then detect an abnormal operating condition thereafter triggering a system shut down.

   The requirement for reactive power support can be addressed through newer technologies such as synthetic inertia and other smart grid mitigation measures against low inertia discussed in 2.5.2. Conventional ancillary services such as spinning reserve and capacitor/reactor compensation technologies that already exist on the grid could be

employed to support a system with high penetration levels of variable renewable power generation.

3. The comparison between Solar PV and Rotational Plant on a MW per MW basis suggests that the Solar PV power plant may possess comparably superior stability characteristics to the rotational plant. However, this may not be the case owing to the reactive power component present in the rotation power plant and normally absent in the Solar PV power plant. This entails the system has to accommodate a higher MVA rating in the case of a rotational power plant.

5.2. Recommendations

5.2.1. Recommendations

Renewable energy generation will form an integral part of future power grids. This will mainly be driven by the scarcity and depletion of conventional power generation resources such as water for hydropower generation and coal, nuclear and petroleum for thermal power plants.

The determination for a transition to renewable energy development has already been demonstrated by world development bodies and lending institution through their sustainable development policies that are fixated on prioritizing funding for renewable energy developments. It is therefore prudent that:

1. Developing countries like Zambia realign their policies to scale up the implementation of renewable energy technologies thereby harnessing the cheaper development funding available on the financial market;

2. Considerations are made to modify the current legislation and grid codes that were developed for conventional power generation so as to enable flexibility in the design, construction and operations of future power infrastructure; and

3. The electricity industry players such as utilities and regulators should refine the so-called Best Operating Practices and policies that are based on high inertial power generators to accommodate the low inertia renewable energy technologies.

5.2.2. Further Studies

Further studies can be carried on the impact of Solar PV power generation on the power quality of the system taking into account some of the critical loads on the network such as electrowinning and copper smelting facilities. This can be done taking into account the detailed design of a solar PV plant and the effects of changes in insolation

.

6. REFERENCES

1. Andreas. U., Theodre, S. B., and Andersson, G. (2014). Impact of Low Rotational Inertia on Power System Stability and Operation. Zurich, Switzerland: ETH Power Systems Laboratory, p.1. p.8. p. 11
2. Ayhan, D. (2006). Global Renewable Energy Resources, Energy Sources Part A: Recovery, Utilization, and Environmental impacts. Ed, 779-792, Milton Park: Taylor and Francis.
3. De Marco, C. (2012). Primary and secondary control for high penetration renewables. Madison-Wisconsin, USA: Power Systems Engineering Research Centre, p.7
4. Delille, G., François, B., and Malarange, G., Dynamic frequency control support: A virtual inertia provided by distributed energy storage to isolated power systems. 2010 IEEE PES Innovative Smart Grid Technologies Conference Europe (ISGT Europe), Gothenberg, 2010, pp. 1-8. doi:10.1109/ISGTEUROPE.2010.5638887
5. DIgSILENT GmbH, (2018). DIgSILENT PowerFactory Version 2018 – User Manual. Gomaringen, Germany, DIgSILENT GmbH, p.1091.
6. Ela, E. and O'Malley, M. (2012). Studying the Variability and Uncertainty of Variable Generation at Multiple Timescales. IEEE Transactions on Power Systems (27:3), pp. 1324-1333.
7. Ela, E. et al. (2013). Impacts of Variability and Uncertainty in Solar Photovoltaic Generation at Multiple Timescales. Denver, USA. National renewable energy laboratory. p.1.
8. ENTSO-E. (2013). Network code for requirements for grid connection applicable to all generators. Technical Report, ENTSO, March 2013
9. ERB, (2019) Energy Sector Report 2019. Energy Regulation Board, Lusaka
10. Fares, R. (2015). Renewable Energy Intermittency Explained: Challenges, Solutions, and Opportunities. Viewed 11 June 2019<https://blogs.scientificamerican.com/plugged-in/renewable-energy-intermittency-explained-challenges-solutions-and-opportunities/>
11. Franke, A. (2016). Building Political Support for a Clean Energy Transition - How arguments on solar power affect public support in Germany and the US How arguments on solar power affect public support in the US and Germany, energy transition, Washington, DC – USA. Heinrich-Böll-Stiftung North America.
12. Gonzalez-Longatt, F., Chikuni, E and Rashayi, E. (2013). Effects of the Synthetic Inertia from wind power on the total system inertia after a frequency disturbance. 2013 IEEE International Conference on Industrial Technology (ICIT), Cape Town. pp. 826-832. doi: 10.1109/ICIT.2013.6505779
13. Holttinen, H. et al. (2009). Design and operation of power systems with large amounts of wind power. Final Report, Phase one 2006-2008. IEA WIND Task 25. Espoo: VTT. http://www.vtt.fi/inf/pdf/tiedotteet/2009/T2493.pdf.
14. IEA. (2018). World Energy Outlook - 2017, International Energy Agency, Paris France
15. IEA. (2020). Electricity Information – Statistics Report 2020, International Energy Agency, Paris France

16. IEEE Task Force Report. (1982). Proposed terms and definitions for power system stability. IEEE Trans. Power Apparatus and Systems, vol. PAS-101, pp. 1894–1897, July 1982.
17. IEEE/CIGRE Joint Task Force on Stability Terms and Definitions, "Definition and Classification of Power System Stability", IEEE Trans. on Power Syst., Vol. 19, No. 2, pp. 1387-1400, May 2004.
18. International Energy Agency. (2018). Renewables Information Renewables Information (2018 edition)2018. Paris, France. 2018 International Energy Agency (IEA). p.xii
19. Irena. (2013). Zambia Renewables Readiness Assessment 2013. Dubai-UAE: International Renewable Energy Agency (Irena). p.15
20. Karlsson Björn (2013) Comparison of PSSE & PowerFactory, Teknisk-naturvetenskaplig fakultet UTH-enheten, Uppsala, Sweden
21. Kumar, B.K. (2014) Power System Stability and Control. Chennai, India. Indian Institute of Technology Madras. P.1.1
22. Kundur, P. et al., (2004). Definition and classification of power system stability IEEE/CIGRE joint task force on stability terms and definitions. IEEE Transactions on Power Systems, vol. 19, no. 3, pp. 1387-1401, Aug. 2004. doi: 10.1109/TPWRS.2004.825981
23. Kundur, P. (1994). Power system stability and control. New York. McGraw-Hill Inc.
24. Mills, A. et al., (2009). Understanding Variability and Uncertainty of Photovoltaics for Integration with the Electric Power System. Berkeley, USA: Berkeley National Laboratory, p.1
25. Mukund R. P. (2006). Wind and Solar Power Systems: Design, Analysis, and Operation. 2nd Ed. New York, USA: Taylor and Francis. p.163.
26. Oudalov, A., Chartouni, D. and Ohler C. (2007). Optimising a battery energy storage system for primary frequency control. IEEE Transactions on Power Systems, Vol. 22, Issue 3, pp. 1259-1266, Aug. 2007. doi: 10.1109/TPWRS.2007.901459
27. Perez, R. et al. (2009). Validation of short and medium term operational solar radiation forecasts in the US. In: Proceedings SES Annual Conference. Buffalo, New York.
28. Rycroft, M. (2017). Synthetic inertia in grids with a high renewable energy content. EE Publishers, viewed 06 July 2019, https://www.ee.co.za/article/synthetic-inertia-grids-high-renewable-energy-content.html
29. Tielens, P. and Van Hertem, D. (2012). Grid inertia and frequency control in power systems with high penetration of renewables. Young Researchers Symposium in Electrical Power Engineering, Delft, vol. 6, April 2012. p.5
30. UNDP 2019, Sustainable Development Goals, UNDP, viewed 07.07.2019, http://www.undp.org/content/undp/en/home/sustainable-development-goals/goal-7-affordable-and-clean-energy.html
31. Wikipedia. (2019). List of photovoltaic power stations. Viewed 11 June 2019 https://en.wikipedia.org/wiki/List_of_photovoltaic_power_stations.
32. Xinhuanet (2021) http://www.xinhuanet.com/english/2020-09/23/c_139388774.htm

7. APPENDICES

7.1. Appendix 1: Utility Scale Solar PV Technology

1. Background

This Appendix 1 gives some of the technologies employed in solar power systems and how the various technologies may interact with the existing grid.

2. Photovoltaic technology and systems

2.1. Solar PV modules

The basic element of a PV System is the photovoltaic (PV) cell or Solar Cell. Solar cells are generally several square centimetres in size and are made of semiconductor materials which have four valence electrons in the outer shell. The material that is used widely in the industry for the production of photovoltaic cells is silicon. A typical solar cell is shown in Fig 1 below.

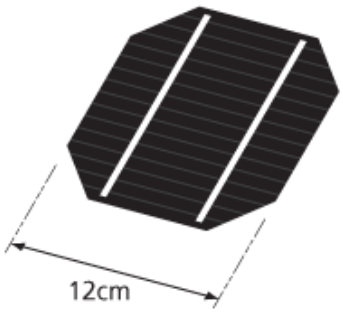

Fig 1: PV / Solar Cell made of Mono-crystalline Silicon
http://www.samlexsolar.com/learning-center/solar-cell-module-array.aspx

When a solar cell is exposed to light, photons in the sunlight will excite electrons in the semiconductor and the negatively charged electrons and the positively charged holes separate. This yields a voltage across the photovoltaic module and current flows through a connected load. This phenomenon is termed as the photovoltaic effect and is depicted in Fig 2 below;

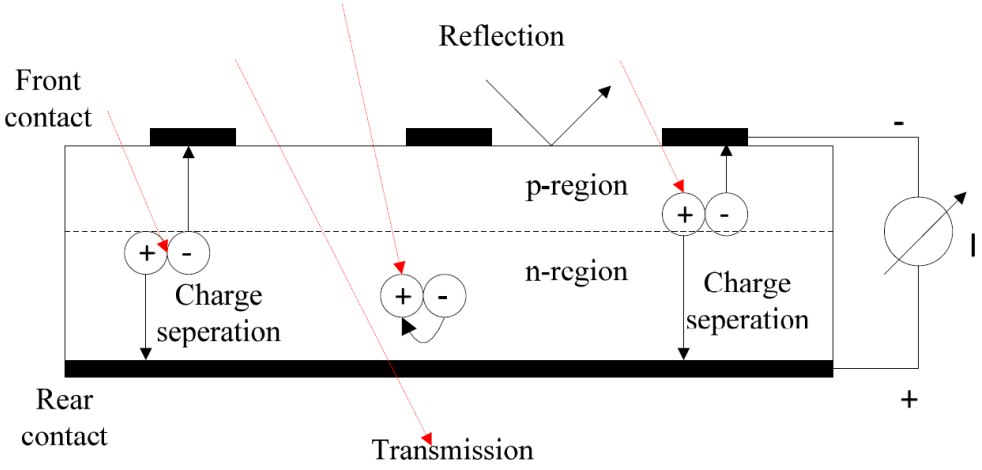

Fig 2: The Photovoltaic Effect (Mukund, 2006)

In order to harness the photovoltaic effect, a number of individual PV cells are interconnected together in a sealed, weatherproof package called a Panel or Module. For a desired output, a number of modules are then wired in alternating series and parallel configuration into what is called a PV Array. This is depicted in Fig 3 below.

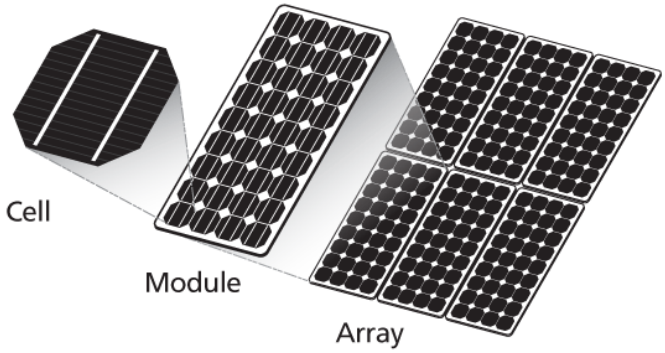

Fig 3: Solar Cell, Module and Array
http://www.samlexsolar.com/learning-center/solar-cell-module-array.aspx

Photovoltaic modules can be classified into five different categories, depending on the structure of the basic material from which they are made and the particular way of their preparation (Zulu, 2014). The types include the following:

- Single crystal (dominant type)
- Multi-crystalline (1 mm – 10 cm)
- Polycrystalline (1μm – 1 mm) e.g., CdTe, CuInSe2
- Microcrystalline (< 1 μm)
- Amorphous (no single crystal region) e.g., a-Si

Solar modules can also be classified according to the thickness of the semiconductor:

- Thick (conventional): 200 – 500 μm [80 % of PVs]
- Thin film: 1 – 10 μm [20 % of PVs]

2.2. Mounting of Solar PV Modules

The power incident on a Solar PV module depends not only on the intensity of the insolation, but also on the angle between the module and the sun. When the absorbing surface and the sunlight are perpendicular to each other, the power density on the surface is equal to that of the sunlight. The power density will always be maximum when the PV module is perpendicular to the sun's rays (Mukund, 2006).

However, as the angle between the sun and a fixed surface is continually changing, the power density on a fixed PV module is less than that of the incident sunlight. Therefore, some

calculations are required to ensure the installation is optimised for power generation. Some of the important geospatial angles that need to be noted in solar PV designs are:

1. Maximum Elevation Angle

   The elevation angle or the altitude angle is the angular height of the sun measured from the horizontal. The elevation is 0° at sunrise and 90° when the sun is directly overhead which only occurs on the equinoxes.

   The elevation angle varies throughout the day. It also depends on the latitude of a particular location and the day of the year.

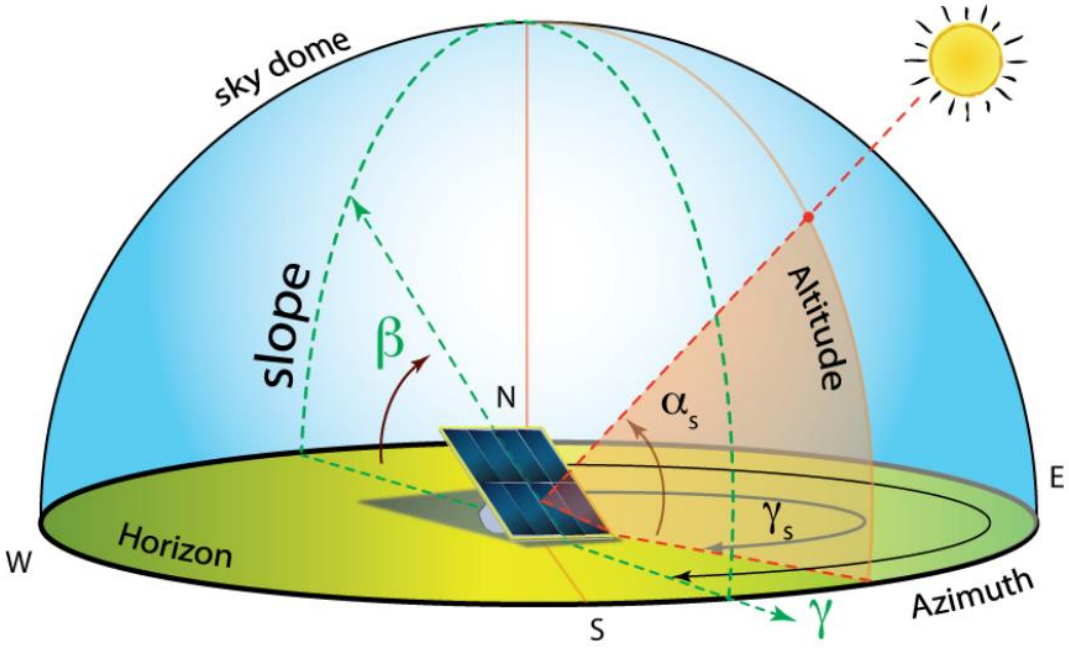

Fig 4: Daily Variation of the Elevation Angle
https://www.e-education.psu.edu/eme810/node/576

The maximum elevation angle (α_{max}) is given by:

$\alpha = 90 - \varphi + \delta$,

where φ is the latitude of the location of interest considering +ve for the northern hemisphere and -ve for the southern hemisphere.

δ is the declination angle. This depends on the day of the year and is given by:

$\delta = 23.45 \sin\left[\frac{360}{365}(284 + d)\right]$, where d is the day of the year.

When the equation above gives a number greater than 90° then subtract the result from 180° meaning the sun at solar noon is coming from the south as is typical of the northern hemisphere.

While the maximum elevation angle is used even in simple PV system design, more accurate PV system simulation requires the knowledge of how the elevation angle varies throughout the day. The relationship which gives this hourly elevation angle is expressed as:

$$\alpha = \sin^{-1}\left[\sin\delta\sin\varphi + \cos\delta\cos\varphi\cos\omega\right]$$

Where, ω is the solar hour angle

2. Tilt angle

The amount of solar radiation incident on a tilted module surface is the component of the incident solar radiation which is perpendicular to the module surface. Fig 5 below shows the calculations for the radiation incident on a tilted surface (S_{module}) given either the solar radiation measured on horizontal surface (S_{horiz}) or the solar radiation measured perpendicular to the sun ($S_{incident}$).

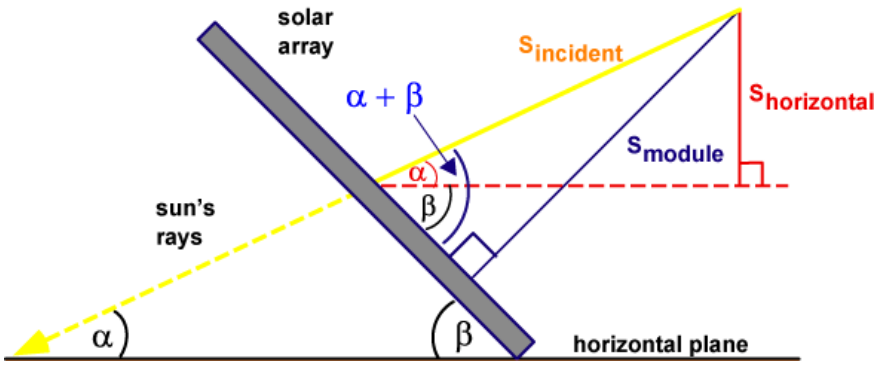

Fig 5: Tilting angles for a solar module
https://www.pveducation.org/pvcdrom/properties-of-sunlight/solar-radiation-on-a-tilted-surface

With β as the tilt angle of the module measured from the horizontal, the equations relating S_{module}, $S_{horizontal}$ and $S_{incident}$ will therefore be:

$$S_{horizontal} = S_{incident}.\sin\alpha$$

$$S_{module} = S_{incident}.\sin(\alpha+\beta)$$

The amount of solar radiation incident on a tilted module surface is therefore a component of the incident solar radiation which is perpendicular to the module surface.

The tilt angle has a major impact on the solar radiation incident on a surface. For a fixed tilt angle, the maximum power over the course of a year is obtained when the tilt angle is equal to the latitude of the location.

3. Zenith Angle

   The Zenith angle is the angle between the sun and the vertical. The zenith angle is similar to the elevation angle but it is measured from the vertical rather than from the horizontal, thus making the zenith angle = 90° - elevation.

$$\zeta = 90^{o} - \alpha$$

4. Azimuth Angle

   The azimuth is the PV array's east–west orientation in degrees. In most solar PV energy. Normally, an azimuth value of zero is facing the equator in both northern and southern hemispheres; +90° degrees is facing due west and –90° degrees is facing due east. The compass angle shows 180° for south, 90° for east and 270° for west.

   The solar azimuth angle measures the relation of the sun facing south, depending on the same three angles as the solar altitude angle. The following equation can be used to calculate the solar azimuth angle γ:

$$\gamma = \sin^{-1}\left[\frac{\cos\delta.\sin\omega}{\cos\alpha}\right]$$

   Variations in the azimuth angle can lead to significant loss in the output power, and also will affect the PV system by various types of faults. In Solar PV development, any factor which reduces the energy output is considered as a fault.

A simplified general orientation of a PV module that is mounted in the northern hemisphere is given in Fig 6 below.

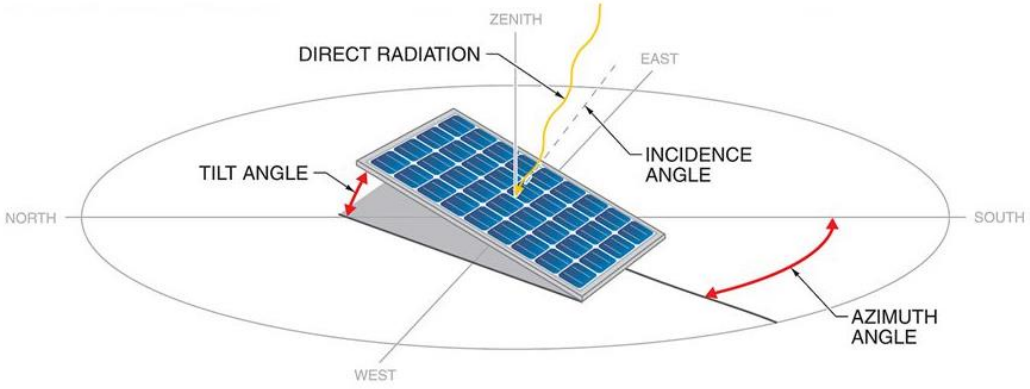

Fig 6: Description of Array Orientation

3. Electrical characteristics of a PV system

An unirradiated solar cell behaves very much like a diode and so the complex physics of the PV cell is usually represented by the equivalent electrical circuit shown in Fig 7 below.

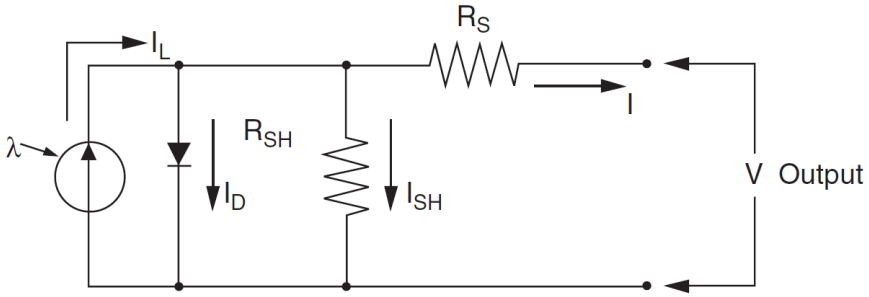

Fig 7: Equivalent circuit for a Solar Cell (Mukund, 2006)

The circuit parameters are defined as follows:

- The current I at the output terminals is equal to the light-generated current I_L, less the diode current I_D and the shunt-leakage current I_{SH};

- The series resistance R_S represents the internal resistance to the current flow, and depends on the p-n junction depth, impurities, and contact resistance;

- The shunt resistance R_{SH} is inversely related to the leakage current to ground.

In an ideal PV cell, $R_S = 0$ (no series loss), and $R_{SH} = \infty\ \Omega$ (no leakage to ground). However, in a typical high-quality 1 in^2 silicon cell, R_S varies from 0.05 to 0.10Ω and R_{SH} from 200 to 300 Ω (Mukund, 2006). The PV conversion efficiency is sensitive to small variations in R_S, but is insensitive to variations in R_{SH}. A small increase in R_S can decrease the PV output significantly.

In the equivalent circuit, the current delivered to the external load equals the current I_L generated by the illumination, less the diode current I_D and the shunt leakage current I_{SH}. The open-circuit voltage V_{OC} of the cell is obtained when the load current is zero, i.e., when I = 0, and is given by the relationship below:

$$V_{OC} = V + IR_{SH}$$

And the diode current is given by the classical diode current expression:

$$I_d = I_D\left[e^{\frac{QV_{OC}}{AkT}} - 1\right]$$

Where,

I_D = the saturation current of the diode

Q = electron charge = 1.6 x10^{-9} C
A = curve-fitting constant (or ideality Factor)
k = Boltzmann constant = 1.38x10^{-23} J/^{0}K
T = temperature on absolute scale ^{0}K

The load current is therefore given by the expression:

$$I = I_L - I_D\left[e^{\frac{QV_{OC}}{AkT}} - 1\right] - \frac{V_{OC}}{R_{SH}}$$

The last term is the leakage current to the ground. In practical cells, it is negligible compared to I_L and I_D and is generally ignored. The diode-saturation current can therefore be determined experimentally by applying a voltage V_{OC} to the cell in the dark and measuring the current going into the cell. This current is often called the dark current or the reverse diode-saturation current.

3.1. Open-Circuit Voltage and Short-Circuit Current

The two most important parameters widely used for describing cell electrical performance are the open-circuit voltage V_{oc} and the short-circuit current I_{sc} under full illumination. The short-circuit current is measured by shorting the output terminals and measuring the terminal current. Ignoring the small diode and ground leakage currents under zero terminal voltage, the short-circuit current under this condition is the photocurrent I_L.

The maximum photo-voltage is produced under the open-circuit voltage. Again, by ignoring the ground leakage current, with I = 0 gives the open-circuit voltage as follows:

$$V_{OC} = \frac{AkT}{Q} Log_n\left(\frac{I_L}{I_D} + 1\right)$$

The term $\frac{KT}{Q}$ is expressed in voltage (0.026 V at 30 ^{0}K). In practical photocells, the photocurrent is several orders of magnitude greater than the reverse saturation current. Therefore, the open-circuit voltage is many times the $\frac{KT}{Q}$ value. Under conditions of constant illumination, $\frac{I_L}{I_D}$ is a sufficiently strong function of the cell temperature, and the solar cell ordinarily shows a negative temperature coefficient of the open-circuit voltage.

3.2. Voltage-Current and P-V characteristics of the photovoltaic system

The electrical characteristic of the PV cell is generally represented by the current vs. voltage (I-V) curve. Fig 8 below shows the I-V characteristic of a PV module under two conditions, in sunlight and in the dark.

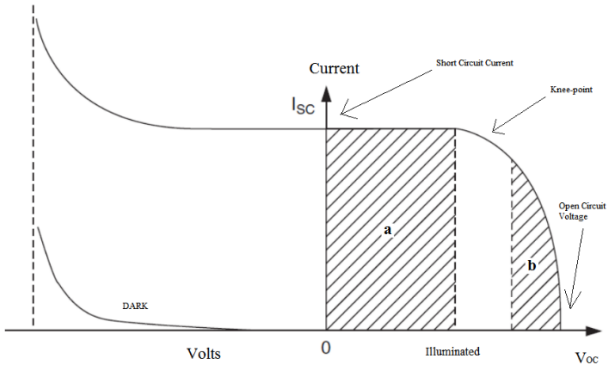

Fig 8: I-V curve for the equivalent circuit for a Solar Cell (Mukund, 2006)

In the first quadrant, the top left of the I-V curve at zero voltage is called the short-circuit current. This current is measured when the output terminals are shorted i.e., at zero voltage. The bottom right of the curve at zero current is called the open-circuit voltage. This voltage is measured when the output terminals are open i.e., at zero current).

In the shaded region **a**, the cell works as a constant current source, generating a voltage to match with the load resistance. In shaded region **b**, the current drops rapidly with a small rise in the voltage. In region **b**, the cell works like a constant voltage source with an internal resistance. Between regions **a** and **b**, the curve has a knee point.

If an external voltage is applied in the reverse direction, usually during a system fault transient, the cell current will remain flat, and power is absorbed by the cell with a negative voltage and positive current. However, beyond a certain negative voltage, the junction breaks down as in a diode, and the current rises to a high value.

3.3. Solar PV Power Output

The power output of a solar cell (panel) is the product of the voltage and current outputs. In Fig 9 below, the power is plotted against the voltage. It therefore follows that the cell produces no power at zero voltage or at zero current. However, the cell produces maximum power at the voltage corresponding to the knee point of the I-V curve. For this reason, PV power circuit is designed to operate close to the knee point with a slight slant on the left-hand side.

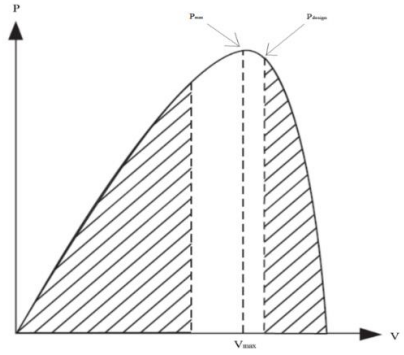

Fig 9: P-V curve for the equivalent circuit for a Solar Cell (Mukund, 2006)

4. Specifying a Solar PV panel

While describing the characteristics of a PV system the main parameters that are very important to be stated are the Maximum Power Point (MPP), the Short-circuit measurement (I_{sc}), the Open circuit measurement (V_{OC}), Fill Factor (FF), the efficiency (η), the Series Resistance (R_S), the shunt resistance (R_{SH}), the Ideality Factor of diode (*m*) and the diode saturation current (I_D) (D. T. Cotfas, et al). Using the equivalent circuit and the I-V characteristics, the important parameters of the cell (panel) can be determined.

4.1. Temperature and irradiance dependence of Solar PV cells

One of the main obstacles that face the operation of photovoltaic panels (PV) is overheating due to excessive solar radiation and high ambient temperatures. Overheating reduces the efficiency of the panels dramatically.

1. Temperature

The ideal P–V characteristics of a solar cell for a temperature variation between 0°C and 75°C are shown in Fig 10. The *P–V* characteristic is the relation between the electrical power output *P* of the solar cell and the output voltage, *V*, while the solar irradiance and module temperature are kept constant. If either temperature or irradiance is changed, the P-V characteristics change.

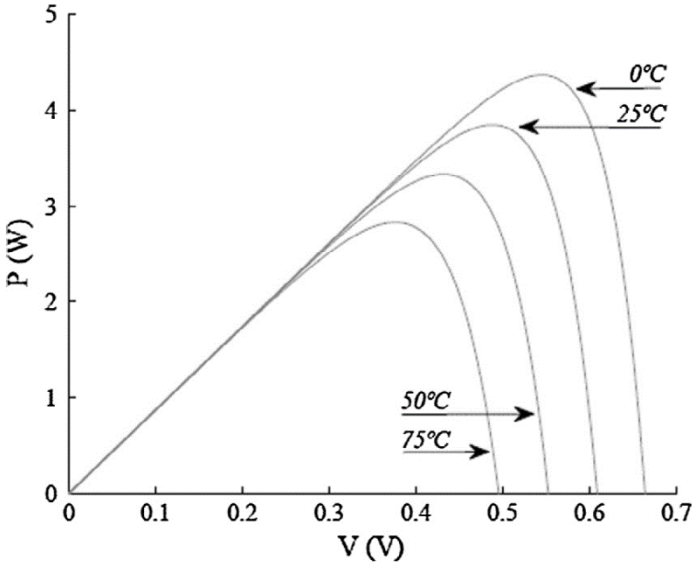

Fig 10: P–V characteristics as a function of the module temperature (Rodrigues et al)

During the design and testing of the panels, the current voltage characteristics are measured at different temperatures from 25°C to 87°C and at different illumination levels from 400 to 1000 W/m^2, because there are locations where the upper limit of the photovoltaic cells working temperature exceeds 80°C. The voltage and current dependence on the change of temperature and irradiation for a typical PV cell is shown in Fig 11 below:

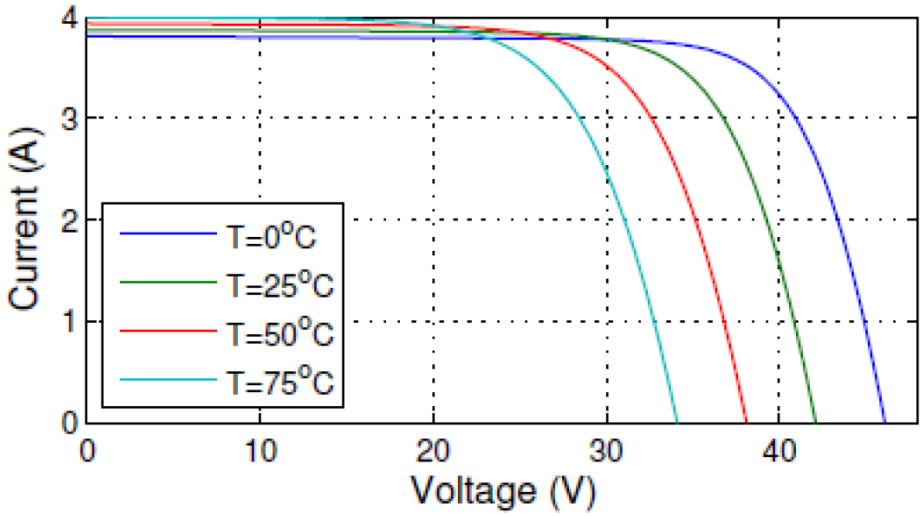

Fig 11: Voltage current dependence on irradiation

From Fig 11, the short circuit current I_{sc} is slightly lower at low temperatures (0^0C) while the corresponding open circuit voltage $V_{OC(0)}$ is relatively higher at high temperatures $V_{OC(75)}$. The dependence of the photovoltaic cell parameter function of the temperature is approximately linear.

$$TC_a(p) = \frac{dp}{dT},$$

$$TC_n(p) = \frac{1}{p}\frac{dp}{dT}\Big|_{T=25^0C}$$

Where *p* represents the parameter of the photovoltaic cell and T is the temperature

Now, as the temperatures of the solar cells rise above 25^0C, the current rises very slightly, but the voltage decreases more rapidly. The net effect is a decrease in output power with increasing temperature. Typical silicon solar panels have a temperature coefficient of about -0.4 to -0.5 percent. This means that for every degree Celsius above 25, the power output from the array would drop by that percentage. At 45 ^{0}C, a 40-watt solar panel with a temperature coefficient of -0.4 would produce less than 37 watts.

For solar installations in temperate regions such as Zambia, cooling techniques such as natural wind flow, evaporative cooling and others can be employed to offset the temperature effect on solar panels.

Hybrid Photovoltaic/Thermal (PV/T) solar system is one of the most popular methods for cooling the photovoltaic panels nowadays. The hybrid system consists of a solar photovoltaic panel combined with a cooling system. The cooling agent, i.e., water or air, is circulated around the PV panels for cooling the solar cells, such that the warm

water or air leaving the panels may be used for domestic applications such as domestic heating.

Basically, there are two types of cooling systems: (i) active cooling, which consumes energy and (ii) passive cooling, which uses natural convection/conduction to enable heat extraction.

From data compiled between the years 1850 and 2015 the average temperature in Zambia was 21.3^0C while the all-time high of 26.28^0C was recorded in October of 2005 and a record low of 15.52^0C recorded in July of 1907. Clearly, it is expected that solar farm blocks designed and implemented with such conditions are not likely to be impacted significantly upon by a rise in such ambient temperature.

Secondly changes in temperature will be manifested on the dc side as a significant voltage drop with a consequence of reduced power generation, while the ac side of the Solar PV model will manifest simply as a reduction in the generated power. Power electronics components will endeavour to retain the system voltage at a constant value however, the power output will be significantly diminished.

Considering that temperature variations will have a more impact on the power output that the voltage and that temperature changes are a gradually phenomenon that would trigger the operation of protective devices that would eventually shut down the affected PV arrays or entire plant, the effects of temperature on PV modules was neglected in the study for impact of Solar PV on the system stability of the Zambia National Grid. However, practical long-term Solar PV design may need to factor in elements of temperature changes in the design of solar power plants considering the reduction in power generation will result in revenue losses.

2. Solar Irradiance

Solar irradiance is the power per unit area received from the Sun in the form of electromagnetic radiation and is measured in watt per square metre (W/m^2). When integrated over time, Solar irradiance gives radiant energy emitted into the surrounding environment in joule per square metre (J/m^2), during that time period. When so integrated, solar irradiance becomes solar irradiation, insolation, or solar exposure. Often irradiance and insolation are used interchangeably in various literature and practices. Previously irradiance was referred to as solar flux.

Depending on the relevance and use of the obtained measurements, various techniques and principles of measuring solar irradiance are employed. However, the main types of irradiance measured are:

a. Total Solar Irradiance (TSI)

The TSI is a measure of the solar power over all wavelengths per unit area incident on the Earth's upper atmosphere measured perpendicular to the incoming sunlight. The measurement of the TSI gives rise to the concept of the Solar Constant. The solar constant is a conventional measure of mean TSI at a distance of one astronomical unit (AU). The generally accepted solar constant of 1368 W/m^2 is a NASA satellite measured yearly average.

b. Direct Normal Irradiance (DNI), or beam radiation

The DNI is the direct solar radiation from the solar disk and the region closest to the sun (circumsolar disk of 5° centred on the sun). It is measured at the surface of the Earth at a given location with a surface element perpendicular to the Sun. It excludes diffuse solar radiation (radiation that is scattered or reflected by atmospheric components). DNI is a component that is involved in thermal (concentrating solar power, CSP) and photovoltaic concentration technology (concentrated photovoltaic, CPV).

c. Diffuse Horizontal Irradiance (DHI), or Diffuse Sky Radiation

DHI is the radiation at the Earth's surface from light scattered by the atmosphere. It is measured on a horizontal surface with radiation coming from all points in the sky excluding circumsolar radiation which is the radiation coming from the sun disk.

d. Global Horizontal Irradiance (GHI)

GHI is the total irradiance from the sun on a horizontal surface on Earth. It is the sum of direct irradiance (after accounting for the solar zenith angle of the sun ζ) and diffuse horizontal irradiance. GHI is a reference radiation for the comparison of climatic zones; it is also essential parameter for calculation of radiation on a tilted plane.

e. Global Tilted Irradiation/Irradiance (GTI),

GTI or total radiation is the radiation received on a surface with defined tilt and azimuth, fixed or sun-tracking. This is the sum of the scattered radiation, direct and reflected. In the case of photovoltaic (PV) applications, GTI can be occasionally affected by shadow.

Generally, the effect of variation in the solar irradiance on the P-V characteristics of the cell is shown in Fig 12 in which it can be deduced that increase in solar irradiance results in overall increase in power output.

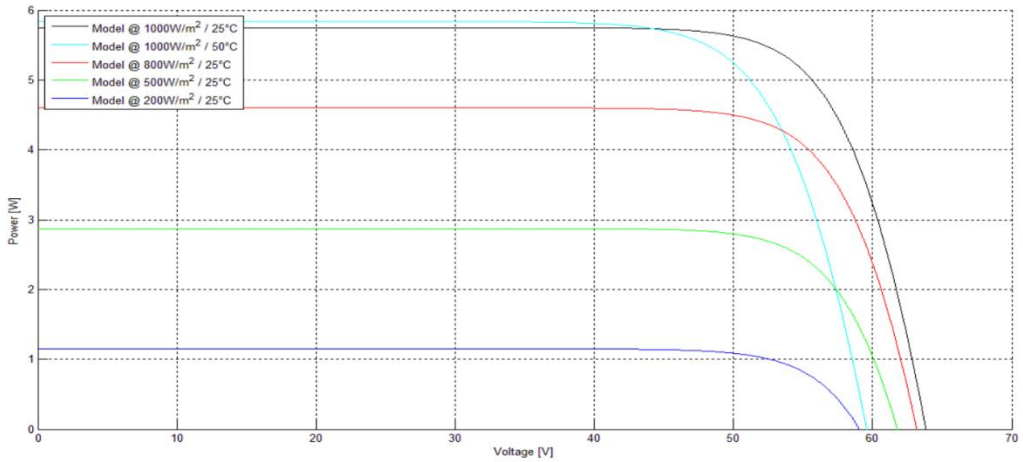

Fig 12: Variation in the Module-voltage with the Module-current for different Irradiances (Watts/sq.mm) and Temperature (in oC)

4.2. Fill Factor

The Fill Factor (FF) is another quantity often used to characterize the performance of a solar module. The fill factor is the ratio of the power at the maximum power point (P_{max}) to the product of V_{OC} and I_{SC}.

$$\text{Fillfactor} = \frac{P_{max}}{V_{OC}I_{SC}} = \frac{V_R I_R}{V_{OC}I_{SC}}$$

The Fill Factor is essentially a measure of quality of the solar cell. Fill factors around 70–75% for crystalline silicon solar modules are typical, while for multi junction amorphous-Si modules, it is closer to 50–60%. The Fill Factor reduces with increase in the temperature of the solar cell.

4.3. Diode Curve Fitting Constant (A)

The Diode Curve Fitting Constant is defined as ***A*** and is sometimes referred to as the Ideality Factor (*m*). In the ideal diode equation, ***A*** is taken as 1 giving the classical diode equation as shown below:

$$I_d = I_D\left[e^{\frac{QV_{OC}}{kT}} - 1\right]$$

However, practical diodes may not be ideal due to various reasons. Therefore, the curve fitting constant (***A***) can be used to describe this characteristic or Ideality.

Basically, the diode equation provides two pieces of information of the diode characteristics; (1) I_D, reverse saturation current, which determines the forward voltage and (2) $\frac{nkT}{Q}$, which determines the slope of current vs. voltage. So, the curve fitting constant describes how far the diode slope differs from an ideal diode slope.

In an ideal diode, ***A*** = 1, the slope is about 18mV per octave (2X) of current change or 60mV per decade (10X) of current change at 27^0C. In a non-ideal diode with ***A*** = 2, the slope is about 36mv per octave (2X) of current change or 120mv per decade (10X) of current change at 27 ^{0}C.

If diode equation is plotted on semi-log scale, the characteristic is a straight line at current >>>I_D. The slope of this line is $Ak\frac{T}{Q}$.

4.4. Efficiency (η)

Efficiency is the ratio of the electrical power output (P_{out}), compared to the solar power input (P_{in}), into the PV cell.

$$\eta = \frac{P_{out}}{P_{in}} \Rightarrow \eta_{\max} = \frac{P_{max}}{P_{in}}$$

P_{out} can be taken to be P_{max} since the solar cell can be operated up to its maximum power output in order to get the maximum efficiency while P_{in} is taken as the product of the irradiance of the incident light, measured in W.m^{-2} or in suns (1000 W.m^{-2}), with the surface area of the solar cell m^2.

5. Solar Energy Yield

The global formula to estimate the electricity generated by a photovoltaic system is given by:

$$E = ArH(PR)$$

Where,

E = Energy (kWh)
A = Total solar panel Area (m^2)
r = Solar panel yield or efficiency (%)
H = Annual average solar radiation on tilted panels (shadings not included)
PR = Performance ratio, coefficient for losses (range between 0.5 and 0.9 with a default value taken as 0.75)

The solar panel yield (*r*) of the solar panel is given by the ratio of electrical power (kWp) of one solar panel divided by the area of one panel. This is a nominal ratio which is used for Standard Test Conditions (STC) i.e., with radiation of 1000 W.m^{-2}, cell temperature of 25^0C, Wind speed of 1m/s, AM=1.5. In such conditions, the unit of the nominal power of the photovoltaic panel is called Watt-peak (Wp).

The Performance Ratio (*PR*) is used to evaluate the quality of a photovoltaic installation. This is because the *PR* gives the performance of the installation independently of the orientation/inclination of the panel. The *PR* includes all losses in the PV installation. These losses depend on many factors such as site conditions, technology used, size of the system etc. Typical values for such losses are;

- Inverter losses (4% to 10 %)
- Temperature losses (5% to 20%)
- DC cables losses (1 to 3 %)
- AC cables losses (1 to 3 %)
- Shadings 0 % to 80% (specific to each site)
- Losses at weak radiation 3% to 7%
- Losses due to dust, snow etc (2%)
- Other Losses

6. Grid connected PV Systems

6.1. Grid Connected PV Systems

Grid connected Solar PV systems as the name implies are PV systems connected to the grid and can be distributed or centralized in nature. A grid-connected PV system consists of solar panels, one or several inverters, a power conditioning system and grid connection equipment. They range from small residential and commercial rooftop systems (distributed) to large utility-scale solar power stations (Centralised). Unlike stand-alone power systems, a grid-connected system rarely includes an integrated battery solution, as they are still very expensive. With increased irradiance, grid-connected PV system may supply excess power beyond the consumption by the connected load and therefore require stringent control processes and curtailments.

6.2. Grid connected PV System subcomponents

There are several factors that affect the design and development of a PV system. The major factors include safety and economics. The objective would be to design and build the system to maximize the return or the invested capital within the safety and operational requirements. In this process of optimization, the selection, design, and development of various parts of the PV system play important roles.

The system performance requirements may include requirements on efficiency, voltage regulation, voltage flicker, dc injection into the utility system, output reactive power, harmonics, and voltage unbalance.

The PV system and the utility systems should be protected against abnormal operating conditions such as under/overvoltage, overcurrent, over or under frequency. Some of these abnormal conditions may originate either in the PV system or the utility system. If the utility bus is de-energized, the PV system should be isolated and should remain isolated until

conditions permit resynchronization. Protection systems should be mutually time-coordinated to disconnect the PV system from the utility under these abnormal conditions.

A block diagram of a grid connected photovoltaic system is shown in Fig 13 below. The system consists of a PV array subsystem, power conditioning subsystem, utility interconnection subsystem, and control subsystem.

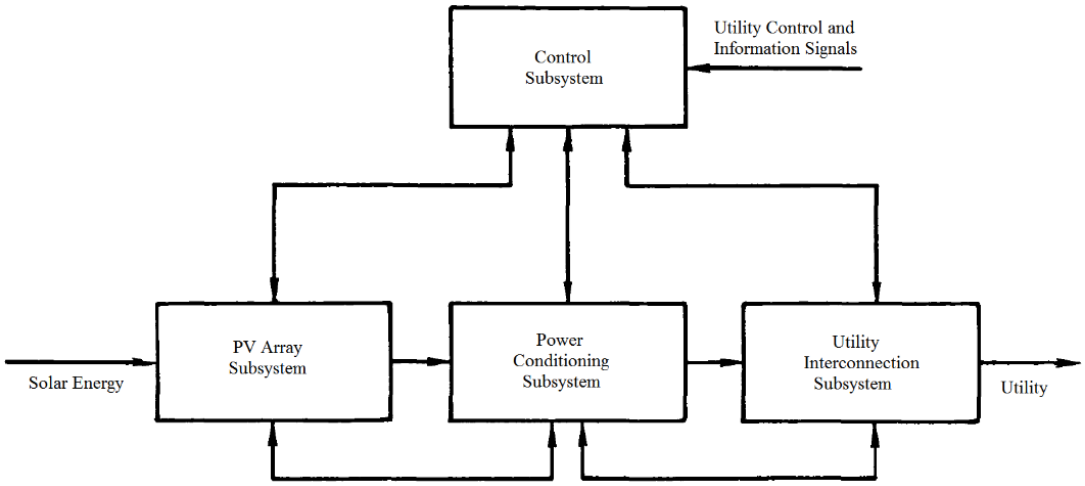

Fig 13: Block Diagram of a Utility Interactive Photovoltaic System

a. PV Array Subsystem

The PV array subsystem converts solar energy into electrical power. It collects dc power and provides protection for PV arrays. The subsystem consists of PV cells assembled into modules, dc cabling and certain protection equipment. The cells and modules (arrays) are electrically connected in series and in parallel to obtain the desired operating voltage and current levels.

The PV arrays are implemented using the aggregated model that computes the total internal resistances, the non-linear integrated characteristic and total generated solar cell photocurrent according to the series and parallel contribution of each parameter.

A three-phase DC-AC voltage source inverter is then employed for connecting to the grid. This three-phase static device is shunt connected to the distribution network by means of a coupling transformer and the corresponding line sinusoidal filter. The output voltage control of this VSI can be efficiently performed using pulse width modulation (PWM) techniques.

Means of protection for the array and means of isolating the array are provided to facilitate the maintenance of the array. The array subsystem includes any field fuses, switches, and disconnects that may be necessary. It may include a distribution panel for array wiring and may also include experimental instrumentation (sun detection, wind measurement etc.).

b. Photovoltaic Power Conditioning System (PCS) model

The selection, design, and development of the power conditioning subsystem (PCS) have a great impact on the economic and technical viability of a given PV system. One of the major challenges of grid-connected solar photovoltaic systems is to attain an optimal compatibility of PV arrays with the existing electricity grid. A power conditioning system is required to meet the amplitude and frequency requirements of the stiff utility AC grid and inject synchronized power into the grid. Such a conditioning circuit is typically a DC-AC converter (or inverter) which inverts the DC output current generated by the PV arrays into a synchronized sinusoidal waveform. This PV interface must generate high quality electric power and at the same time be flexible, efficient, and reliable, and is expected to operate safely.

One key of grid-connected PV systems is the procedure employed for power extraction from solar radiation and is mostly related to the nature of PV arrays. Each PV module is a nonlinear system with a power output mostly influenced by atmospheric conditions, such as solar radiation and temperature. To transfer maximum power into the utility grid for all operating conditions, a maximum power point tracking (MPPT) technique is usually implemented. Therefore, each grid-connected PV generating system has to perform two essential functions, i.e., to extract the maximum output power from the PV array, and to generate a sinusoidal current from the dc source into the grid

c. Utility Interconnection Subsystem

The utility interconnection subsystem provides means for synchronising Solar PV plant with to the interconnected grid. It also provides the means for the isolation of the PV system from the utility when necessary. Typical equipment under this subsystem includes power transformers, circuit breakers, voltage transformers, current transformers and the associated protective relaying system

The interconnection subsystem protects the PV system from utility abnormal conditions and vice versa. The subsystem may include appropriate metering and instrumentation equipment as specified within the grid interface requirements.

d. Control Subsystem

The Control Subsystem oversees the operation of the PV system and performs the following functions:

i. It provides overall coordination of system protection;
ii. It provides tracking signals for the PV arrays
iii. It communicates status information to the utility dispatch centre, and
iv. Receives operational commands from the utility dispatch.

Supervisory Control and Data Acquisition (SCADA) systems form the core of the control subsystems for Solar PV power plants as well as any power generation or processing facility.

7. PV system operation

There are three possible conditions under which a PV system may be operated and these are: (1) constant current operation, (2) constant voltage operation, and (3) maximum power operation.

Independent of the operating mode, the primary objective is to be able to extract maximum energy from the PV array. Therefore, an understanding of the array characteristics for a specific site is essential in designing an efficient PV system.

7.1. Constant Current Operation

Because the PCS consists of solid-state components that are limited by current ratings, the PV array may be operated in a constant current mode. As a result, a fluctuation in array output power will cause PCS input voltage to change. If the dc voltage is within specified limits, constant current operation will continue; otherwise, the PCS will be shut off.

7.2. Constant Voltage Operation

In this operation, the dc array voltage is compared with a reference value and the difference is kept to a minimum. In general, however, fixed-voltage operation does not guarantee maximum power output. Adjusting reference voltage may improve efficiency, but it requires adjustment seasonally.

7.3. Maximum Power Operation

In this mode of operation, a closed-loop feedback control system is used, PCS output power is sensed, and operation at maximum power is achieved by continuously shifting the operating point on the array characteristics (maximum power point tracking).

There are many methods of Maximum Power Point Tracking (MPPT). However, these methods can be classified into three main categories: (1) lookup table methods, (2) computational methods which include neural networks and fuzzy logic and (3) hill climbing methods. The methods vary in the degree of sophistication, processing time and memory requirements.

7.2. Appendix 2: Classical Methods for Analysis of Power System Stability

1. Introduction

The general analysis of power system stability involves the representation of the power system through a model in which the individual components are expressed mathematically.

The basic representation of such a model depicts a single synchronous generator connected to an infinite busbar through a transformer and transmission lines. Such a type of system is called as Single Machine Infinite Bus (SMIB) system and has been advocated for by Kimbark (1948) and Crary (1945).

Though this model is not appropriate for current generators with fast acting exciters, governors, power system stabilizers, it is nevertheless useful in understanding the basic phenomenon of stability (Kumar, 2014). In order to make the representation of such a basic power system easy, the following four (04) assumptions are normally made:

1. The exciter dynamics are not considered and the field current is assumed to be constant so that the generator stator induced voltage is always constant. In this way, the dynamics of the exciter are neglected;

2. The effect of damper windings, present on the rotor of the synchronous generators, is neglected. Thus, the dynamics of the damper windings, and rotor windings are neglected;

3. The input mechanical power to the generator is assumed to be constant during the period of study. In this way, the dynamics of the turbine and turbine speed governor are neglected. The change in the mechanical input power takes more time, in the order of 2 to 10 minutes, due to the involvement of mechanical systems where as the electrical power output can change within in milliseconds.

4. The saliency of the generator is neglected, that is the generator is assumed to be of cylindrical type rotor.

A typical Single Machine Infinite Bus (SMIB) system is shown in Fig 14 below:

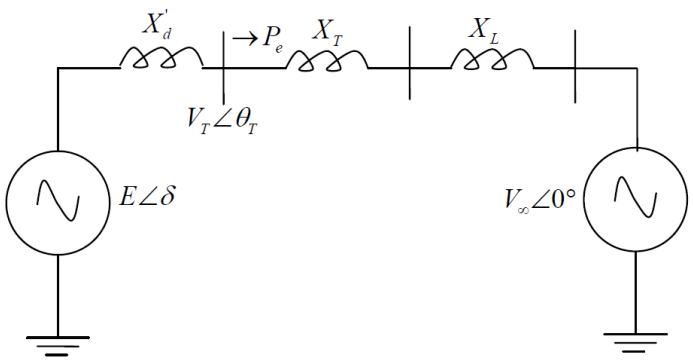

Fig 14:Single Machine Infinite Bus (SMIB) System (Kumar, 2014)

The analysis of the SMIB is centred around the reactance since the resistances of the synchronous generator stator, transformer and the transmission line are relatively negligible as compared to the corresponding reactances. In this case, X'_d represents the reactance of the synchronous generator during transients, X_T is the reactance for the transformer and X_L is the transmission line reactance.

The infinite bus represents the rest of the grid, where the voltage magnitude and frequency are held constant thereby acting as an infinite source or sink. The infinite bus can also be considered as a generator with infinite inertia and fixed voltage. In the case of the SMIB of Fig 14 above, $V_T\angle\theta_T$ is the terminal voltage of the synchronous generator while $V_\infty\angle 0^o$ is the infinite bus (reference bus).

The generator internal voltage angle δ is defined with respect to the infinite bus voltage angle. The input mechanical power is represented as P_m and the output electrical power is defined by P_e. H is the inertia constant of the generator. H_∞ is the inertia constant of the grid equivalent generator connected at the infinite bus and its value can be taken as ∞.

2. Rotor Angle Stability

2.1 Background

From the discussion above, the real power output of the generator, P_e can be computed as

$$P_e = \text{Real}\left(V_T e^{j\theta_T} . \frac{\left(V_T e^{-j\theta_T} - V_\infty e^{-j0} \right)}{j\left(X_T + X_L \right)} \right) = \text{Real}\left(E e^{j\delta} . \frac{\left(E e^{-j\delta} - V_\infty e^{-j0} \right)}{j\left(X'_d + X_T + X_L \right)} \right)$$

$$P_e = \frac{EV_\infty}{X'_d + X_T + X_L} \sin\delta$$

Where the maximum real power output of the synchronous generator transferable to the infinite bus in this case is

$$P_{\max} = \frac{EV_\infty}{X'_d + X_T + X_L}, \text{ at } \delta = 90^o$$

Hence, the synchronous generator real power output can be represented as:

$$P_e = P_{\max} . \sin\delta$$

The mechanical systems of Fig 14 above are modelled as a prime mover giving mechanical energy to the generator rotor and in turn the generator converts the mechanical energy into electrical energy through magnetic coupling. The dynamics of such a rotational mechanical system can thus be represented as shown in Fig 15 below:

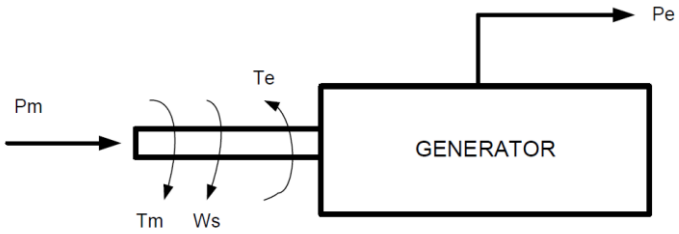

Fig 15:Mechanical Representation of (SMIB) System (Kumar, 2014)

Now

$$J\frac{d^2\theta_m}{dt^2} = T_m - T_e$$

Where, J is the moment of inertia of the rotating machine in kg.m^2. The mechanical input torque due to the prime mover is represented as T_m in N.m and the electrical torque acting against the mechanical input torque is represented by T_e in N.m.

The angle θ_m is the mechanical angle of the rotor field axis with respect to the stator reference or fixed reference frame. As the rotor is continuously rotating at synchronous speed in steady-state θ_m will also be continuously varying with respect to time. To make the angle θ_m constant in steady-state it can be measure with respect to a synchronously rotating reference instead of a stationary reference. Hence, this can be written as:

$$\theta_m = \delta_m + \omega_{ms}t$$

Where, θ_m is the angle between the rotor field axis and the reference axis rotating synchronously at ω_{ms} rps. The result of differentiating θ_m with respect to time yields:

$$\frac{d\theta_m}{dt} = \frac{d\delta_m}{dt} + \omega_{ms}$$

$$\frac{d^2\theta_m}{dt^2} = \frac{d^2\delta_m}{dt^2}$$

Knowing that the rate of change of the rotor mechanical angle θ_m with respect to time is in fact rotor speed, $\frac{d\theta_m}{dt}$ is thus ω_{ms}. Consequently,

$\frac{d\delta_m}{dt} = \omega_m - \omega_{ms}$, and

$$J\frac{d^2\delta_m}{dt^2} = T_m - T_e$$

And, when ω_{ms} is multiply on both the side of the above torque equation we get the power equation below:

$$J\omega_m\frac{d^2\delta_m}{dt^2} = P_m - P_e$$

Multiplying both sides of the power equation by $\frac{1}{2}\omega_{ms}$ and then dividing the resultant equation with the base MVA by S_B in order to express the equation in per unit values yields:

$$\frac{\frac{1}{2}J\omega_m\omega_{ms}}{S_B}\frac{d^2\delta_m}{dt^2} = \frac{1}{2}\omega_{ms}\left(\frac{P_m}{S_B} - \frac{P_e}{S_B}\right)$$

This in turn defines a new parameter called machine inertia constant where:

$$H = \frac{\frac{1}{2}J\omega_{ms}{}^2}{\text{Base MVA}} = \frac{\frac{1}{2}J\omega_{ms}{}^2}{\text{Base MVA}}\frac{\text{MW.S}}{\text{MVA}}$$

This relationship is derived from the assumption that $\omega_m \cong \omega_{ms}$ since the variation of the speed, even during transients, from synchronous speed is quite less. This assumption does not however mean that the speed of the rotor has reached the synchronous speed but instead $\frac{1}{2}J\omega_{ms}{}^2 \cong \frac{1}{2}J\omega_m\omega_{ms}$ consequently,

$$H\frac{d^2\delta_m}{dt^2} = \frac{1}{2}\omega_{ms}\left(P_m - P_e\right) \text{ per unit.}$$

δ_m and ω_{ms} are expressed in mechanical radians and mechanical radians per second, in order to convert them in to electrical radians and electrical radians per second respectively we have to take the number of poles (P) of the synchronous machine rotor into consideration. Hence, the electrical angle and electrical speed can be represented as:

$$\delta = \frac{P}{2}\delta_m \text{ elec.rad}$$

$$\omega_{ms} = \frac{P}{2}\omega_{ms} \text{ elec.rad.s}^{-1}$$

Replacing the electrical quantities in the per unit power equation,

$$\frac{d^2\delta}{dt^2} = \frac{\omega_s}{2H}\left(P_m - P_{\max}\sin\delta\right) \text{ per unit}$$

$$\frac{d^2\delta}{dt^2} = \frac{\pi f_s}{H}\left(P_m - P_{\max}\sin\delta\right) \text{ per unit}$$

This gives what is known as the *classical swing equation* where f_s is the system frequency. For the Zambian system f_s = 50 Hz, while for other jurisdictions such as the United States of America, f_s = 60 Hz. Japan is known to use both 50 Hz and 60 Hz split into the northern half which is at 50 Hz and the southern half at 60 Hz.

From the classical swing equation above, it can be deduced that $P_m = P_{\max}\sin\delta$ then there will be no speed change nor voltage angle change. But, if $P_m \neq P_{\max}\sin\delta$ due to disturbance in the system then either the speed increase or decrease with respect to time.

Where there is more input mechanical power than the electrical power output, $P_m > P_{\max}\sin\delta$ and since the energy has to be conserved, this will lead to an increase in the kinetic energy of the rotor and the speed will increase.

Likewise, where the input power is less than the required electrical power output, $P_m < P_{\max}\sin\delta$, the balance power will be drawn from the kinetic energy stored in the rotor due to which the rotor speed will decrease.

2.2 Rotor angle stability analysis for a SMIB System

Stability analyses for a typical Single Machine Infinite Bus (SMIB) system is provided below.

2.2.1 Small-signal stability analysis of a SMIB System

Small Signal Stability analysis is sometimes referred to as Modal Analysis or Eigenvalue Calculation (DIgSILENT, 2018).

a. Criteria for stability

The classical swing equation can be rewritten as:

$$\frac{H}{\pi f_s}\frac{d^2\delta}{dt^2} = \left(P_m - P_{\max}\sin\delta\right)$$

At steady-state, the speed of the generator rotor is constant at synchronous speed therefore the rate of change of rotor speed will become zero ($\frac{d^2\delta}{dt^2} = 0$) from which $P_m = P_{\max}\sin\delta$.

But the mechanical power input P_m and the maximum power output of the generator P_{max} are known for a given system topology and load, the rotor angle δ can be calculated from:

$$\delta = \sin^{-1}\left(\frac{P_m}{P_{\max}}\right) \text{ or } \pi - \sin^{-1}\left(\frac{P_m}{P_{\max}}\right)$$

The rotor angle (δ) thus has two solutions for $P_m = P_{\max}\sin\delta$ and these can be denoted as $\delta_o = \sin^{-1}\left(\frac{P_m}{P_{\max}}\right)$ and $\delta_{\max} = \pi - \sin^{-1}\left(\frac{P_m}{P_{\max}}\right) = \pi - \delta_o$.

The solution of δ_o and $\delta_{\max}$ has very important implications of the two on the stability of the system and can be clearly understood from the so-called swing curve or $P - \delta$ curve, which is a plot of electrical power output P_e with respect to the rotor angle δ. The $P - \delta$ curve as shown in Fig 16: below, is basically a sine curve with δ varying from 0 to π.

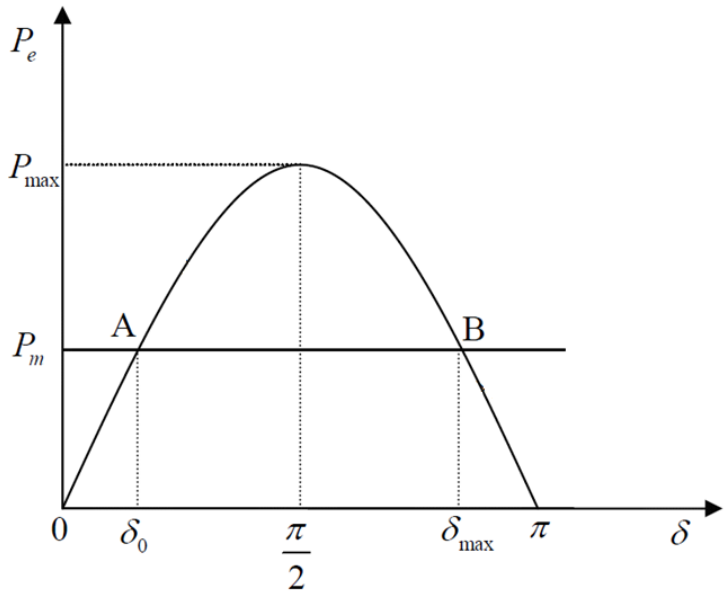

Fig 16:Swing (P – δ) Curve of a SMIB System (Kumar, 2014)

From Fig 16 above, the maximum power output of the generator $P_{\max}$ occurs at $\delta = \frac{\pi}{2}$ while the constant mechanical power (P_m) is a straight line which cuts the $P - \delta$ curve at

points A and B in which case the mechanical power input P_m is equal to the electrical power P_e. At points A and B, the rotor angles are δ_o and $\delta_{\max}$.

The stability characteristics of points A and B are then interrogated by considering each point and then introducing a small disturbance into the system. Considering Point A on the swing curve in Fig 16 above, a small positive angle ($\Delta\delta_o$) disturbance introduced onto the rotor will result in a new operating point which can be labelled as C as shown in Fig 17 below:

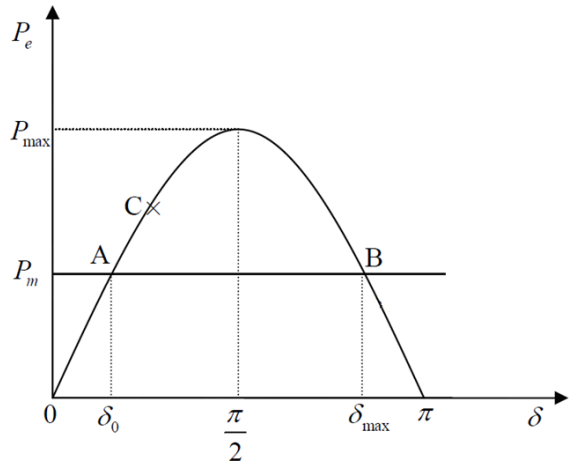

Fig 17:Small signal disturbance as point A

At Operating point C, the electrical power output is expected to increase to $P_{\max}\sin(\delta_o + \Delta\delta_o)$ resulting in the electrical power being more than the input mechanical power. At Point C where $P_m < P_{\max}\sin(\delta_o + \Delta\delta_o)$, the rotor will start to decelerate due to which the angle δ will be pulled back to the point A. But since the rotor has some form of inertia, it will not stop at the point A but will decelerate further due to which δ moves to the point say D in Fig 18 below.

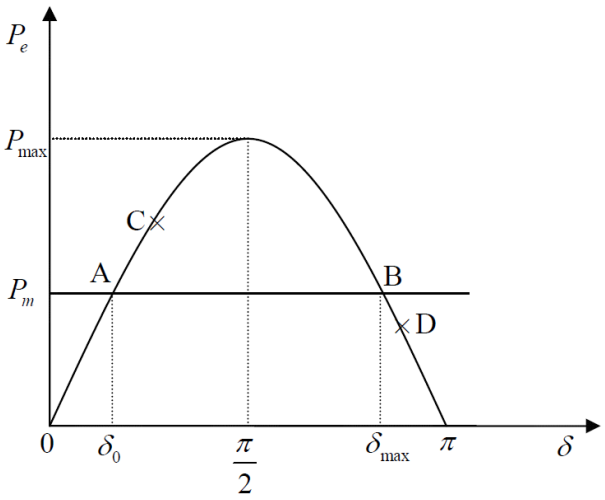

Fig 18:Small signal disturbance resulting to operating point D

At point D, the input mechanical power will become more than the electrical power output and ($P_m > P_e$) hence the rotor starts accelerating with a consequent increase in the rotor angle δ. The rotor angle δ will reach point A and due to inertia, it will not stop there but again move to point C. Theoretically, this A-C-A-D-A movement will repeat itself indefinitely if if there are no means to consume the access energy resulting from the rotor oscillations. This extraction of access energy is a loose reference to the damping action on the rotor oscillation.

If we consider point B on the P – δ of Fig 16: at which $\delta = \delta_{max}$, a small positive angle ($\Delta\delta_{max}$) disturbance introduced onto the rotor will result in a new operating point at which the electrical power output will be $P_{max}\sin\left(\delta_{max} + \Delta\delta_{max}\right)$ and hence being less than the input mechanical power $P_m > P_{max}\sin\left(\delta_{max} + \Delta\delta_{max}\right)$. This leads to acceleration of the rotor due to which the angle will increase further and this will lead to further decrease in the electrical power output, thereby leading to unstable operation of the generator.

Kumar (2014) thus concluded that out of the two operating points A and B, with rotor angles δ_o and δ_{max}, operating point A is stable and operating point B is unstable for small disturbances. Kumar (2014) calls these points Stable Equilibrium Point for point A and Unstable Equilibrium Point for point B. Similarly, δ_o was defined as the Stable Steady State Rotor Angle while δ_{max} was defined as the Unstable Steady State Rotor Angle.

b. Linearization of the SMIB System

The classical swing equation for SMIB system is a nonlinear function. There is therefore a need to present the swing equation for SMIB in state-space form through linearization. Now, a linear autonomous system can be represented in the form of state space as:

$$\dot{X} = AX + BU$$

Where, *X* is the vector of state variables, *A* is the state matrix, *B* input matrix and *U* is the vector of the control inputs. In an autonomous system, the state vector and the input vector are not explicit functions of time and from linear control theory, the stability of such an autonomous system can be assessed by computing the eigen values of the state matrix *A*. Eigen values for a given matrix *A* can be computed as the solution of the equation below:

$$\left|\lambda I - A\right| = 0$$

Where, λ is vector of eigen values and *I* is an identity matrix and is of the same order of the state matrix *A*. If the order of the state matrix *A* is *n x n* then there will be *n* eigen values

which could be real or complex. The stability of the system can be found out from the eigen values so computed. There are three scenarios:

1. All the eigen values have negative real part
2. Some of the eigen values have positive real part
3. Some of the eigen values have zero real part

If all the eigen values have negative real parts irrespective of their imaginary parts then the system is said to be asymptotically stable. If at least one eigen value has positive real part then the system is unstable. If at least one complex conjugate pair of eigen values have zero real parts then the system is called as marginally stable with sustained oscillations. This test is summarized in Tab 1 below:

Tab 1: Test for Stability

No.	Condition	Status
1.	All the eigen values have negative real part	Asymptotically Stable
2.	Some of the eigen values have zero real part	Marginally Stable
3.	Some of the eigen values have positive real part	Unstable

From the foregoing, the stability of the nonlinear SMIB model can be assessed using linear control theory provided that the model is linearized.

As was demonstrated from the *P – δ curve* above, a small positive angle disturbance ($\Delta\delta$) on the rotor for the operating point at A in Fig 18, the rotor angle would oscillate between points C and D. If observed closely it can be seen that the *P – δ curve* falling between the points C and D is almost linear if $\Delta\delta$ is very small and therefore we can assume that the system behaves in a linear fashion around the operating point A between points C and D. Mathematically this can be written by supposing the angle δ_o is disturbed by an angle $\Delta\delta$ then we can express the classical swing equation as:

$$\frac{H}{\pi f_s}\frac{d^2\left(\delta_o+\Delta\delta\right)}{dt^2} = P_m - P_{\max}\sin\left(\delta_o-\Delta\delta\right)$$

When $\sin\left(\delta_o-\Delta\delta\right)$ is expanded, we get

$$\frac{H}{\pi f_s}\frac{d^2\delta_o}{dt^2}+\frac{H}{\pi f_s}\frac{d^2\Delta\delta}{dt^2} = P_m - P_{\max}\left(\sin\delta_o\cos\Delta\delta+\cos\delta_o\sin\Delta\delta\right)$$

But since, $\Delta\delta$ is a very small disturbance angle, then $\cos(\Delta\delta)\cong 1$ and $\sin\left(\Delta\delta\right)=\Delta\delta$ and with this approximation, the swing equation becomes

$$\frac{H}{\pi f_s}\frac{d^2\delta_o}{dt^2}+\frac{H}{\pi f_s}\frac{d^2\Delta\delta}{dt^2}=P_m-P_{\max}\sin\delta_o-P_{\max}\cos\delta_o\Delta\delta$$

Since at initial operating point A,

$$\frac{H}{\pi f_s}\frac{d^2\delta_o}{dt^2}=P_m-P_{\max}\sin\delta_o=0 \text{ then,}$$

$$\frac{H}{\pi f_s}\frac{d^2\Delta\delta}{dt^2}=-P_{\max}\cos\delta_o\Delta\delta$$

A synchronizing torque (P_s) can thus be defined as the torque required to pull in the rotor in to synchronization, where $P_s=P_{\max}\cos\delta_o$. Consequently,

$$\frac{H}{\pi f_s}\frac{d^2\Delta\delta}{dt^2}+P_s.\Delta\delta=0,$$

which is a linear differential equation of order two and can be solved through Laplace transformation. With $s=j\omega$, the relationship can be converted from time domain to frequency domain, where,

$$\frac{H}{\pi f_s}s^2\Delta\delta(s)+P_s.\Delta\delta=0 \text{ from which we get,}$$

$$s=\pm\sqrt{-\frac{\pi f_s}{H}P_s}$$

Since, the swing equation is of second order it has two roots.

Now if P_s is positive then there will be two roots on the imaginary axis with values

$$s=\pm j\sqrt{-\frac{\pi f_s}{H}P_s}$$

and if P_s is negative i.e., $\delta_o>90^o$ then the roots are

$$s=+\sqrt{-\frac{\pi f_s}{H}P_s} \quad , \quad -\sqrt{-\frac{\pi f_s}{H}P_s},$$

In which case one root has a positive real part and other root has a negative real part and thus signifies an unstable system.

In practice, the rotor of a synchronous generator does have damper windings due to which it acts as an induction motor during transients and this effect has to be considered while evaluating the stability of the system. This effect of damper winding is called as damping torque and depends on the rate of change of the rotor angle i.e.

$$P_d = D\frac{d\delta}{dt}$$

Where D is the damping coefficient. Arising from D, the classical swing equation is presented as:

$$\frac{H}{\pi f_s}\frac{d^2\Delta\delta}{dt^2} + D\frac{\Delta\delta}{dt} + P_s.\Delta\delta = 0$$

Applying the Laplace transform yields:

$$s^2 + \frac{\pi f_s}{H}Ds + \frac{\pi f_s}{H}P_s = 0$$

Now, the characteristic equation of a standard second order system, is given by

$$s^2 + 2\xi\omega_n s + \omega_n^2 = 0$$

A comparison of the two equations yields:

$$\omega_n = \sqrt{\frac{\pi f_s}{H}P_s} \qquad \text{and} \qquad \xi = \frac{D}{2}\sqrt{\frac{\pi f_s}{H.P_s}}$$

In which case ω_n is the natural frequency and ξ is the damping ratio of the oscillations of the system while the eigen values can be obtained from the characteristic equation as:

$$s = -\xi\omega_n \pm j\omega_n\sqrt{1-\xi^2}$$

Now if P_s>0 then ω_n, ξ>0 and the system will have two complex conjugate roots with negative real parts making the system unstable.

By applying inverse Laplace transform to $S^2 + \frac{\pi f_s}{H} Ds + \frac{\pi f_s}{H} P_s = 0$, the time response of the synchronous generator in a SMIB system when subjected to a small disturbance $\Delta\delta$ can be observed. With an initial condition of $\delta = \delta_o = \sin^{-1}\left(\frac{P_m}{P_{\max}}\right) = 0$, we get:

$$\delta = \delta_o + \frac{\Delta\delta}{\sqrt{1-\xi^2}} e^{-\xi\omega_n t} \sin\left(\left(\omega_n\sqrt{1-\xi^2}\right)t + \cos^{-1}(\xi)\right)$$

$$\omega = \omega_o - \frac{\omega_n\Delta\delta}{\sqrt{1-\xi^2}} e^{-\xi\omega_n t} \sin\left(\left(\omega_n\sqrt{1-\xi^2}\right)t\right)$$

Clearly, if ξ>0 then the time response is a damped sinusoid and the effect is that from an initial condition of δ_o and ω_o, when subjected to a disturbance $\Delta\delta$, there will be oscillations in the angle δ and speed around the initial angle δ_o and ω_o, and these oscillations will be damped out after certain time and finally the angle δ and speed ω will settle down to the initial angle δ_o and initial speed ω_o. The initial speed of the generator rotor in this case is the synchronous speed that is $\omega_o = \omega_s$ (Kumar, 2014)

2.2.2 Transient stability analysis of a SMIB System

a. Criteria for stability

Transient stability analysis is mostly concerned with the analysis of system behaviour following large system disturbances such as short circuit, loss of generation, load rejection etc. In transient disturbances, the resulting system response involves large excursions of generator rotor angles and is influenced by the nonlinear power-angle relationship.

The main difference between small-disturbance and large-disturbance stability analysis is that in small-disturbance it can be assumed that over a small range around an operating condition the power system can be considered linear and thereby can be linearized around that operating condition. Whereas in case of large disturbances the change in the angle or speed of the generator will be high and we can no longer assume that the system is linear.

The transient stability of a SMIB system can be analysed through the so-called Equal Area Criterion (EAC) method. One of the main appealing characteristics of the EAC is that its use eliminates the need of computing the swing curves of the system, thus saving a considerable amount of work. The EAC can be obtained from the swing equation as follows:

From $\frac{d^2\delta}{dt^2} = \frac{\pi f_s}{H}\left(P_m - P_{\max}\sin\delta\right)$

we get $2\frac{d\delta}{dt}\frac{d^2\delta}{dt^2} = \frac{\pi f_s}{H}\left(P_m - P_{\max}\sin\delta\right)\left(2\frac{d\delta}{dt}\right)$

if both sides are multiplied by $\left(2\frac{d\delta}{dt}\right)$.

But because $\frac{d}{dt}\left[\frac{d\delta}{dt}\right]^2 = 2\frac{d\delta}{dt}.\frac{d^2\delta}{dt^2}$ we get

$$\frac{d}{dt}\left[\frac{d\delta}{dt}\right]^2 = \frac{\pi f_s}{H}\left(P_m - P_{\max}\sin\delta\right)\frac{d\delta}{dt}$$

$$d\left[\frac{d\delta}{dt}\right]^2 = \frac{\pi f_s}{H}\left(P_m - P_{\max}\sin\delta\right)d\delta$$

Integrating on both sides and taking square root we get

$$\frac{d\delta}{dt} = \sqrt{\frac{\pi f_s}{H}\int_{\delta_0}^{\delta}\left(P_m - P_{\max}\sin\delta\right)d\delta}$$

For the system to be stable the rotor angle δ should settle down to its steady state value and hence $\frac{d\delta}{dt} = \sqrt{\frac{\pi f_s}{H}\int_{\delta_0}^{\delta}\left(P_m - P_{\max}\sin\delta\right)d\delta}$ should be zero. Therefore,

$$\frac{d\delta}{dt} = 0 \Rightarrow \int_{\delta_0}^{\delta}\left(P_m - P_{\max}\sin\delta\right)d\delta$$

b. Equal area criteria (EAC)

The implication of $\frac{d\delta}{dt} = 0 \Rightarrow \int_{\delta_0}^{\delta}\left(P_m - P_{\max}\sin\delta\right)d\delta$ on system stability can be analysed through a three phase to ground fault in the SMIB system as shown in Fig 19 below:

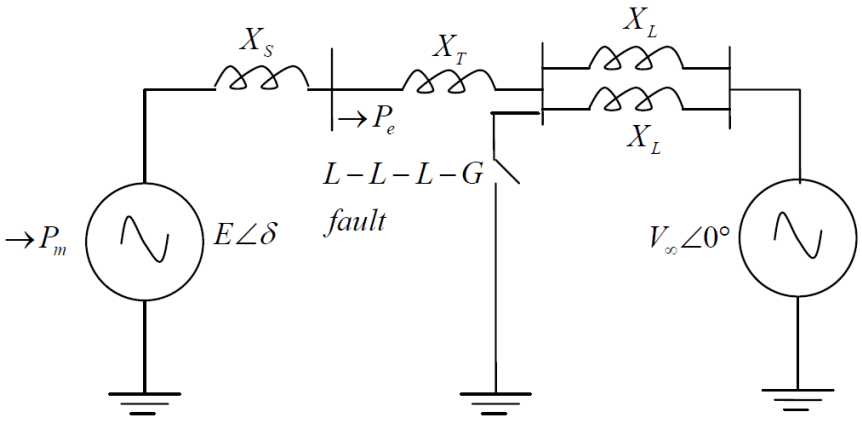

Fig 19:SMIB system with a three-phase to ground fault (Kumar, 2014)

The corresponding *P – δ curve* for the system in Fig 19 above is given in Fig 20 below:

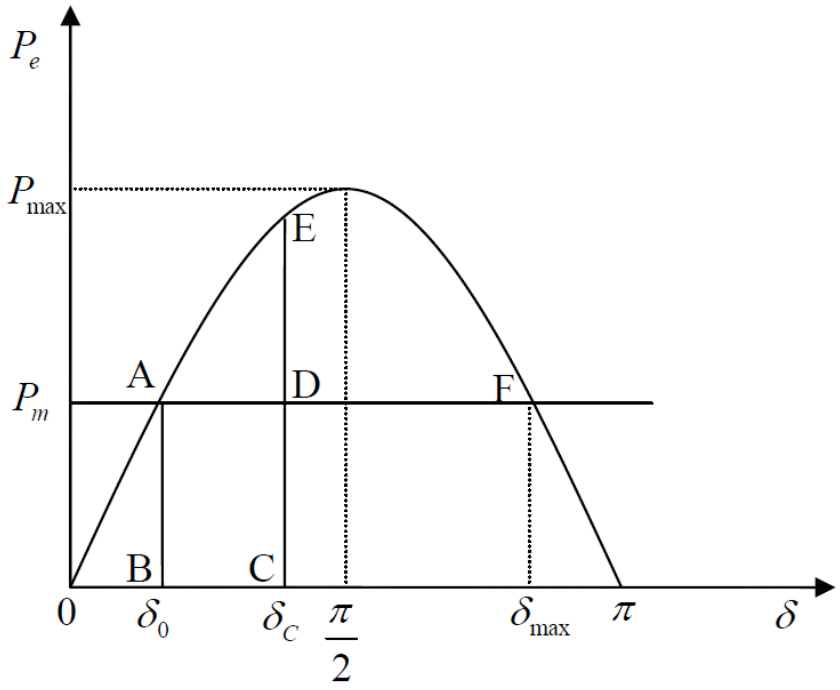

Fig 20:Swing curve demonstrating equal area criterion (Kumar, 2014)

P_m is the mechanical input power and is assumed constant while the stable operation point is considered to be $\delta_o\left(=\sin^{-1}\left(\frac{P_m}{P_{\max}}\right)\right)$ and the unstable operation point is considered to be $\delta_{\max}\left(=\pi-\sin^{-1}\left(\frac{P_m}{P_{\max}}\right)\right)$

In steady state before the fault is applied the rotor angle is at the stable equilibrium point A. When a three-phase to ground fault is applied on one of the transmission lines, towards

the generator, then the electrical power output of the generator will be zero and hence the operating point moves to point B on the *P – δ curve*.

Since, electrical power output ($P_{\max}\sin\delta$) has become zero and the mechanical input power (P_m) is constant the rotor angle starts to increase as can be observed from swing equation. The imbalance in input and output power will lead to rotor gaining kinetic energy and the rotor starts accelerating. Hence, the operating point starts moving from point B on the *P – δ curve* along the *δ-axis* towards infinity. If the fault is cleared say at point C, which corresponds to an angle δ_c, then since electrical power output is not zero but it is $P_{\max}\sin\delta_c$ the operating point moves to point E on the swing curve.

It can be observed that at point E the electrical power output is greater than the mechanical power input and hence the rotor starts decelerating. Since, rotor has finite inertia it cannot change its speed suddenly and hence the rotor acceleration will decrease slows due to which angle will swing from point E to point F. The rotor angle will increase until the rotor losses all the kinetic energy it gained during the fault period is exhausted. Once, the rotor exhausts the kinetic energy gained during fault period it will swing back from point F and will move towards the point A. But if the rotor swing causes the rotor angle to cross the unstable operating point δ_{max} from point E then the system will become unstable. Hence, the rotor can swing maximum up to δ_{max} before becoming unstable. Consequently,

$$\int_{\delta_0}^{\delta_{\max}} \left(P_m - P_{\max}\sin\delta\right) d\delta = 0$$

With the intervals of integration as δ_o - δ_c and δ_c - δ_{max}, the above relationship becomes:

$$\int_{\delta_0}^{\delta_c} \left(P_m - P_{\max}\sin\delta\right) d\delta + \int_{\delta_c}^{\delta_{\max}} \left(P_m - P_{\max}\sin\delta\right) d\delta = 0$$

Rearranged to

$$\int_{\delta_0}^{\delta_c} \left(P_m - P_{\max}\sin\delta\right) d\delta = \int_{\delta_c}^{\delta_{\max}} \left(P_{\max}\sin\delta - P_m\right) d\delta$$

From Fig 20: it can be observed that:

$$\int_{\delta_0}^{\delta_c} \left(P_m - P_{\max}\sin\delta\right) d\delta = \text{Area of ABCD} \text{ and}$$

$$\int_{\delta_c}^{\delta_{\max}} \left(P_{\max}\sin\delta - P_m\right) d\delta = \text{Area of DEF}$$

Consequently, it can be concluded that the energy gained during acceleration (Area ABCD) should be exactly equal to the energy lost during deceleration (Area DEF) for the system to be stable. Therefore, for stability the EAC requires that:

Area of P - δ curve during acceleration = Area during deceleration

With this understanding, in intention thus is to ensure the fault is cleared below a critical clearing angle δ_c such that area of acceleration is equal to area of deceleration. If the fault is cleared later than critical clearing angle then area of acceleration will become more than area of deceleration due to which the rotor angle will swing beyond the point F and will become unstable. In order to find the critical clearing angle δ_c therefore have to solve

$$\int_{\delta_0}^{\delta_c} \left(P_m - P_{\max}\sin\delta\right) d\delta = \int_{\delta_c}^{\delta_{\max}} \left(P_{\max}\sin\delta - P_m\right) d\delta \text{ for } \delta_c.$$

During a fault event, the electrical output power is zero hence $P_e = P_{\max}\sin\delta = 0$. With this relationship,

$$\int_{\delta_0}^{\delta_c} P_m d\delta = \int_{\delta_c}^{\delta_{\max}} \left(P_{\max}\sin\delta - P_m\right) d\delta \text{ for which } \delta_c \text{ can be solved as:}$$

$$\text{Cos}\,\delta_c = \frac{P_m}{P_{\max}}\left(\delta_{\max} - \delta_o\right) + \delta_{\max} \quad \text{or}$$

$$\delta_c = \cos^{-1}\left(\frac{P_m}{P_{\max}}\left(\delta_{\max} - \delta_o\right) + \delta_{\max}\right)$$

δ_c is the critical clearing angle at which if the fault is cleared the system becomes stable. However, there is also need to know the clearing time corresponding to the critical clearing angle δ_c. Again, we consider the swing equation during the fault (P_e=0).

$$\frac{d^2\delta}{dt^2} = \frac{\pi f_s}{H} P_m$$

Double integration on both sides yields:

$$\delta = \frac{\pi f_0}{2H} P_m t^2 + \delta_0$$

If $\delta = \delta_c$ and t the critical clearing time is set at t_c, then,

$$t_c = \sqrt{\frac{(\delta_c - \delta_0).2H}{\pi f_s P_m}} \quad \text{s}$$

The above assessment is based on a three-phase to ground fault near the generator bus resulting in the electrical power output from the generator being zero during the fault. In the case of a three-phase to ground fault is at some distance from the generator terminal then the electrical power output will not become zero but will transmit power along the healthy transmission line at a reduced level which depends on the distance of the fault from the generator terminal.

Considering the SMIB system shown in Fig 19 above, where instead of the fault being at the generator terminals let it be at the centre of the second transmission line due to which the maximum power that can be transferred to the infinite bus reduces P_{max2} and after the fault is cleared the faulted line is disconnected from the system hence the maximum power that can be transferred to the infinite bus post fault also reduced, due to increased reactance. Let this reduce power be P_{max3}. In such a case, three *P – δ curves* are developed to represent the pre-fault, during-fault and post-fault conditions as shown in Fig 21 below:

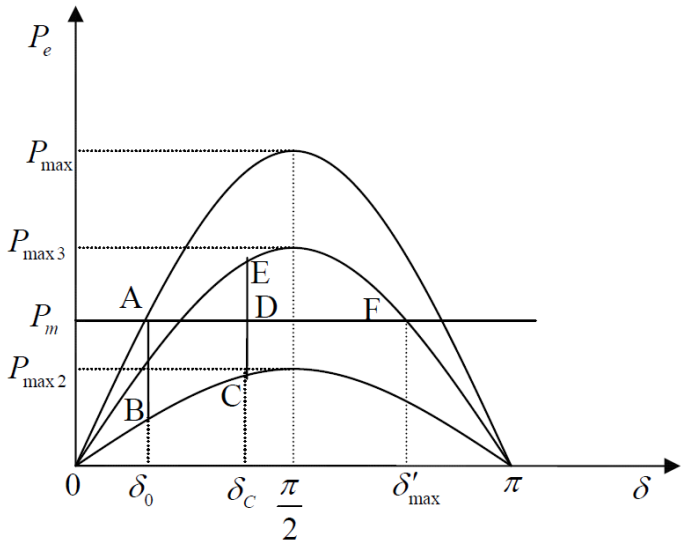

Fig 21: Swing curve during pre, post and during the fault (Kumar, 2014)

In pre-fault case the system is stable at operating point A. At the time of the fault the operating point moves to point B on the *P – δ curve* with maximum power transfer P_{max2}. As the mechanical input power P_m is greater than $P_{max2}sin\delta$ the rotor will accelerate and the operating point movies from point B to point C where the fault is cleared followed by tripping of the faulted line. At operating point C as the fault is cleared the rotor angle will move to point E on post fault *P – δ curve* with maximum power transfer P_{max3}.

Due to inertia of the rotor the rotor angle will swing from point E and will move up to the point F before becoming unstable.

Here $\delta_0 = \sin^{-1}\left(\frac{P_m}{P_{\max}}\right)$ and $\delta'_{\max} = \pi - \sin^{-1}\left(\frac{P_m}{P_{\max 3}}\right)$.

It has to noted that δ_{max} in $\int_{\delta_0}^{\delta_c}\left(P_m - P_{\max}\sin\delta\right)d\delta = \int_{\delta_c}^{\delta_{\max}}\left(P_{\max}\sin\delta - P_m\right)d\delta$ corresponds to the pre-fault equilibrium point of post-fault system. Applying equal area criterion to this system and equating the area of acceleration and area of deceleration we get

$$\int_{\delta_0}^{\delta_c}\left(P_m - P_{\max 2}\sin\delta\right)d\delta = \int_{\delta_c}^{\delta'_{\max}}\left(P_{\max 3}\sin\delta - P_m\right)d\delta$$

From which,

$$\text{Cos}\,\delta_c = \frac{P_m\left(\delta'_{\max} - \delta_0\right) + P_{\max 3}\cos\delta'_{\max} - P_{\max 2}\cos\delta_0}{P_{\max 3} - P_{\max 2}}$$ or

$$\delta_c = \cos^{-1}\left(\frac{P_m\left(\delta'_{\max} - \delta_0\right) + P_{\max 3}\cos\delta'_{\max} - P_{\max 2}\cos\delta_0}{P_{\max 3} - P_{\max 2}}\right)$$

c. Numerical integration of swing equation

The EAC gives an analytic way of assessing the stability of the system however, transient stability of the system can also be found out by numerically integrating the swing equation. But since the swing equation is nonlinear it cannot be resolved using analytical methods. In order to solve the swing equation numerical methods have been used. Such numerical methods include the Euler's method.

Solutions of the swing equation using numerical methods shall not be discussed further in this discussion.

3. Frequency Stability

The frequency of a given power network is expected to be the same at all points of the network at steady state. However, when a significant disturbance occurs, the frequency varies in time and space, and in many ways, it exhibits the characteristics of electromechanical wave propagation phenomena.

Abnormalities in the frequencies would lead to damage of power system equipment and therefore maintaining the grid frequency within an acceptable range is a necessary requirement for the stable operation of power systems. Frequency stability and in turn also stable operation both depend on the active power balance, meaning that the total power feed-in minus the total load consumption (including system losses) is kept close to zero. In normal operation small variations of this balance occur spontaneously. Deviations from its nominal value f_0, e.g., 50 Hz, should be kept small, as damaging vibrations in synchronous machines and load shedding occur for larger deviations.

Because the loss of a large generator is much more likely than a sudden loss of load, frequency response is typically discussed in the context of a loss of a large generator.

3.1 Frequency Response for a SMIB System

Frequency response is best explained by considering the changes in kinetic energy of the conventional generation equipment in the event of system disturbances. The kinetic energy stored in the rotating masses of the conventional generators is released following a disturbance, rendering the power system frequency dynamics slower and, hence, easier to regulate. The rotational energy in a conventional generator of a SMIB is given as:

$$E_{kin} = \frac{1}{2} J \left(2\pi f_m\right)^2$$

with J as the moment of inertia of the synchronous machine and f_m the rotating frequency of the machine. The inertia constant $H = \frac{\frac{1}{2} J \omega_{ms}{}^2}{\text{Base MVA}}$ for this machine can be rewritten as

$$H = \frac{E_{kin}}{S_B} = \frac{J\left(2\pi f_m\right)^2}{2S_B}$$

with S_B as the rated power of the generator and H denoting the time duration during which the machine can supply its rated power solely with its stored kinetic energy. Typical values for H are in the range of 2 – 10 s (Kundur, 1994).

The inertial response of such a synchronous generator following a power imbalance will thus be described by swing equation as the change in rotational frequency f_m or indeed the rotational speed $\omega_m = 2\pi f_m$ of the generator and can be represented as:

$$dE_{kin} = J\left(2\pi\right)^2 f_m.df_m = \frac{2\mathrm{H}S_B}{f_m}.df_m = \left(P_m - P_e\right)$$

Where P_m is the mechanical power supplied by the generator and P_e is the electric power demanded by the system. And since frequency excursions are usually small deviations around the reference value, f_m can be replaced with f_0 and P_m with P_{m0}, and complete then adding a frequency-dependent load damping (D) to the classical swing equation we get:

$$df_m = -\frac{f_0}{2\mathrm{H}S_B D_{\text{load}}} f_m + \frac{f_0}{2\mathrm{H}S_B}\left(P_{m,0} - P_e\right)$$

D_{load} is the frequency-dependent load damping constant which is basically the self-stabilizing property inherent in power systems. D_{load} can also be presented as K_{load} and the relationship is that:

$$K_{\text{load}} = \frac{1}{D_{\text{load}}}$$

3.2 Frequency Response for a Multiple Machine System

In a multi-machine interconnected system, frequency response modelling for different aggregated generator and load nodes can be realized in a similar fashion as modelling individual generators by reformulating the classical Swing Equation to include *n* generators, *j* loads and *l* connecting tie-lines to obtain what is known as the Aggregated Swing Equation. The Aggregated Swing Equation is shown below:

$$df = -\frac{f_0}{2\mathrm{H}S_B D_{\text{load}}} f + \frac{f_0}{2\mathrm{H}S_B}\left(P_m - P_{\text{load}} - P_{\text{loss}}\right)$$

Where,

$$f = \frac{\sum_{i=1}^{n} H_i S_{B,i} f_i}{\sum_{i=1}^{n} H_i S_{B,i}}, \qquad S_B = \sum_{i=1}^{n} S_{B,i}, \qquad H = \frac{\sum_{i=1}^{n} H_i S_{B,i}}{S_B},$$

$$P_m = \sum_{i=1}^{n} P_{m,i} \qquad P_{\text{load}} = \sum_{i=1}^{j} P_{\text{load},i} \qquad P_{\text{loss}} = \sum_{i=1}^{l} P_{\text{loss},i}$$

In which case, *f* is the Centre of Inertia (COI) grid frequency, H the aggregated inertia constant of the *n* generators, S_B the total rated power of the generators, P_m the total mechanical power of the generators, P_{load} the total system load of the grid and P_{loss} the total transmission losses of the *l* lines making up the grid topology and f_0 = 50 Hz. The term D_{load} is the frequency damping of the system load.

The Aggregated Swing Equation model is valid for a highly meshed grid, in which all units can be assumed to be connected to the same grid bus, representing the Centre of Inertia of the given grid (Andreas et al, 2014).

Since load-frequency disturbances are relatively small, linearized swing equations with $\Delta f_i = f_i - f_0$ can be used. Following a system disturbance and assuming $\Delta P_{loss} = 0$, the Aggregated Swing Equation can be presented as:

$$\Delta df = -\frac{f_0}{2\mathrm{H}S_B D_{\text{load}}} \Delta f + \frac{f_0}{2\mathrm{H}S_B}\left(\Delta P_m - \Delta P_{\text{load}}\right)$$

In frequency stability analysis often, the assumption is used that the (aggregated) inertia constant H is constant (and the same) for all swing equations of a multi-area system. This assumption is being tested by reality as more variable power generators are integrated onto the grid. The aggregated inertia H_{agg} is highly time-variant and fluctuates between its nominal value of 6 s, i.e., at times when only conventional generators are dispatched, and significantly lower levels of 3–4 s at times when significant shares of variable power generators are deployed (Andreas et al, 2014).

4. Voltage Stability

Voltage stability is the ability of a power system to maintain acceptable voltages at all busbars in the system under normal condition and after being subjected to a disturbance. In the normal operating condition, the voltage of a power system is stable, but when the fault or disturbance occurs in the system, the voltage becomes unstable this result in a progressive and uncontrollable decline in voltage. Voltage stability is sometimes also called load stability.

The voltage stability problem is now a serious concern to the electric utility industry due to the ever-increasing complexity in their operation and modified structures (Thannimalai et al, 2015). With an open access market, poorly scheduled generation for the competitive bidding is one of many reasons for voltage instability problem in the deregulated electricity environment.

Voltage stability may be classified as Large-disturbance Voltage Stability which, is concerned with a system stability to control voltages following a large disturbance such as system faults, loss of load, or loss of generation, and Small-Disturbances Voltage Stability which is concerned with a system's ability to control voltages following small perturbations such as incremental changes in system load.

4.1 Voltage Stability Limit

The voltage stability limit has been defined as the limiting stage in a power system beyond which no amount of reactive power injection will raise the system voltage to its nominal state (Circuit Globe, 2020). The system voltage can only be adjusted by reactive power injections till the system voltage stability is maintained.

From previous discussions, the power transfer over a lossless line can be presented as:

$$P = \frac{V_s V_r}{X} \sin \delta$$

Where,

P is the power transferred per phase
V_s is the sending-end phase voltage
V_r is the receiving-end phase voltage
X is the transfer reactance per phase; and
δ is the phase angle between V_s and V_r.

now since the line is lossless then $P_s = P_r = P$. And assuming constant power generation,

$$\frac{dP_r}{dV_s} = 0$$

$$\frac{V_r}{X}\sin\delta + \frac{V_s V_r}{X}\cos\delta\frac{d\delta}{dV_s} = 0$$

$$\frac{d\delta}{dV_s} = -\frac{\tan\delta}{V_s}$$

From which maximum power transfer is obtained at δ = 90^o so that $\frac{d\delta}{dV_s} = -\infty$ signifying the location of the critical point on the δ versus V curve provided that the receiving end voltage is constant.

On the other hand, the reactive power expression at the receiving-end bus may also be written as

$Q_r = \frac{V_s V_r}{X}\cos\delta - \frac{V_r^2}{X}$ leading to:

$\frac{dQ_r}{dV_r} = \frac{1}{X}\left[V_s\cos\delta - V_s V_r\sin\delta\frac{d\delta}{dV_r} - 2V_r\right]$ and,

Now knowing that a similar result to $\frac{d\delta}{dV_s} = -\frac{\tan\delta}{V_s}$ can be obtained on the receiving end assuming the sending end voltage constant and analysing the system taken V_r as a variable parameter in which case $\frac{d\delta}{dV_r} = -\frac{\tan\delta}{V_r}$. Then,

$$\frac{dQ_r}{dV_r} = \frac{1}{X}\left[V_s\cos\delta - V_s V_r\sin\delta\left(-\frac{\tan\delta}{V_r}\right) - 2V_r\right]$$ broken down further to

$$\frac{dQ_r}{dV_r} = \frac{1}{X}\left[V_s\cos\delta + V_s\frac{\sin^2\delta}{\cos\delta} - 2V_r\right] = \frac{1}{X}\left[V_s\left(\frac{\cos^2\delta + \sin^2\delta}{\cos\delta}\right) - 2V_r\right]$$ and consequently,

$$\frac{dQ_r}{dV_r} = \frac{1}{X}\left[\frac{V_s}{\cos\delta} - 2V_r\right]$$

At steady state, δ = 90^o so that $\frac{dQ_r}{dV_r} = \infty$ representing the steady-state voltage stability limit.

$\frac{dQ_r}{dV_r} = \infty$ shows that, at steady state stability limit, the reactive power becomes infinite. This means that $\frac{dQ}{dV_r}$ becomes zero. Hence the rotor angle stability limit under steady state conditions is coincident with steady state voltage stability limit. The voltage stability at steady state may also be affected by the load.

4.2 Voltage Stability of a SMIB System

Voltage stability of a SMIB system can be accessed arising from the relationships:

$$P = \frac{EV}{X}\sin\delta \text{ and } Q = \frac{EV}{X}\cos\delta - \frac{V^2}{X}$$

when these relations are normalised by using

$$v = \frac{V}{E},\ p = P\frac{X}{E^2} \text{ and } q = Q\frac{X}{E^2} \text{ then}$$

$$p = v\sin\delta \text{ and } q = -v^2 + v\cos\delta$$

When *p* and *q* are squared on both sides, and following some appropriate rearrangements, we get

$$v^2(\sin^2\delta + \cos^2\delta) = p^2 + \left(q + v^2\right)^2 \text{ or}$$

$$v^4 + v^2(2q-1) + \left(p^2 + q^2\right) = 0$$

And the positive real solutions of *v* are given by:

$$v = \sqrt{\frac{1}{2} - q \pm \sqrt{\frac{1}{4} - p^2 - q}}$$

A plot of v on the *p – q – v plane* is shown in Fig 22 below:

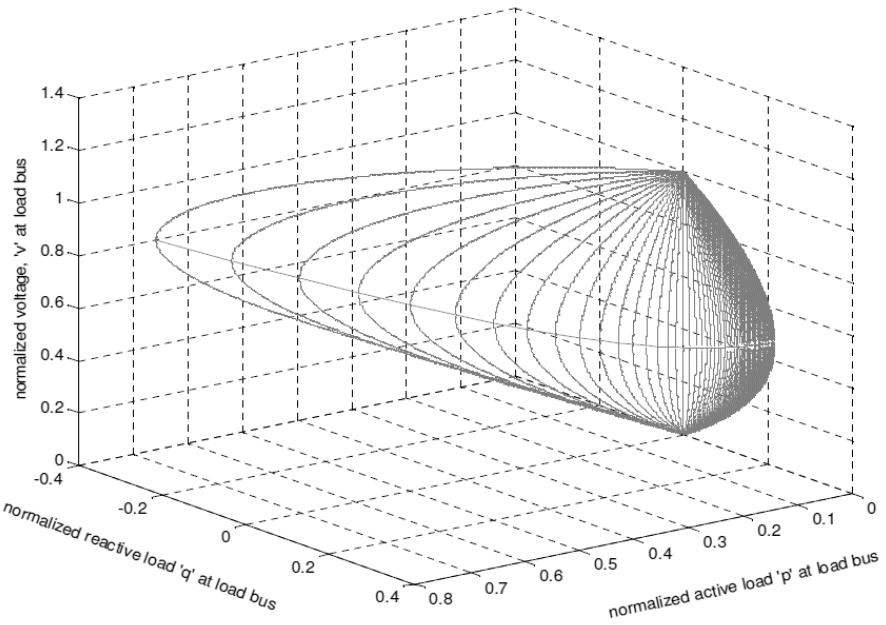

Fig 22: Variation of bus voltage with active and reactive loading for a typical SMIB system (S. Chakrabarti)

Corresponding to each point (*p*,*q*), there are two solutions for voltage, one is the high voltage or stable solution, which is the actual voltage at the bus, and the other one is the low voltage or unstable solution. The equator, along which the two solutions of *v* are equal, represents maximum power points.

Starting from any operating point on the upper part of the surface, an increase in p or q or both brings the system closer to the maximum power point. An increase in p or q beyond the maximum power point makes the voltage unstable.

4.3 Tools for voltage stability analysis

There are numerous methods for analysing the voltage stability of such a given network. The conventional analysis methods can broadly be classified into four (04) types and these are:

1. **The *P – V Curve* Method**
   The *P – V Curve* is one of the widely used methods of voltage stability analysis. *P – V Curve* gives the available amount of active power margin before the point of voltage instability. For radial systems, the voltage of the critical bus is monitored against the changes in real power consumption. For large meshed networks, *P* can be the total active load in the load area and *V* can be the voltage of the critical or representative bus (Chakrabarti, S.,).

   For the SMIB discussed in (4.2) above, the relationship $v = \sqrt{\frac{1}{2} - q \pm \sqrt{\frac{1}{4} - p^2 - q}}$

   gives real solutions of v^2 as

   $\left(1 - 4q - 4p^2\right) \geq 0$

Assuming a constant power factor load such that $q/p = k$ (constant), the inequality can be expressed as,

$$p \le \frac{1}{2}\left(\left(1+k^2\right)^{1/2} - k\right)$$

Thus, there are two solutions for p,

$$v_1 = \left(\frac{1}{2} - pk + \left(\frac{1}{4} - pk - p^2\right)^{1/2}\right)^{1/2}$$

$$v_2 = \left(\frac{1}{2} - pk - \left(\frac{1}{4} - pk - p^2\right)^{1/2}\right)^{1/2}$$

For the real values of v_1 and v_2, the terms under the square roots should be positive.

Hence,

$$\left(\frac{1}{2} - pk - \left(\frac{1}{4} - pk - p^2\right)^{1/2}\right) \ge 0$$

Or

$$P^2\left(k^2+1\right) \ge 0$$

Hence $p \le \frac{1}{2}\left(\left(1+k^2\right)^{1/2} - k\right)$ is the relationship that determines the maximum value of p. Thus, representing the load as a constant power factor type, with a suitably chosen power factor, the active power margin can be computed. For different values of load power factors, i.e., for different corresponding values of 'k', the normalized values of load active power are shown in Fig 23 below:

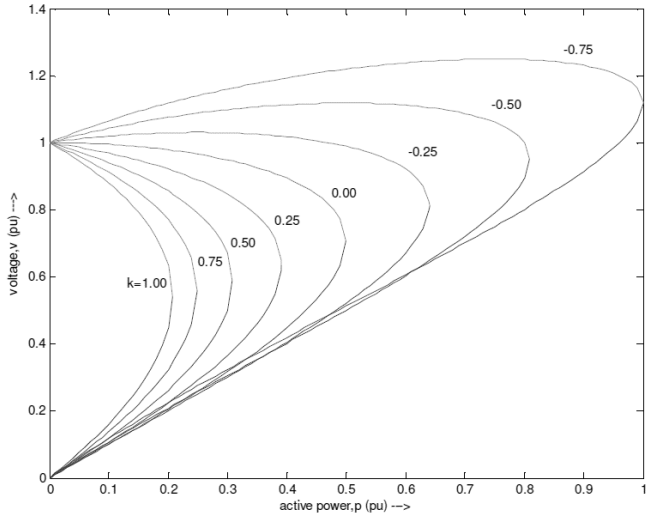

Fig 23: Normalized P-V curves for the a typical SMIB system (Cutsem and Vournas, 1998)

2. The V – Q Curve method and reactive power reserve

The V-Q curve method is a popular to investigate voltage instability issues power systems during the post transient period (Chakrabarti, S.,). Unlike the P-V curve method, it doesn't require the system to be represented as a two-bus equivalent (SMIB). Voltage at a test bus or critical bus is plotted against reactive power at that bus. A fictitious synchronous generator with zero active power and no reactive power limit is connected to the test bus. The power-flow program is run for a range of specified voltages with the test bus treated as the generator bus. Reactive power at the bus is noted from the power flow solutions and plotted against the specified voltage. The operating point corresponding to zero reactive power represents the condition when the fictitious reactive power source is removed from the test bus.

Voltage security of a bus is closely related to the available reactive power reserve, which can be easily found from the *V – Q Curve* of the bus under consideration. The reactive power margin is the MVAR distance between the operating point and either the nose point of the *V – Q Curve* or the point where capacitor characteristics at the bus are tangent to the *V – Q Curve* (Taylor, 1994). Stiffness of the bus can be qualitatively evaluated from the slope of the right portion of the *V – Q Curve*. The greater the slope is, the less stiff is the bus, and therefore the more vulnerable to voltage collapse it is. Weak busses in the system can be determined from the slope of *V – Q Curve*.

For the SMIB above discussed, equations of *V - Q Curves* for constant power loads can be derived using $p = v\sin\delta$, in which the power angle δ is computed for specified active power. Thereafter, δ is used in $q = -v^2 + v\cos\delta$. For a range of values of voltage and different active power levels, normalized V – Q Curves are shown in Fig 24 below:

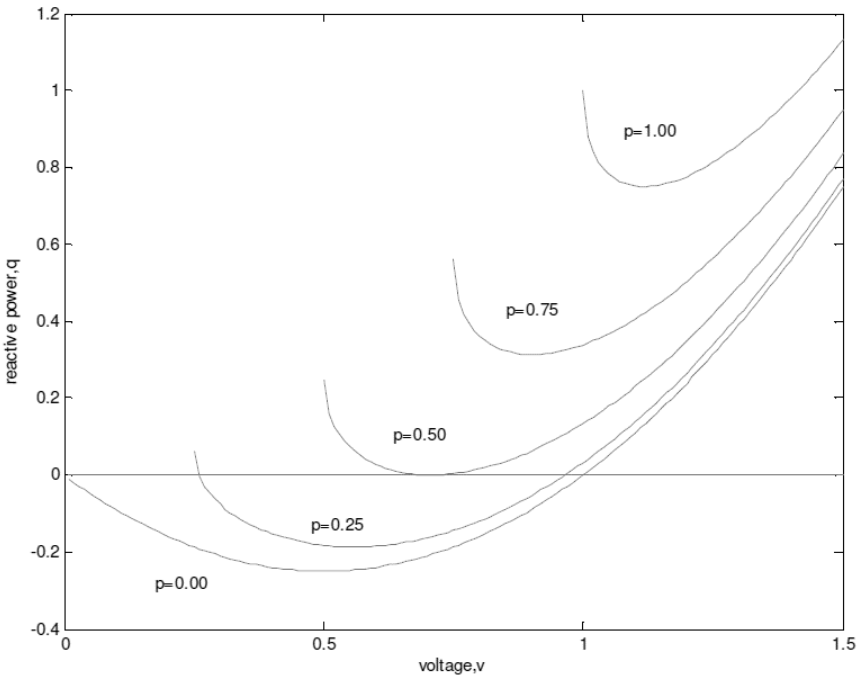

Fig 24:Normalized V – Q Curves for the a typical SMIB system (Chakrabarti, S.,)

The critical point or nose point of the characteristics corresponds to the voltage where dQ/dV becomes zero. If the minimum point of the *V – Q Curve* is above the horizontal axis, then the system is reactive power deficient. Additional reactive power sources are needed to prevent a voltage collapse. In this case, curves for p=1.00 and p=0.75 in Fig 24 signify reactive power deficient buses.

On the other hand, buses having *V – Q Curves* below the horizontal axis have a positive reactive power margin. The system may still be called reactive power deficient, depending on the desired margin (Chakrabarti, S.,).

3. Method based on singularity of power-flow Jacobian matrix at the point of voltage collapse

These methods ride on the principle that the power flow Jacobian matrix becomes singular at the point of voltage collapse and modal analysis of the Jacobian matrix is one of the most popular methods. Modal analysis involves the investigation of eigenvalues and eigen vectors and that is:

For a (n x n) square matrix **A**, left and right eigenvectors are defined as follows:

$Ax=\lambda x$
$yA=\lambda y$

5. Disadvantages of Classical Method of Stability Analysis

There are several disadvantages of using simplistic model of synchronous generators and these include:

1. The rotor flux decay, the damper windings on the generator rotor and the effect of rotor core on the stability are totally neglected in the classical model. But they can affect the stability of a system significantly.

2. The internal voltage of the generator behind the synchronous reactance is assumed to be constant on the basis that the rotor field current is held constant. This assumption is not true and the rotor field current is controlled through an excitation system and automatic voltage regulator (AVR). Also, it is well observed phenomenon that high gain fast acting exciters can cause small signal instability (Concordia, 1944). Hence, the exciter and AVR dynamics have to be taken into account;

3. It is assumed throughout the analysis that the mechanical power input is held constant. Again, the input mechanical power depends on turbine speed governor and turbine dynamics. By controlling the mechanical power input according to the variation in the electrical power input we can improve the transient stability of the system. Hence, the dynamics of speed governor and turbine have to be considered.

4. Important generator external controllers like power system stabilizer (PSS) improve the system stability significantly and need to be modelled.

5. Dynamic loads like induction motors, synchronous motors, power electronic devices etc can affect the stability drastically. These are not taken into consideration in the classical model.

Due, to these limitations the classical method cannot give an accurate idea about the stability of the system. Detailed modelling of synchronous generator, excitation system, speed governor, turbine, external controllers and loads would be required to accurately analyse a typical power system.

6. References

1. Babu, R. (2010). Numerical Methods, Pearson Education, India
2. Chakrabarti, S., Notes on Power System Voltage Stability, Dept. of EE, IIT, Kanpur
3. Concordia, C. (1944). Steady-state stability of synchronous machines as affected by voltage regulator characteristics, AIEE Trans., Vol. 63, pp. 215-220.
4. Crary, S. B. (1945). Power System Stability Volume I: Steady State stability, John Wiley, New York.
5. Cutsem, T. V. and Vournas, C. (1998). Voltage Stability of Electric Power Systems, Kluwer Academic Publishers.
6. DIgSILENT PowerFactory. (2018). User Manual, DIgSILENT GmbH, Gomaringen, Germany
7. https://circuitglobe.com/voltage-stability-in-power-system.html accessed 23 November, 2020
8. Kimbark, E. W. (1948). Power System Stability, Volume I: Elements of Stability Calculations, John Wiley (New York)
9. Kundur, P. (1994). Power system stability and control, McGraw-Hill Inc., New York.
10. NERC Training resource working group, (2003). Understand and calculate frequency response, NERC Training Document
11. Thannimalai P., Raman R.R., Nair P., and Nithiyananthan k. (2015). Voltage Stability Analysis and Stability Improvement of Power System, International Journal of Electrical and Computer Engineering (IJECE), Vol. 5, No. 2, April 2015, pp. 189~197, ISSN: 2088-8708

7.3. Appendix 3: System Setup for the Model Zambia National Grid

The model for the study was built with reference to a ZESCO file of 2010 which was then updated using reports on recent power projects and system upgrades. Key system parameters were set as follows:

1. Generators

Table 1.1: List of Generators in Zambia

S/N	Location	Description	Installed Capacity (MVA)	Operating (MVA)	Power Factor	Voltage Set Point (pu)	Operator	Comment
1.	Kariba North	Gen # 1	200	165	0.92	1.03	ZESCO Ltd	
		Gen # 2	200	165	0.92	1.03		
		Gen # 3	200	165	0.92	1.03		
		Gen # 4	200	165	0.92	1.03		
		Gen # 5	200	165	0.92	1.03		Peaking Plants, Out of Service
		Gen # 6	200	165	0.92	1.03		
2.	Kafue Gorge	Gen # 1	200	165	0.8988	1.02	ZESCO Ltd	Reference Machine
		Gen # 2	200	165	0.8988	1.02		
		Gen # 3	200	165	0.8988	1.02		
		Gen # 4	200	165	0.8988	1.02		
		Gen # 5	200	165	0.8988	1.02		
		Gen # 6	200	165	0.8988	1.02		
3.	Victoria Falls	Gen # A1	1.25	0.9	1	1.00	ZESCO Ltd	
		Gen # A2	1.25	0.9	1	1.00		
		Gen # A3	3.75	3.0	1	1.00		
		Gen # A4	3.75	3.0	1	1.00		
		Gen # B1	11.7	9.9	1	1.00		
		Gen # B2	11.7	9.9	1	1.00		
		Gen # B3	11.7	9.9	1	1.00		
		Gen # B4	11.7	9.9	1	1.00		
		Gen # B5	11.7	9.9	1	1.00		
		Gen # B6	11.7	9.9	1	1.00		
		Gen # C1	11.77	6	1	1.00		
		Gen # C1	11.77	6	1	1.00		
		Gen # C1	11.77	6	1	1.00		
		Gen # C1	11.77	6	1	1.00		
4.	Maamba	Gen # 1	150	120	0.9	-	IPP	Constant Q
		Gen # 2	150	120	0.9	-	IPP	Constant Q
5.	Itezhi Tezhi	Gen # 1	89	63	0.85	1.00	IPP	Not precise
		Gen # 2	89	63	0.85	1.00	IPP	Not precise
6.	Mulungushi	Gen # 1	2.5	2.5	0.85	1.00	IPP	
		Gen # 2	6.25	6.25	0.85	1.00	IPP	
		Gen # 3	6.25	6.25	0.85	1.00	IPP	
		Gen # 4	8.00	8.00	0.85	1.00	IPP	
7.	Lunsemfwa	Gen # 1	6.00	6.00	0.85	1.00	IPP	
		Gen # 2	6.00	6.00	0.85	1.00	IPP	
		Gen # 3	6.00	6.00	0.85	1.00	IPP	
8.	Lusiwasi	Gen # 1	3.50	2.97	0.9417	-	ZESCO Ltd	
		Gen # 2	3.50	2.97	0.9417	-		

		Gen # 3	3.50	2.97	0.9417	-		
		Gen # 4	3.50	2.97	0.9417	-		
9.	Musonda Falls	Gen # 1	1.20	1.20	0.85	-	ZESCO Ltd	
		Gen # 2	1.20	1.20	0.85	-		
		Gen # 3	1.20	1.20	0.85	-		
		Gen # 4	1.20	1.20	0.85	-		
10.	Chishimba Falls	Gen # 1	1.40	1.2	0.87	-	ZESCO Ltd	
		Gen # 2	1.40	1.2	0.87	-		
		Gen # 3	1.40	1.2	0.87	-		
		Gen # 4	1.40	1.2	0.87	-		
11.	Lunzua	Lunzua	Omitted					

2. Transmission Lines

All existing transmission lines were in service except for:

i. 66kV Msoro – Chipata
ii. 88kV Muzuma – Maamba
iii. 330kV Mumbwa (Nambala) – Kalumbila line 2

Some of the newer transmission lines that were not modelled include:

iv. North-western grid extension
v. Kafue Town – Livingstone via Mukuni substation

3. Compensation

S/N	Location	Description	Capacity (MVar)	Type	Status
1.	Victoria Falls	33kV Bus Reactor	11.8	R-L	Out of Service
2.	Maamba	330kV Bus Reactor	25	R-L	In Service
3.	Muzuma	330kV Bus Reactor	80	R-L	In Service
4.	Sesheke	220kV Sesheke Victoria Falls Line Reactor	15	R-L	Out of Service
		220kV Bus Capacitor	6	R-L	Out of Service
5.	Mongu	66kV Bus Reactor	2.4	C	Out of Service
		66kV Bus Reactor	2	R-L	Out of Service
6.	Lusaka West	330kV Bus Reactor	30	R-L	In Service
7.	Nambala	330kV Nambala-Kalumbila Line 1 Reactor	35	R-L	In Service
		330kV Nambala-Kalumbila Line 2 Reactor	35	R-L	Out of Service
		330kV Bus Reactor	30	R-L	In Service
8.	Kalumbila	330kV Kalumbila-Nambala Line 1 Reactor	40	R-L	Out of Service
		330kV Kalumbila-Nambala Line 2 Reactor	40	R-L	Out of Service
		33kV Bus Capacitor	25	C	Out of Service
9.	Lumwana	330kV Bus Reactor	10	R-L	In Service
		330kV Bus Capacitor	25.2	C	In Service
		33kV Bus Capacitor No. 1	25	C	Out of Service
		33kV Bus Capacitor No. 2	25	C	Out of Service
		33kV Bus Capacitor No. 3	25	C	Out of Service
		33kV Bus Capacitor No. 4	25	C	Out of Service
10.	Kansanshi	330kV Bus Capacitor	25	C	Out of Service
		33kV Bus Capacitor No. 1	20	C	Out of Service
		33kV Bus Capacitor No. 2	25	C	Out of Service
		33kV Bus Capacitor No. 3	15	C	Out of Service
		33kV Bus Capacitor No. 4	10	C	Out of Service
11.	Luano	11kV Bus Capacitor No. 1	20	C	Out of Service
		11kV Bus Capacitor No. 2	30	C	Out of Service

		11kV Bus Capacitor No. 3	30	C	Out of Service
		11kV Bus Capacitor No. 4	30	C	Out of Service
		220kV Compensator	40	C	In Service
12.	Stadium	11kV Bus Reactor	16.7	R-L	In Service
13.	Michelo	66kV Bus Capacitor	15	C	In Service
		66kV Bus Capacitor	0.96	C	In Service
14.	Bancroft Central	66kV Bus Capacitor No. 1	8	C	In Service
		66kV Bus Capacitor No. 2	8	C	In Service
		66kV Bus Capacitor No. 3	8	C	In Service
15.	Chambishi East	66kV Bus Capacitor	30	C	In Service
16.	Kansuswa	66kV Bus Capacitor No. 1	15	C	In Service
		66kV Bus Capacitor No. 2	15	C	Out of Service
17.	Kankoyo	66kV Bus Capacitor No. 1	8	C	In Service
		66kV Bus Capacitor No. 2	8	C	In Service
		66kV Bus Capacitor No. 3	8	C	In Service
18.	Cosak	33kV Bus Capacitor No. 1	15	C	In Service
		33kV Bus Capacitor No. 2	15	C	In Service
19.	Kitwe	11kV Bus Capacitor No. 1	29	C	In Service
		11kV Bus Capacitor No. 2	29.4	C	In Service
		11kV Bus Reactor	20	R-L	Out of Service
		11kV Bus Capacitor No. 3	25	C	In Service
		11kV Bus Capacitor No. 4	33.3	C	In Service
		11kV Bus Capacitor No. 5	20	C	Out of Service
		11kV Bus Capacitor No. 6	20	C	Out of Service
20.	Nkana	66kV Bus Capacitor No. 1	1	C	Out of Service
		66kV Bus Capacitor No. 2	1	C	Out of Service
		66kV Bus Capacitor No. 3	1	C	Out of Service
		66kV Bus Capacitor No. 4	1	C	Out of Service
21.	Mill	66kV Bus Capacitor No. 1	1	C	In Service
		66kV Bus Capacitor No. 2	1	C	In Service
		66kV Bus Capacitor No. 3	1	C	In Service
22.	Mindola	66kV Bus Capacitor No. 1	1	C	In Service
		66kV Bus Capacitor No. 2	1	C	In Service
		66kV Bus Capacitor No. 3	1	C	In Service
		66kV Bus Capacitor No. 4	1	C	In Service
		66kV Bus Capacitor No. 5	1	C	In Service
23.	Maposa	66kV Bus Capacitor No. 1	15	C	In Service
		66kV Bus Capacitor No. 2	15	C	Out of Service
24.	Pensulo	330kV Pensulo-Msoro Line Reactor	30	R-L	In Service
		330kV Pensulo-Kasama Line Reactor	60	R-L	In Service
		66kV Bus Reactor	30	R-L	In Service
25.	Kasama	330kV Kasama-Pensulo Line Reactor	60	R-L	In Service
		330kV Bus Reactor	30	R-L	In Service
		66kV Bus Capacitor	7.5	C	Out of Service
		66kV Bus Reactor	7.5	R-L	Out of Service
26.	Mpika	66kV Bus Capacitor	7	C	Out of Service
27.	Isoka	66kv Bus Reactor	1.5	R-L	Out of Service
28.	Lusiwasi	66kV Bus reactor	2.5	R-L	Out of Service
29.	Msoro	330kV Msoro-Pensulo Line Reactor	30	R-L	Out of Service
		330kV Msoro-Chipata Line Reactor	30	R-L	Out of Service
		330kV Bus Reactor	30	R-L	In Service
30.	Chipata	330kV Chipata-Msoro Line reactor	60	R-L	In Service

7.4. Appendix 4: Modelling and Simulation in PowerFactory DIgSILENT

1. Introduction

In PowerFactory DIgSILENT, the modelling philosophy is targeted towards a strictly hierarchical system modelling approach, which combines both graphical and script-based modelling methods. The basis for the modelling approach is formed by the basic hierarchical levels of time-domain modelling:

- The DSL Block Definitions, based on the "DIgSILENT Simulation Language" (DSL), form the basic building blocks to represent transfer functions and differential equations for the more complex transient models;

- There are built-in models and common models. The built-in models or elements are the transient PowerFactory models for standard power system equipment, i.e., for generators, motors, static VAr compensators, etc. The common models are based on the DSL Block Definitions and are the front-end of the user-defined transient models.

- The composite models are based on composite frames and are used to combine and interconnect several elements (built-in models) and/or common models. The composite frames enable the reuse of the basic structure of the composite model.

  Fig 25 below shows a typical configuration of a synchronous generator with power system stabiliser, voltage controller, primary controller, and prime mover model.

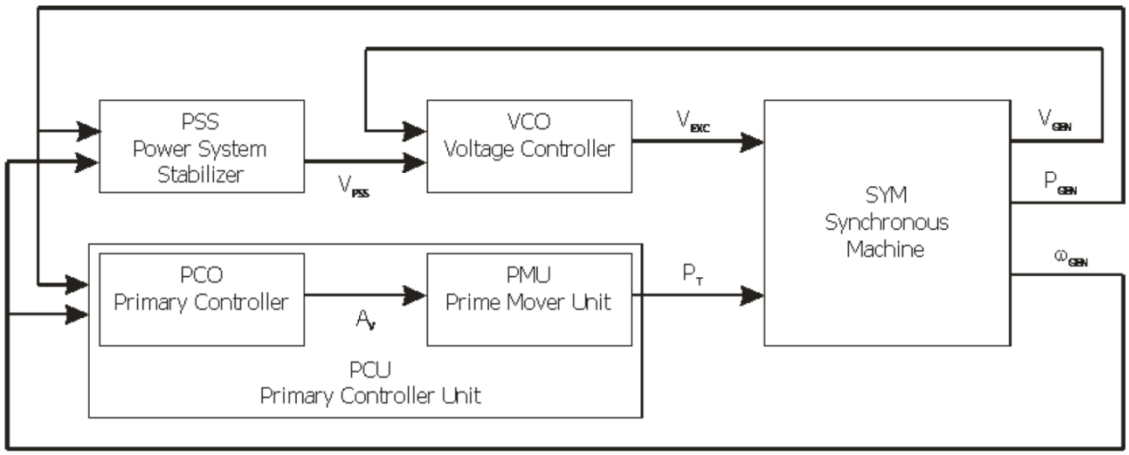

Fig 25: Typical Composite or Power Plant Model

In DIgSILENT, Time domain analyses are typically based on such predefined system models. In the majority of cases the standard IEEE definitions for models are used.

2. Hydro Generators

Generators are usually represented by a synchronous machine with the generator mode selected. The same standard element can be used as a motor depending on the applicable mode of operation. The Active and Reactive power or alternatively the Apparent Power and the Power Factor are then defined accordingly. The machine is then provided with a composite frame and a station controller where necessary.

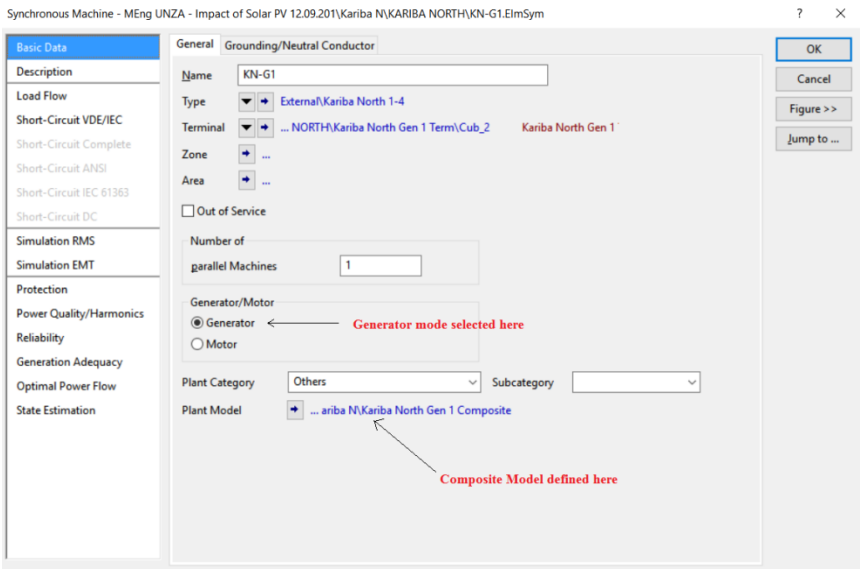

Fig 26: Definition of a synchronous machine

A composite model is a specific combination of mathematical models. These models may be power system elements such as synchronous generators, or block definitions, such as voltage controllers, primary mover models or power system stabilisers.

Composite models may be used to create new objects, such as protection devices, to dress-up power system elements such as synchronous machines with controllers, prime movers' models, etc., or for the identification of model parameters on the basis of measurements.

In the ZESCO simulation model, the major hydro generators are represented by the IEEE composite frame. The IEEE frame has slots that provide for dynamic controls such as governor control (primary controller unit or pcu slot), Automatic Voltage Regulation (Voltage Control or vco slot), Power system stabilizer (pss slot) etc.

Fig 27 below shows a screen shot defining the IEEE Composite Model whereas Fig 28 shows a schematic of the model.

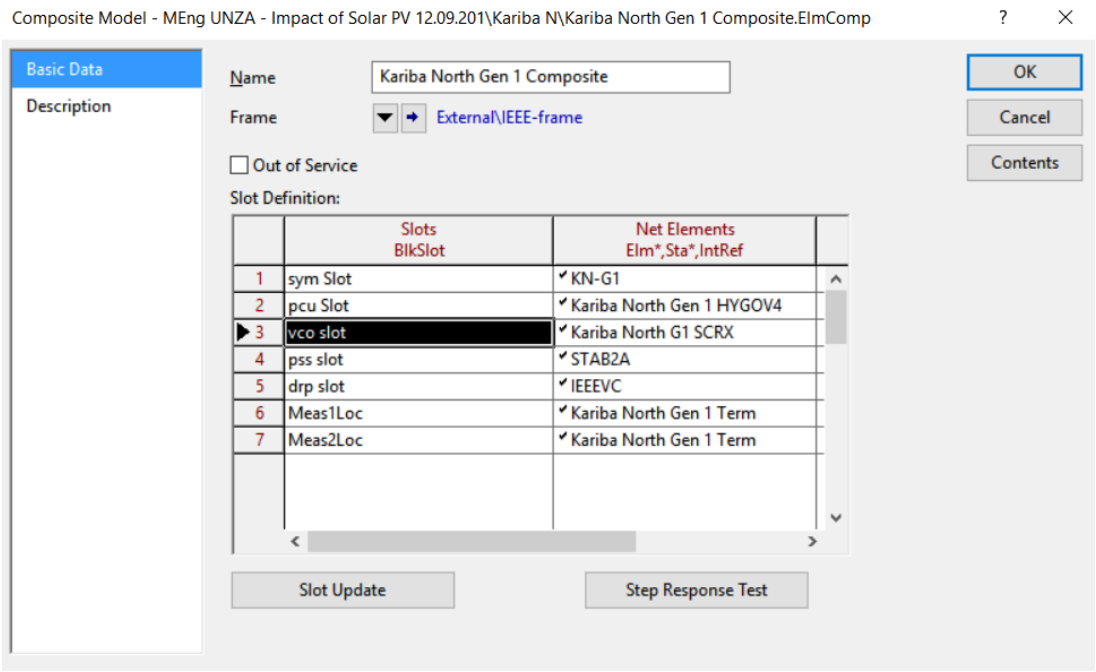

Fig 27: Screen shot - Example of a Composite Model Using the IEEE-Frame

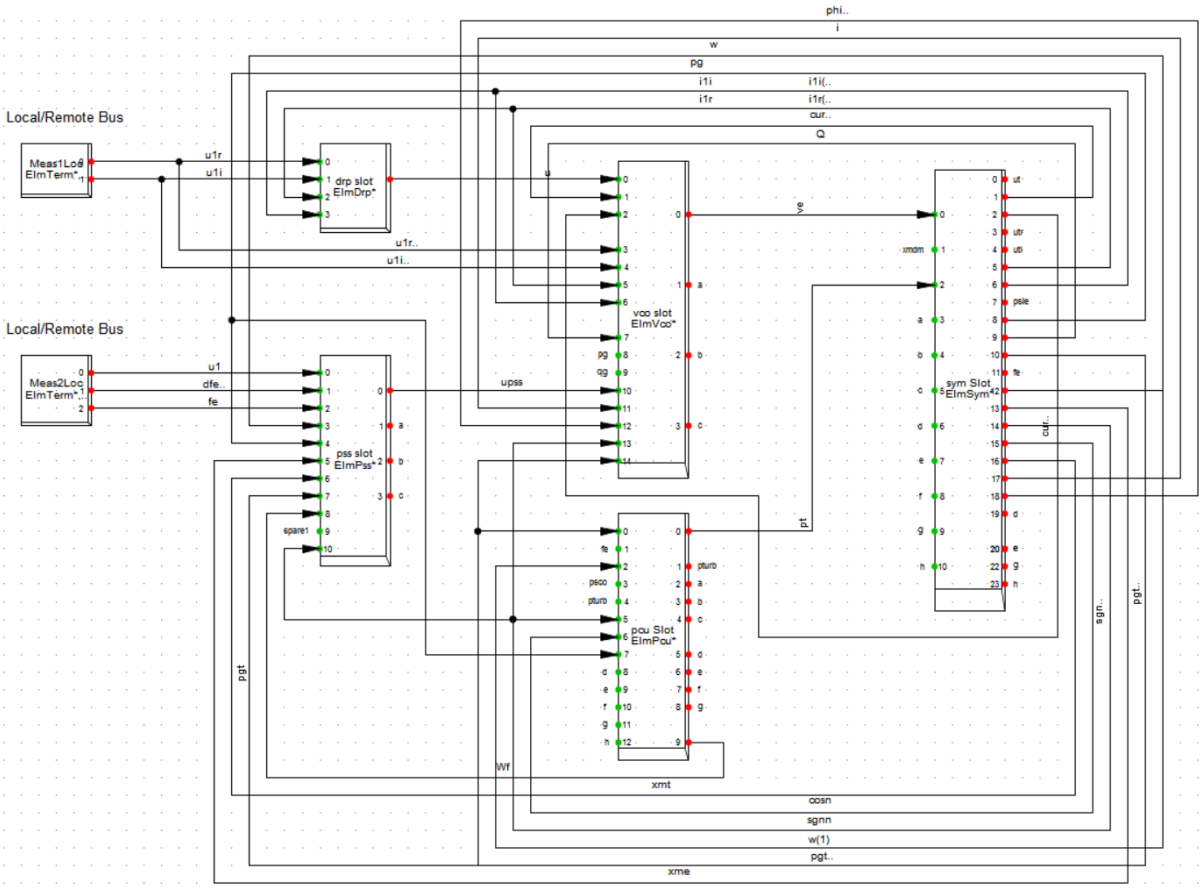

Fig 28: Screen shot of the IEEE-Frame Synchronous machine signal interconnection (DIgSILENT)

3. Governors

Governing system or governor is the main controller of the hydraulic turbine. Governor control system in Hydro Turbines is basically a feedback control system which senses the speed and power of the generating unit or the water level of the forebay of the hydroelectric installation etc. and takes control action for operating the discharge/load controlling devices in accordance with the deviation of actual set point from the reference point. Governing system as per IEEE std. -75 includes following. a) Speed sensing elements b) Governor control actuators c) Hydraulic pressure supply system d) Turbine control servomotors which are normally supplied as part of turbine

Governors are also known as primary controller Units (pcu). Shortly after a disturbance, the governors of the units participating in primary control will increase/decrease their turbine power and drive the frequency close to its nominal value. There are many ways of achieving this physically, but mostly in hydrogenators, these involves altering the volumetric flow rate by adjusting the guide vanes in the turbines.

Now the change in the generator power is proportional to the frequency deviation and is divided among participating units according to the gain (K_{pf}) of their primary controllers and which is depicted in Fig 29 below. If the Active Power Control Option According to Primary Control is selected in PowerFactory´s load flow command, the power balance is established by all generators having a primary controller gain value different than zero (parameter Prim. Frequency Bias in the Load Flow page Fig 30). The modified active power of each generator is then calculated according to the following equation:

$$P_i = P_{i-dispatch} + \Delta P_i$$

Where,
P_i is the modified active power of generator i,
$P_{i-dispatch}$ is the initial active power dispatch of generator i and
ΔP_i is the active power change in generator i.

The active power change of each generator (ΔP_i) will be determined by its corresponding primary controller gain value (K_{pf-i}) and the total frequency deviation.

$$\Delta P_i = K_{pf-i} . \Delta f$$

Where,
K_{pf-i} is the primary controller gain parameter of generator i and Δf is the total frequency deviation.

The total frequency deviation (Δf) can be obtained according to:

$$\Delta f = \frac{\Delta P_{Tot}}{\sum K_{pf}}$$

where ΔP_{Tot} corresponds to the active power change sum of every generator:

$$\Delta P_{Tot} = \sum_{j=1}^{n} \Delta P_j$$

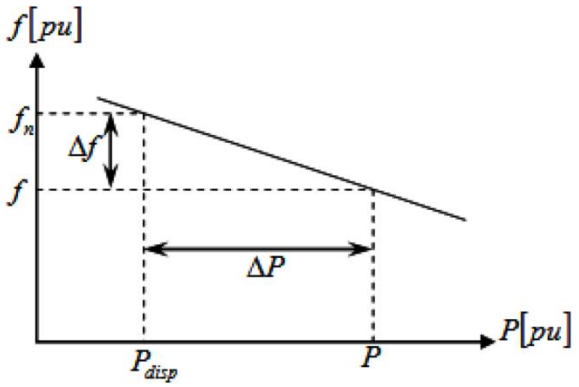

Fig 29: Primary Frequency Bias

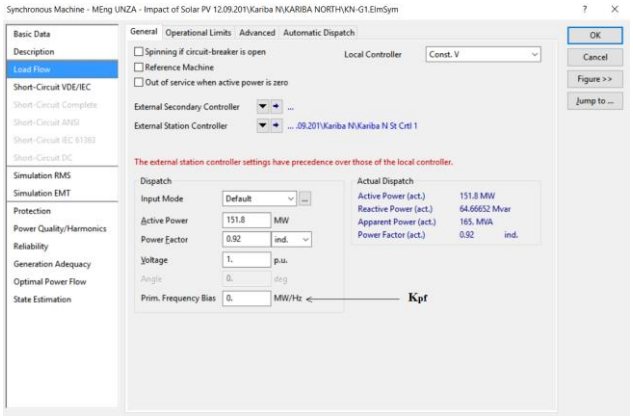

Fig 30: Primary Frequency Bias (K_{pf}) Setting in the Load Flow Page of the Synchronous Machine Element (ElmSym)

In the study, governors in the major generation stations were modelled using the IEEEG3 model. Fig 31 below shows typical settings of a governor while Fig 32 shows the block diagram.

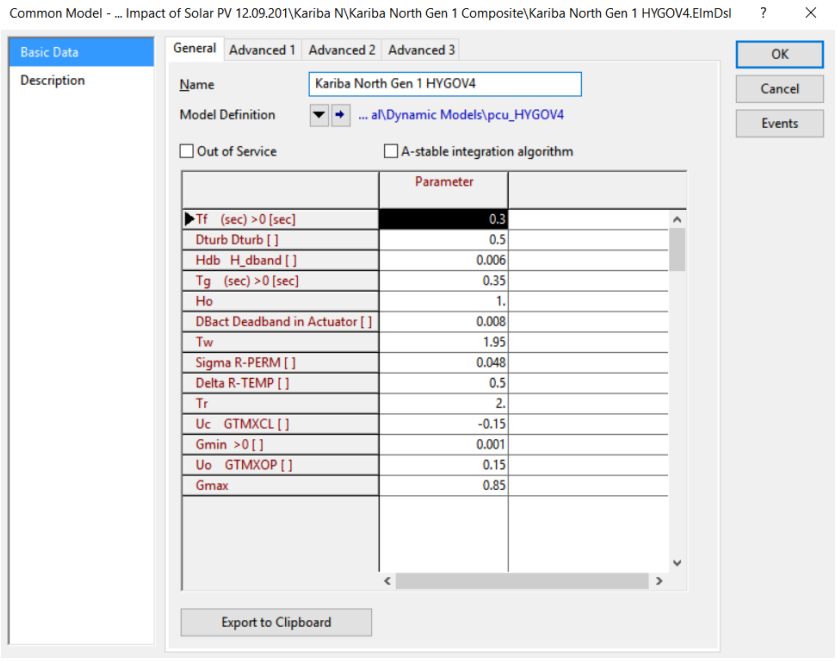

Fig 31: Typical general definition for a Hydropower governor

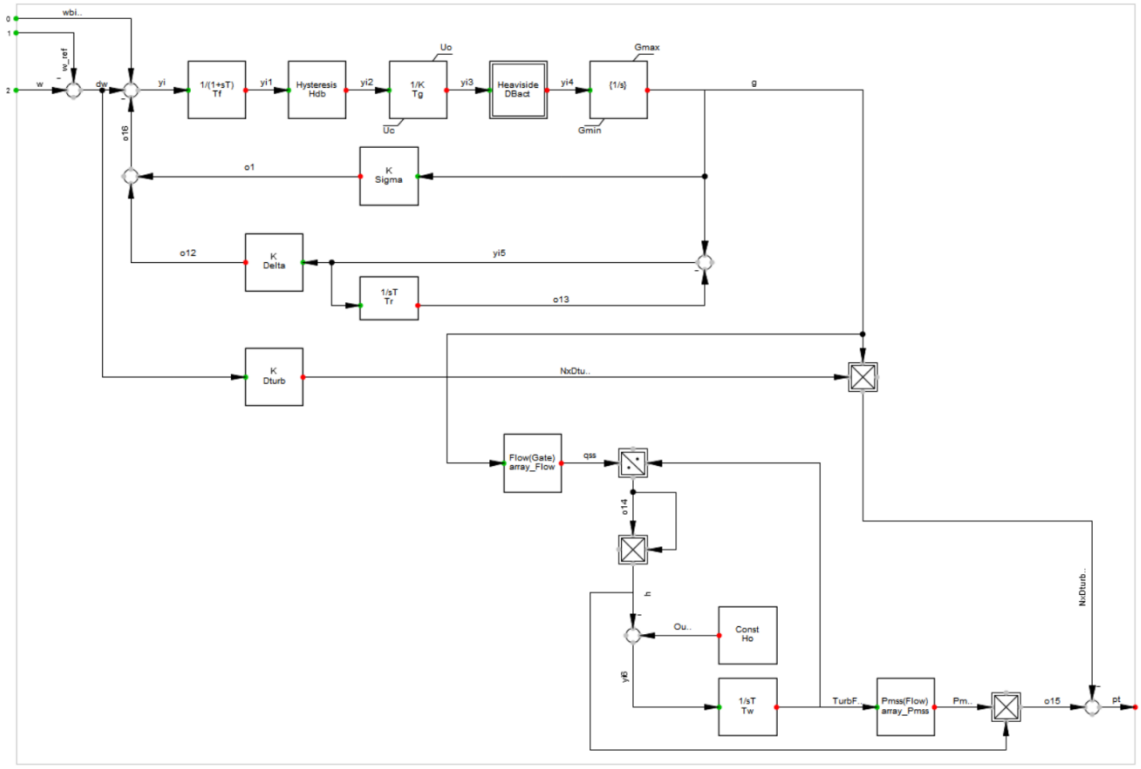

Fig 32: Block Diagram of the IEEEG3 Governor –pcu_HYGOV4

4. Automatic Voltage Regulators (AVRs)

For constant power, Voltage (V) is inversely proportional to current I. That is V decreases with increase in I. However, at the generator end, no matter how much the load is increased terminal voltage should remain unchanged. To achieve this, the Automatic Voltage Regulator (AVR) is employed.

The voltage regulator is an adjustment device that controls the generator output voltage within a specified range. Its function is to automatically control the generator voltage and keep it constant when the rotating speed of the generator changes, so as to prevent the generator voltage from being too high at the same time, it also prevents the generator voltage from being too low.

The AVR senses changes in output voltage and then alters the excitation current, thereby maintaining the output voltage constant. When the terminal voltage and reactive power of the synchronous motor change, the output current of the exciter is automatically controlled according to the corresponding feedback signal to achieve the purpose of automatically regulating the terminal voltage or reactive power of the synchronous motor.

In DIgSILENT PowerFactory, Automatic Voltage Regulators are modelled using the standard SCRX model as shown in Fig 33 below while the modified version is shown in Fig 34.

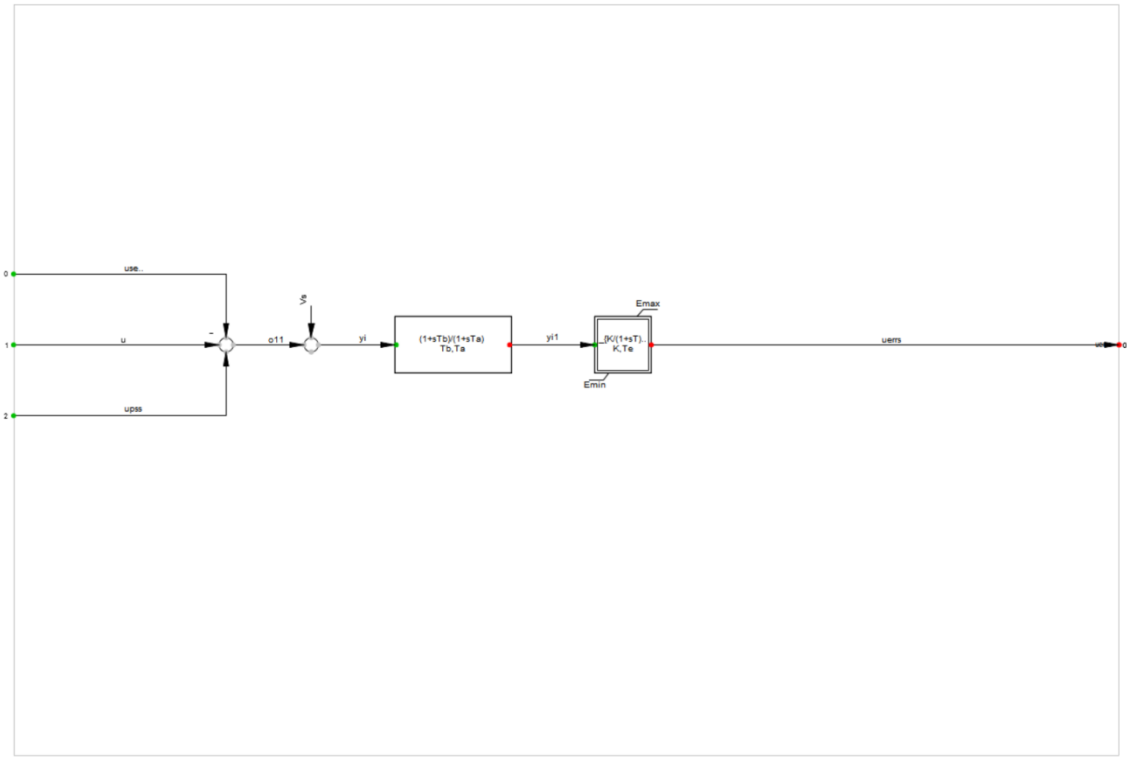

Fig 33: Block diagram for the vco_SCRX bus fed or solid fed static exciter

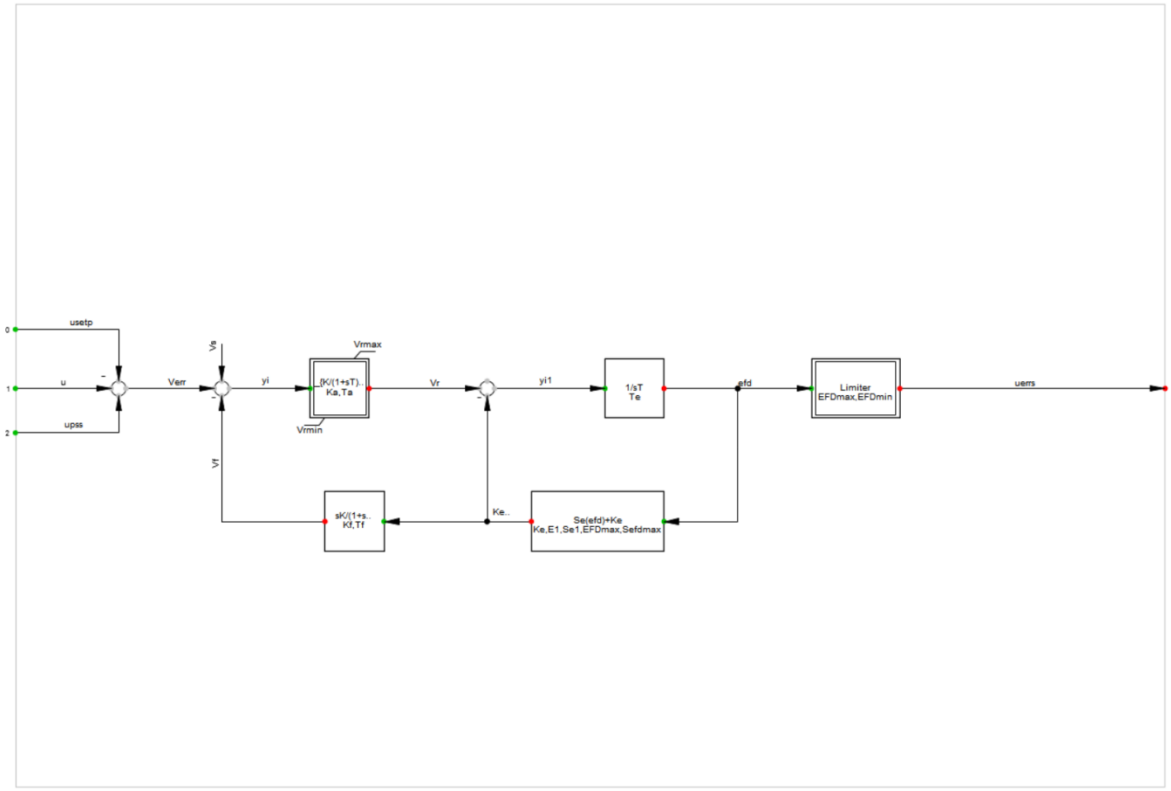

Fig 34: Block diagram for the 1968 modified IEEE vco_IEEEA1 excitation system

5. Power system stabilising Unit

Governors and automatic voltage regulator normally provide the needed feedback to regulate generator outputs. However, these systems are not fast enough when sudden disturbances occur. Power system stabilisers (Fig 35) are therefore added to enable faster damping of the output frequency and voltage.

Power system stabilizer (PSS) control provides a positive contribution by damping generator rotor angle swings, which are in a broad range of frequencies in the power system. These range from low frequency intertie modes (typically 0.1 - 1.0 Hz), to local modes (typically 1 - 2Hz), to intra-plant modes (about 2 -3 Hz). The low frequency modes, commonly called intertie or interarea modes, are caused by coherent groups of generators swinging against other groups in the interconnected system. These modes are present in all interconnected systems and the damping is a function of tie line strength and unit loading factors. Weak ties due to line outages and heavy system loads can lead to poorly damped intertie modes.

PSS control can generally provide significant improvements in intertie mode damping, by applying stabilizers to most units that participate in power swing modes. Stabilizers damp generator electro-mechanical oscillations protecting the shaft line and stabilising the grid. They damp generator rotor angle swings, which are of greater range in frequencies in power system.

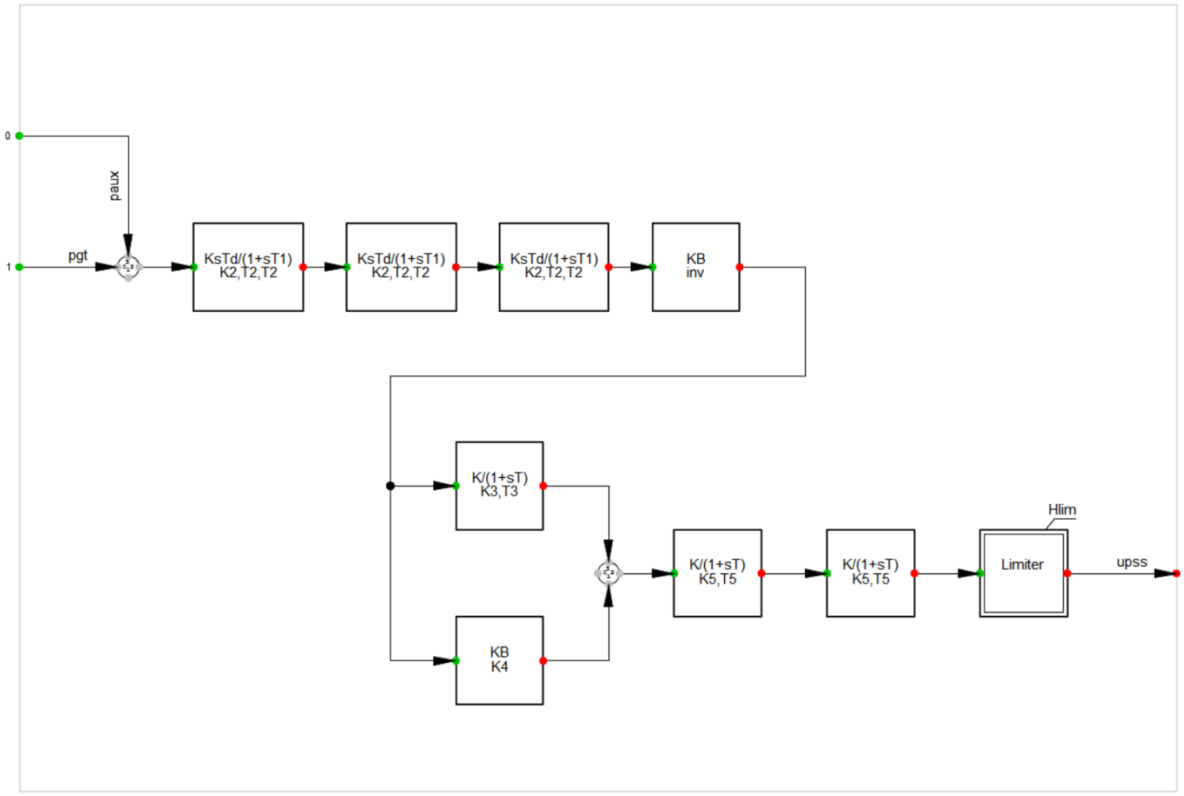

Fig 35: pss_STAB2A: Power system stabilising Unit (ASEA)

The general definition of a PSS is sown in *Fig 36* below:

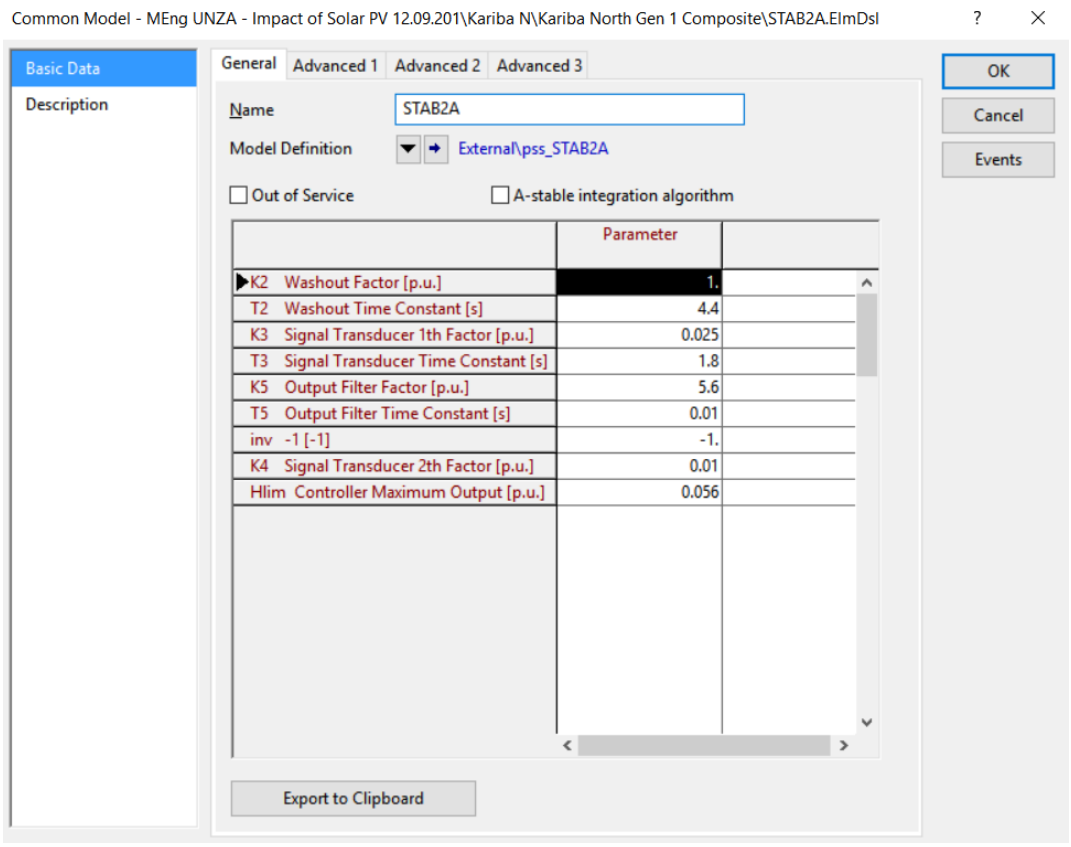

Fig 36: General definition of a Power system stabiliser

6. Load Flow Controllers

1. Station Controller (ElmStactrl)

The station controllers are used to control the reactive power during a load flow. They combine several sources of reactive power to control the voltage at a given bus. The reactive power reserves of synchronous generators in transmission network control the voltages at specific nodes in the system and/or the reactive power exchange with neighbouring network zones.

In PowerFactory´s load flow calculation, the voltage regulator of the generators has a voltage set-point which can be set manually defining a PV bus type or can be controlled from an Automatic Station Controller (ElmStactrl).

Fig 37 below shows a typical load flow definition of a station controller.

2. Power Frequency Controller (ElmSecctrl)

If an unbalance occurs between the scheduled active power values of each generation unit and the loads plus losses, primary control (Governors, VAR & PSS) will adapt

(increase/decrease) the active power production of each unit, leading to an over- or under-frequency situation. Secondary frequency control is then needed to bring the frequency back to its nominal value, re-establishing cost-efficient generation delivered by each unit.

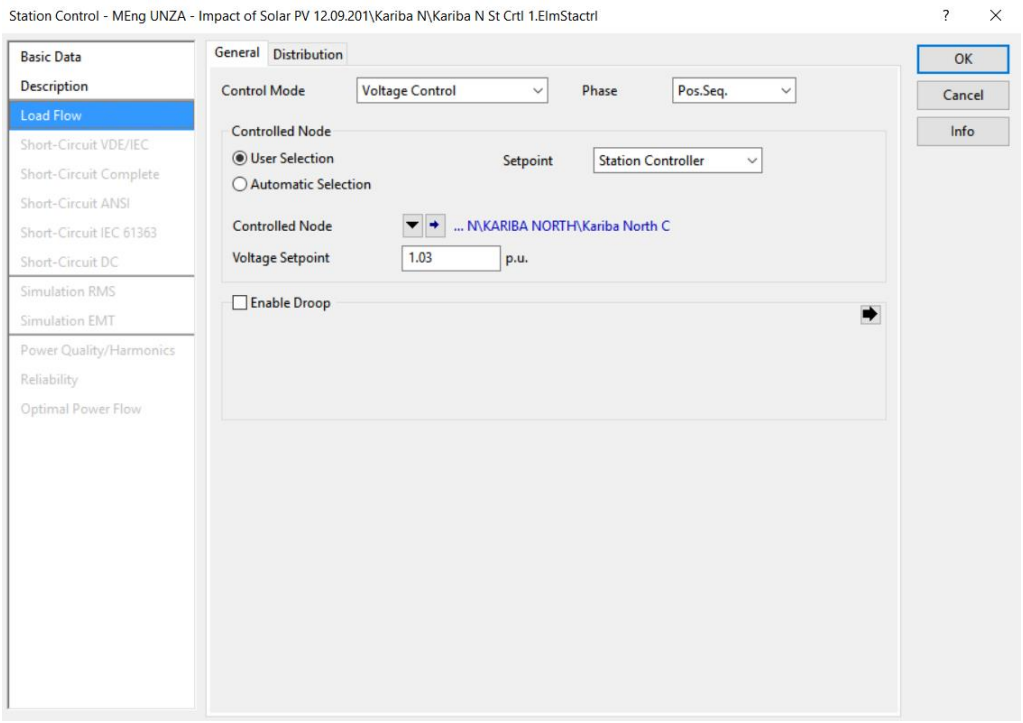

Fig 37: Typical load flow definition of a station controller (DIgSILENT)

In DIgSILENT, secondary control is represented in load flow calculations by network components called Power Frequency Controllers (ElmSecctrl). If the Active Power Control option According to Secondary Control is selected, the generators considered by the Power Frequency Controller establish the active power balance according to their assigned participation factors. It is also possible, within the group of controlled generators, to implement a merit order priority; if this option is selected in the Power Frequency Controller, generators with the highest merit order priority will be dispatched first, as far as their operational limits allow, then the generators with successively lower merit order priorities as required.

In cases where the total required MW change in generation exceeds the total available on generators with a non-zero merit-order, the remainder will be distributed between generators with a zero-merit order, according to the Primary Frequency Bias (K_{pf}) of these generators, those with a higher K_{pf} being used first.

3. Tap-Controller (ElmTapctrl)

The tap controller element represents a tap controlling logic for a group of transformers.

7. Steam Power Plant

DIgSILENT PowerFactory provides several models representing steam turbine governors, all TGOVs, IEEEG1, IEEESGO, and others. The SYM Frame_no droop model can be used to represent thermal power plants except for combined cycle power plants.

For combined cycle there is no standard frame, so it has to be created from information relating to each specific unit. If no detailed information is available, the standard thermal model IEEG1 may be used for the governor, enabling as many stages (HP, MP and/or LP) as required; for a more generic and simplified model, TGOV1 can be also used. The AVR for this kind of application strongly depends on the excitation system of the machine, predominantly AC or static systems, except for old installations, where DC systems may be still in operation.

8. Internal Combustion Model

A diesel or gas with synchronous generator is no different to any other type of synchronous generator unit, only their total inertia is usually lower, and they are usually salient pole machines. For the AVR, the ESAC8B, AC8B or EXAC1 and EXAC1A standard types from the DIgSILENT library may be used. The only diesel governor available in the standard library is the DEGOV1.

9. Modelling of a PV Model

1. The basic Photovoltaic System

A generic model in PowerFactory is already available in the form of a PV template in the library. This model gives the basic understanding of the operation of PV system and has some basic control systems in it. But there are many deficiencies of this model that need to be addressed.

This model has PV panel model with many assumptions and approximations. Also, it does not have any MPPT control to ensure PV system always operate on maximum power. There is only one type of reactive power control is available based upon voltage deviation. And there is no AC voltage and active power regulation is available. Under these circumstances, there arises a need of an extensive model with all the essential control system to have detailed grid studies. The basic Solar PV plant in DIgSILENT is shown in *Fig 38* below:

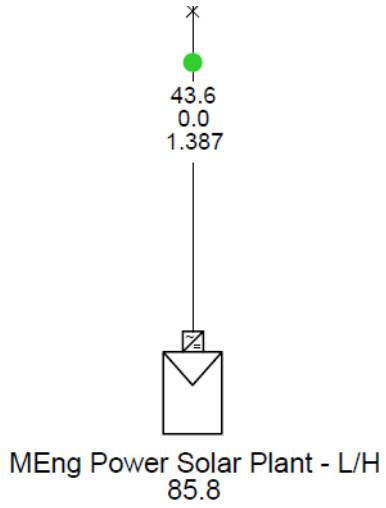

Fig 38: Typical Solar PV Module in DIgSILENT

2. Frame of Generic PV Model

The control frame of the PV System in generic model is shown in *Fig 39*.

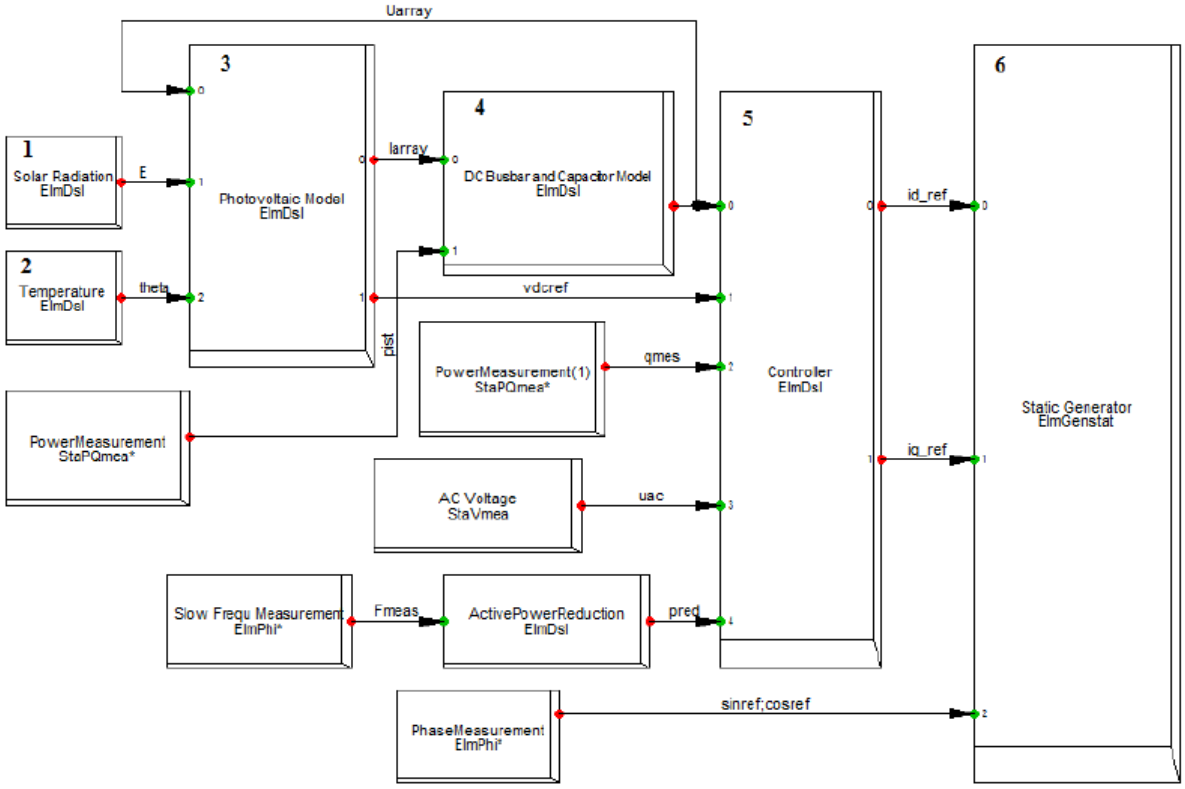

Fig 39: Frame of Generic PV Model

It is necessary to model the PV array, DC link capacitor dynamics by DSL functions. The same can be observed in the control frame and the main blocks will be explained in brief in the following sections.

a. Solar radiation and temperature

Solar radiation and temperature both are modelled as limited time integrators. The purpose of these slots is to accumulate change of irradiance per second or change of temperature per second and integrate them over a period of time. The output of these blocks is given to slot 3 which is the photovoltaic model.

b. Slot 3: Photovoltaic model

Photovoltaic model takes DC voltage, irradiance and temperature as the inputs. Based upon PV equations written as DSL codes, the PV array is modelled and provides array current and reference DC voltage as the outputs. It can be noticed that in this PV model there is no maximum power point tracker (MPPT) control available. The output voltage of this model is assumed to operate on maximum power point and is taken as equal to the reference dc voltage "vdcref" for the controller.

There are many unknown approximations used to calculate the final module current. Inside the PV panel model variables and parameters used for calculation are unknown and undefined. So, it is very difficult to identify any scientific reference of these equations.

c. Slot 4: DC bus bar and capacitor model

This slot represents the mode of DC bus bar and capacitor. With the help of this block the dynamics of the DC side capacitor is included in the PV system. This slot has two inputs one from the PV model in the form of array current and other from power measurement device in the form of active power signal. The output of the block is the DC voltage across the capacitor considered as the actual DC voltage, which is given as feedback to the PV module as well as the input to the controller.

d. Slot 5: Controller block

Controller is the one most important part of the PV system and the control frame is shown in Fig 40. It is necessary to regulate the active and reactive power outputs of the static generator according to the DC side output of the PV system consisting of the PV array and the DC side capacitor. This purpose is realized with the help of the controller block. This block has four inputs and two outputs. DC voltage from the capacitor model as actual DC voltage, reference DC voltage from PV model, measured AC voltage and active power are the inputs.

The reference values of the id (for active power) and iq (for reactive power) are the outputs of this controller. These currents values are given as input to the static generator, which is the interfacing converter.

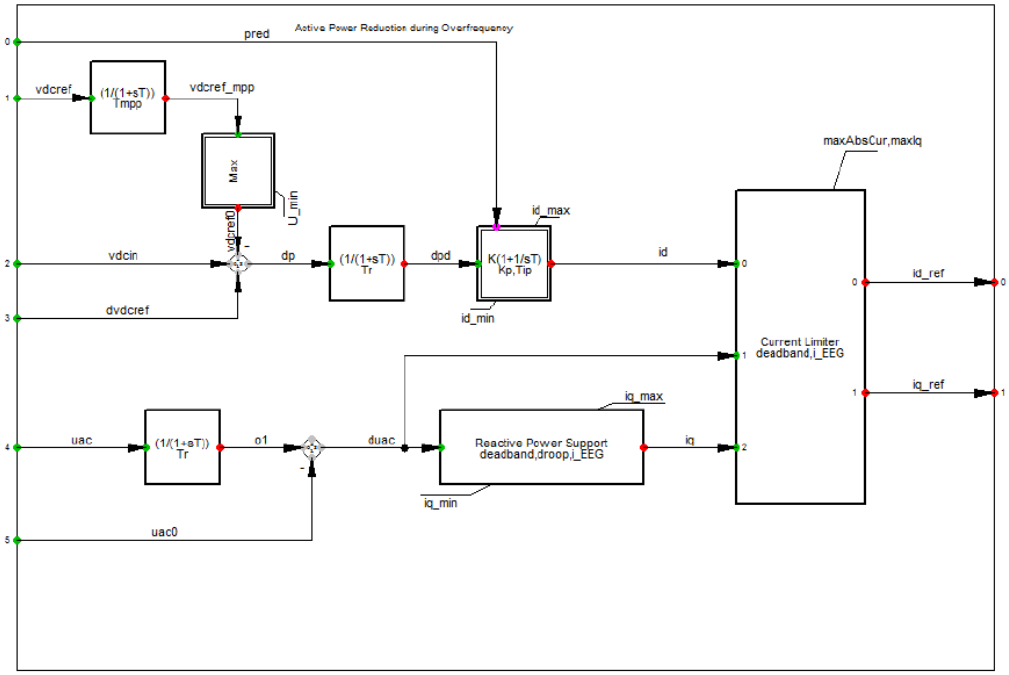

Fig 40: Control frame of Generic Model

The upper part of the control frame is the DC voltage regulation which is implemented to control the active power output of the PV system. The inputs are 'vdcref', 'vdcin' and 'dvdcref' and the output is the d-axis component of the reference current, id_ref. The lower part is the reactive power control. For the control the inputs are 'uac and 'uac0' and the output is the q-axis reference current component, iq_ref.

The equations represented in this block use a dead band of 10% of the nominal voltage and determine the iq (q-axis component of the current). A dead band of 10% means, that it will not provide or absorb the reactive power as long as voltage deviation would be within 10 % of nominal voltage. This dead band value can be changed according to the requirement of the system.

The q-axis component of the current is calculated as follows:

$$i_q = K\left(du_{ac}\right)$$

Where,
K = droop
du_{ac} = Difference in actual voltage and state voltage

e. Slot 6: Static generator block

This block represents the static generator in the control frame. The additional inputs that are to be given to the static generator can be given to this block which

is internally connected to the actual one. So, the output from the controller block that is the d-axis and q-axis reference current components as well as the ‘cosref’ and ‘sinref’ values from the phase measurement unit are given to slot 6. Based upon which the output of the static generator is regulated.

7.5. Appendix 5: Causes of System Collapse in PowerFactory DIgSILENT

1. Introduction

This Appendix 5 gives an outline on some of the causes of system failure in DIgSILENT Power Factory or in indeed in an operational power system

2. Out-of-Step

Out-of-Step or Loss of Synchronism is a condition where a generator experiences a large increase in the angular difference of the Electro Motive Force (EMF) with other generators or portions of a system to which it is connected, usually following a major power system disturbance. Depending on the severity of the disturbance, one or more generators may no longer maintain synchronism with the rest of the system. When a generator still connected to but is no longer in synchronism with other generators or with the power system, the condition is referred to as out of step.

If the generator EMF angle exceeds the critical level, then the generator loses synchronism with the system. This condition can also be introduced by malfunctions in the Automatic Voltage Regulator (AVR) system. Unstable swings (actual OOS conditions) will require tripping generators or possibly system islanding to minimize the scale of the system disturbance.

The out-of-step condition produces high peak currents, winding stresses, pulsating torques and mechanical resonances within the generator, which usually requires separation of the generator from the system. Usually, this separation is accomplished by out-of-step tripping (OOST) relays.

If the disturbance is not so severe, the system remains stable and the load angle of the generator will also oscillate (i.e., the angle will increase and decrease in synchronism with the power system oscillations). Such a “stable” system may or may not be well damped. In the case of stable power swings, it is never desirable to trip.

When generators experience out of step conditions and OOST relays separate them from the system, it is common that nearby generators and transmission system terminals will also experience oscillations similar to those experienced by the OOS generator. Often it is desirable that these other facilities do not trip during the generator OOS event. These facilities may require Power Swing Blocking (PSB) relays in order to avoid undesirable tripping.